THE
PHYSICAL REVIEW
A Journal of Experimental and Theoretical Physics Established by E. L. Nichols in 1893
VOL. 54, NO. 6 SEPTEMBER 15, 1938 SECOND SERIES

Radioactive Manganese Isotopes

J. J. LIVINGOOD, *Radiation Laboratory, Physics Department, University of California*
AND
G. T. SEABORG, *Chemistry Department, University of California, Berkeley, California*
(Received July 11, 1938)

Five radioactive decay periods of manganese have been obtained by bombarding cobalt, iron, manganese, chromium and vanadium with neutrons, deuterons and alpha-particles. Arguments are given for the assignment to various isotopes, as follows:

REACTION	HALF-LIFE	REACTION	HALF-LIFE
$Cr^{50}(d,n)Mn^{51}$	46±2 min. (+)	$Mn^{55}(n,\gamma)Mn^{56}$	2.59±0.02 hours (−)
$Fe^{54}(d,\alpha)Mn^{52}$	21±2 min. (+)	$Mn^{55}(d,p)Mn^{56}$	
	6.5±1 days (+)	$Cr^{53}(\alpha,p)Mn^{56}$	
$Fe^{56}(d,\alpha)Mn^{54}$	310±20 days (*k* electron capture)	$Fe^{56}(d,\alpha)Mn^{56}$	
$Cr^{53}(d,n)Mn^{54}$		$Fe^{56}(n,p)Mn^{56}$	
$V^{51}(\alpha,n)Mn^{54}$		$Co^{59}(n,\alpha)Mn^{56}$	

No evidence has been found for radioactive Mn^{53}. Chemical identification has been made in all instances, except for the case of the bombardment of vanadium with alpha-particles. The 46-minute period emits positrons with a range 0.9 gram/cm² Al and annihilation radiation absorbed to half-value by 5.0 grams/cm² Pb. The positrons from the 6.5-day activity have a range 0.2 gram/cm² Al. The 310-day activity consists of a soft radiation, whose absorption coefficient is consistent with that of the Cr $K\alpha$ x-ray line, and also a gamma-ray reduced to half-value by 8.4 grams/cm² Pb. The range of the electrons from the 2.6 hour Mn^{56} has been measured as 1.3±0.1 grams/cm² Al, while the gamma-ray is brought to half-value by 11.4 grams/cm² Pb.

INTRODUCTION

THE artificial radioactivities reported in this investigation were produced by the Berkeley cyclotron with deuterons at 5.5 Mev and 7.6 Mev and with helium ions at 16 Mev. The activities were observed with a quartz fiber electroscope. C.P. carbonates and oxides of manganese were supported in an envelope of thin aluminum foil; chromium was bombarded either as the oxide (similarly supported) or as the metal plated onto copper. Iron and vanadium were used in the metallic form. Short periods of the order of a few minutes were not looked for, in general.

The bombarded samples were dissolved in a mixture of HCl and HNO_3 and small amounts of the appropriate elements were added to act as carriers for the radioactive transmutation products. The solution was adjusted to a concentration of 16 *N* in HNO_3 for the precipitation of the manganese, which was brought down as MnO_2 by the addition of solid $KClO_3$ to the boiling solution. The MnO_2 was usually purified by redissolving it in an acid solution of H_2O_2 and by again precipitating from a boiling solution of 16 *N* HNO_3 by the addition of solid $KClO_3$.

Figure 1 shows the percent abundance of the stable isotopes in the region near manganese, as compiled by Livingston and Bethe.[1] The identity of the radioactive isotopes, shown in circles, is that derived from the present investigation.

[1] Livingston and Bethe, Rev. Mod. Phys. **9**, 380 (1937).

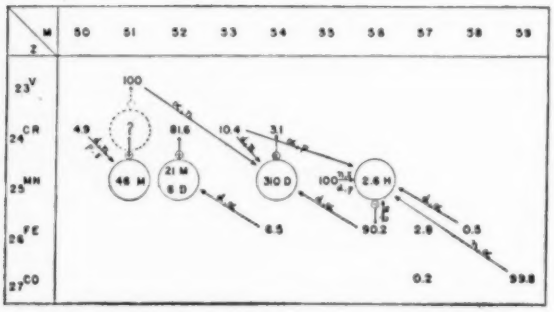

FIG. 1. Percent of stable isotopes in the neighborhood of Mn. The half-lives of radioactive isotopes are shown in circles, with arrows indicating known transmutations.

Mn^{51} FROM Cr+D AND Cr+H: HALF-LIFE 46±2MIN. (+)

We have briefly reported[2] the formation of a chemically identified manganese isotope with half-life 46 minutes that is formed by deuteron bombardment of chromium. Positrons are emitted. The $Cr(d,n)Mn$ reaction could lead to Mn^{51}, Mn^{53} and Mn^{54}, and of these possibilities we believe the 46-minute activity must be assigned to Mn^{51}. If Mn^{54} were responsible, the activity should be apparent after deuteron bombardment of iron, through $Fe^{56}(d,\alpha)Mn^{54}$, and this is not found to occur; neither have we been able to produce this period by fast neutron bombardment of manganese, which would be expected to develop such a short-lived activity with considerable intensity, by the transmutation $Mn^{55}(n,2n)Mn^{54}$. Mn^{53} may be eliminated as the choice since radioactive Fe^{53}, with half-life 8.9 minutes, should then decay into Mn^{53} and ultimately show the 46-minute period. We have previously shown[3] that this does not occur, when Fe^{53} is produced by $Cr^{50}(\alpha,n)Fe^{53}$ and by $Fe^{54}(n,2n)Fe^{53}$. Ridenour and Henderson, who have also reported[4] the 8.9-minute iron activity after irradiating chromium with alpha-particles, were also unable to observe any second period corresponding to Mn^{53}.

The assignment of the 46-minute activity to Mn^{51} is consistent with the report by DuBridge[5] and his associates that proton bombardment of chromium gives rise to a positron emitting radioactivity of 42-minute period. Although chemical analysis was not made, this is doubtless the same isotope and the two modes of production are

$$_{24}Cr^{50}+{}_{1}D^{2}\rightarrow{}_{25}Mn^{51}+{}_{0}n^{1},$$
$$_{24}Cr^{50}+{}_{1}H^{1}\rightarrow{}_{25}Mn^{51}+\gamma$$

followed by

$$_{25}Mn^{51}\rightarrow{}_{24}Cr^{51}+{}_{+1}\varepsilon^{0}\ (46\text{ minutes}).$$

Neither DuBridge nor ourselves have detected a second activity corresponding to the decay of Cr^{51} to stable V^{51}; this indicates that Cr^{51} has a very short or a very long lifetime (or is possibly stable). This is consistent with the fact that the literature discloses no radioactive periods that are definitely due to chromium; in particular none ascribed to Cr^{51}.

The possibility that the 46-minute period could be due to Mn^{50} rather than to Mn^{51} cannot be excluded definitely, since the reactions $Cr^{50}(d,2n)Mn^{50}$ and $Cr^{50}(p,n)Mn^{50}$ might be the sources of the activity, which would then lead to stable Cr^{50}. A decision between Mn^{50} and Mn^{51} could be made by the bombardment of chromium with protons: a study of the excitation function for the 46-minute period would reveal whether the reaction $Cr^{50}(p,\gamma)Mn^{51}$ or $Cr^{50}(p,n)$

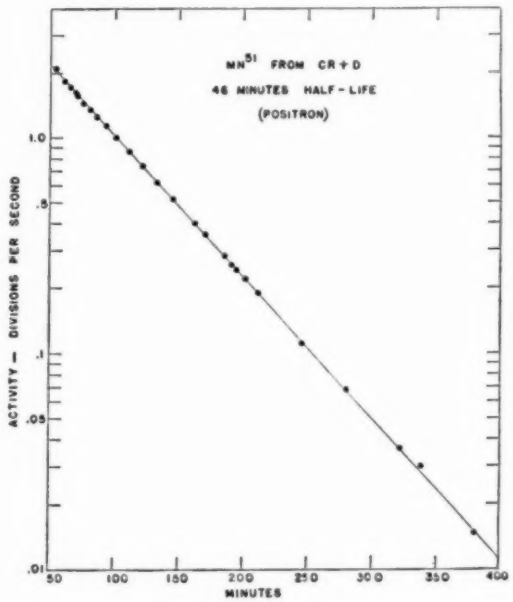

FIG. 2. Decay of Mn^{51}.

[2] Livingood, Seaborg and Fairbrother, Phys. Rev. **52**, 135 (1937).
[3] Livingood and Seaborg, Phys. Rev. **54**, 51 (1938).
[4] Ridenour and Henderson, Phys. Rev. **52**, 889 (1937).
[5] DuBridge, Barnes, Buck, Strain, Phys. Rev. **53**, 447 (1938).

Mn^{50} occurs, since the latter should exhibit a fairly sharp threshold.

Figure 2 shows the decay of manganese precipitated from chromium metal plated onto copper that was activated for 3 minutes with 5 microamperes of deuterons at 5.5 Mev. The half-life, as found from several determinations, may be given as 46 ± 2 minutes. Absorption curves are given in Fig. 3; the positrons have a range of 0.9 gram/cm² Al, unless modified by a line spectrum of electrons as pointed out below. This corresponds to a maximum energy of 2.0 Mev through the relation of Widdowson and Champion:[6]

$$\text{Energy (Mev)} = \frac{\text{Range (grams/cm}^2\text{)} + 0.165}{0.0536}.$$

The gamma-ray, as is to be expected from a positron emitter, is absorbed to half-value by

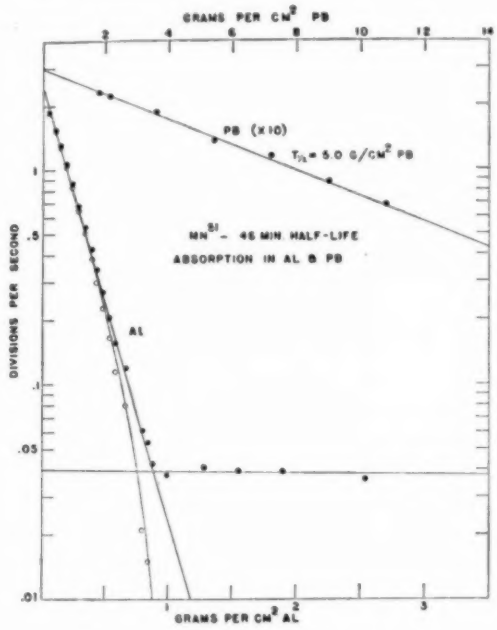

FIG. 3. Absorption curves of Mn^{51}.

5.0 grams/cm² Pb, which represents, according to the data of Gentner,[7] the 0.5 Mev annihilation radiation.

The aluminum absorption curve is somewhat anomalous, in that the softer component of the total radiation appears to be linear (on a semi-log plot). If the gamma-ray is subtracted, the curve for the particles is then concave towards the origin; this may indicate the presence of a homogeneous group of electrons. A possible explanation could be K electron capture as an alternative method of decay, followed by the emission of a gamma-ray that is highly internally converted.

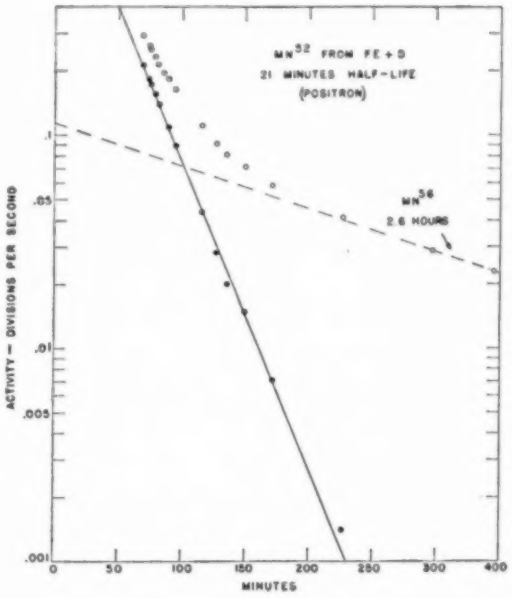

FIG. 4. Decay of Mn^{52}.

Mn^{52} FROM Fe+D: HALF-LIVES 21 ± 2 MIN. (+) AND 6.5 ± 1.0 DAYS (+)

A short account of manganese isotopes with half-lives 21 minutes and 6 days, formed by deuteron bombardment of iron, has already been given.[2] Both activities are positron emitters and chemical identification has been carried out. The 21-minute period has also been observed by Darling, Curtis and Cork[8] after the same type of bombardment.

Two positron emitting manganese isotopes, Mn^{52} and Mn^{54}, can be expected through the disintegration type $Fe(d,\alpha)Mn$; nevertheless, we believe both these activities must be described as isomers of Mn^{52}. This follows from the fact that neither period is obtained by deuteron bombardment of chromium, and the reaction $Cr(d,n)Mn$ could lead to Mn^{54} but not to Mn^{52}. Furthermore, neither activity has been found

[6] Widdowson and Champion, Proc. Phys. Soc. **50**, 192 (1938).

[7] Gentner, J. de phys. et rad. **6**, 274 (1935).

[8] Darling, Curtis and Cork, Phys. Rev. **51**, 1011 (1937).

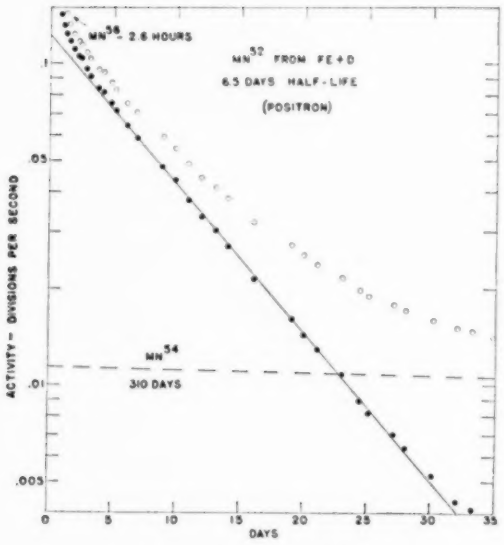

FIG. 5. Decay of Mn^{52}.

after the bombardment of manganese with the fast neutrons from Li+D, wherein the reaction $Mn^{55}(n,2n)Mn^{54}$ could be expected. And finally, this identification is consistent with our failure to detect either activity after neutrom bombardment of cobalt; if either were due to Mn^{54} the reaction $Co^{57}(n,\alpha)Mn^{54}$ might occur, in analogy with the known transmutation $Co^{59}(n,\alpha)Mn^{56}$. The scarcity of Co^{57}, however, could be used to vitiate this last argument.

We therefore conclude the two activities to be isomers, formed according to

$$_{26}Fe^{54}+{}_{1}D^{2}\rightarrow{}_{25}Mn^{52}+{}_{2}He^{4}$$
$$_{25}Mn^{52}\rightarrow{}_{24}Cr^{52}+{}_{+1}e^{0}\ (21\text{ minutes; }6.5\text{ days}).$$

The decay of the 21-minute positron activity is shown in Fig. 4. The manganese was separated from iron that had been exposed to 6 microamperes of 5.5 Mev deuterons for 10 minutes. Even with so short a bombardment, the 2.6-hour activity of Mn^{56} is relatively strong.

Figure 5 exhibits the decay of the 6-day positron emitter, intermixed with the 2.6-hour Mn^{56} and the 310-day Mn^{54} activities (see below). This sample was obtained from iron activated by a 4-hour bombardment with 15 microamperes of 5.5 Mev deuterons. The average value of the half-life, obtained from four specimens, is 6.5 ± 1.0 days.

The absorption in aluminum of this activity is given in Fig. 6. Inasmuch as the 310-day activity was also present during the lifetime of the 6-day period, this figure was obtained by correcting for the contribution of this long period to the composite absorption data obtained at the early age of a few days. The resultant curve is therefore subject to more than the usual amount of error, but suggests a range for the 6-day activity equal to 0.20 ± 0.05 gram per cm^2 Al, or a maximum energy for the positrons of about 0.7 Mev. The gamma-ray has not been examined but is probably the 0.5 Mev annihilation radiation.

Mn^{54} FROM Fe+D, Cr+D AND V+He: HALF-LIFE 310 ± 20 DAYS (*K* ELECTRON CAPTURE)

It has previously been shown by us[2] that a chemically identified manganese isotope of half-life several months is produced by deuteron bombardment of iron. Only electrons were reported to have been observed. More complete studies of this activity have been carried out on three samples that have been followed from 10 to 15 months, and we can now give the half-life more precisely as 310 ± 20 days. Absorption measurements indicate that the electrons are not disintegration particles, but are photoelectrons ejected from the extranuclear structure following "disintegration" of the radioactive nucleus by *K* electron capture, rather than by positron emission. This will be discussed more fully in a subsequent paragraph.

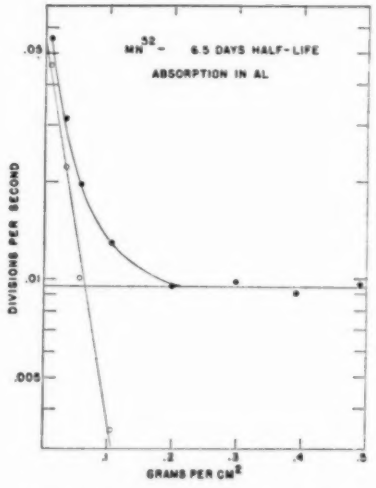

FIG. 6. Absorption curves of Mn^{52}.

Only two choices are available for this isotope when produced from iron by deuteron bombardment: Mn^{52} and Mn^{54}. We have given evidence above for the assignment to Mn^{52} of the isomeric activities with 21 minutes and 6 days half-lives, so that the 310-day period probably is to be associated with Mn^{54}. This supposition is confirmed by the fact that we have been able to produce the same activity, also chemically shown to be due to manganese, by activating chromium with deuterons. Here the reaction $Cr(d,n)Mn$ could lead to Mn^{54} but not to Mn^{52}. Additional evidence that this activity is identical with that produced from iron is the similarity of their absorption curves (see below).

The excessively long period is an adequate explanation for our inability to produce this activity through $Mn^{55}(n,2n)Mn^{54}$, and the scarcity of Co^{57} is an additional reason why the reaction $Co^{57}(n,\alpha)Mn^{54}$ has not been detected.

Study of the isotopic structure of the elements suggests that a conclusive identification of Mn^{54} should be obtained by alpha-particle bombardment of the single isotope of vanadium, since the only radioactive nucleus that could be formed by any known reaction should be Mn^{54}, through $V^{51}(\alpha,n)Mn^{54}$.

Ridenour and Henderson[4] have bombarded vanadium with 9 Mev alpha-particles and reported two activities with half-lives 1.2 minutes and about 67 minutes. No chemical separation was made. We have activated vanadium with 16 Mev alpha-particles and have obtained a decay curve showing a number of short periods and a very much longer activity, of much larger yield than the short periods, which is apparently going into the 310-day period to be expected on the basis of the data

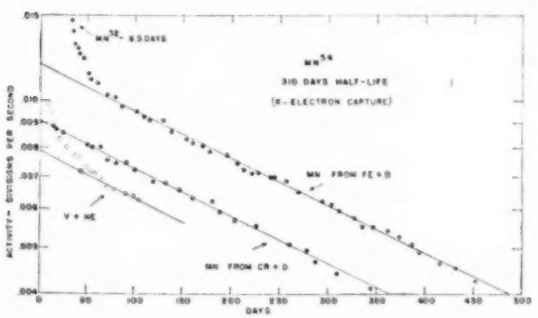

FIG. 7. Decay of Mn^{54}.

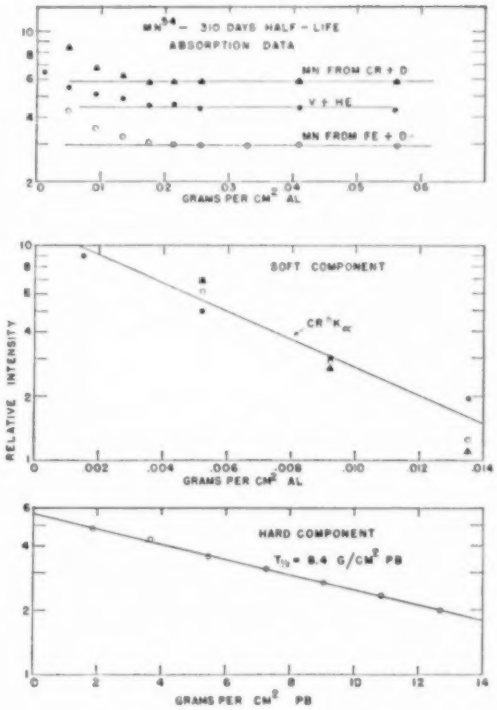

FIG. 8. Absorption curves of Mn^{54}.

given above. We have not been at liberty to perform a chemical analysis on the vanadium, which is supposed to be spectroscopically pure, so that this identification with Mn^{54} is somewhat speculative. Nevertheless, an absorption curve taken on the long-lived activity shows characteristics approximately identical with the 310-day manganese from the deuteron activated chromium and iron, so that we feel reasonably assured the assignment is justified. The other activities induced in the vanadium, might be due to impurities or possibly to neutrons (produced during transmutation of V^{51} to Mn^{54}) or to residual deuteron activation.

The 310-day period has therefore been produced by the transmutations

$$_{26}Fe^{56}+{}_{1}D^{2}\rightarrow{}_{25}Mn^{54}+{}_{2}He^{4},$$
$$_{24}Cr^{53}+{}_{1}D^{2}\rightarrow{}_{25}Mn^{54}+{}_{0}n^{1}$$

and possibly also by

$$_{23}V^{51}+{}_{2}He^{4}\rightarrow{}_{25}Mn^{54}+{}_{0}n^{1}.$$

Each is followed by

$$_{25}Mn^{54}+{}_{-1}e^{0}\rightarrow{}_{24}Cr^{54}\ (310\ \text{days}).$$

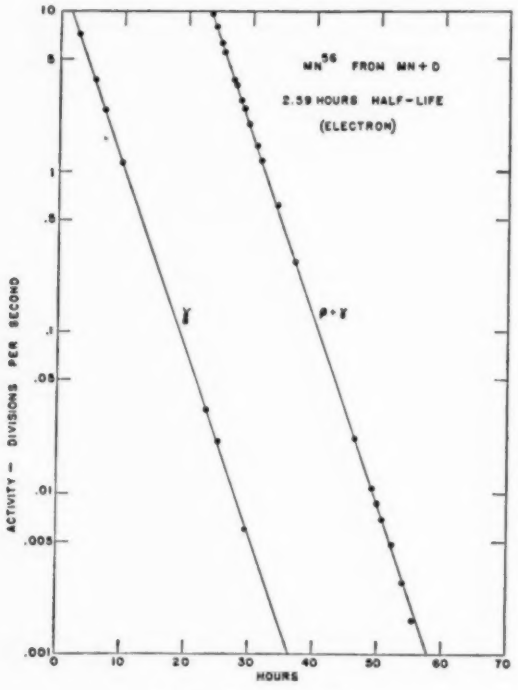

FIG. 9. Decay of Mn^{56}.

Figure 7 shows the decay of these long-lived samples. The iron was activated for 4 hours with 15 microamperes of 5.5 Mev deuterons, the chromium for 1 hour with 25 microamperes of 5.5 Mev deuterons and the vanadium for 2 hours with 0.1 microampere of 16 Mev helium ions.

The absorption data taken on the 310-day samples from Fe+D, Cr+D and V+He are decidedly anomalous, as may be seen in Fig. 8. Ordinarily the ionization due to the soft component (electrons or positrons) is 30 to 70 times as much as that due to the gamma-ray, when observed with an electroscope with a thin aluminum window (0.0001 inch). In the present instances, however, the gamma-ray causes more ionization than does the soft component. Absorption curves were taken on the manganese from an Fe+D bombardment with and without a magnetic field of 3600 gauss in the 10 cm gap between the active specimen and the electroscope; the identity of these curves indicated that there were no appreciable numbers of disintegration particles that were capable of penetrating the window. This suggests, on the basis of the work of Alvarez[9] with Ga^{67}, that the decay of Mn^{54} is neither by electron emission to Fe^{54} nor by positron emission to Cr^{54}, but rather that the Mn^{54} nucleus captures one of its extranuclear K electrons and thus becomes a nucleus of Cr^{54}. The vacancy in the K shell is then filled and the Cr $K\alpha$ x-ray line is emitted. The gamma-ray is only slightly internally converted.

The absorption curves of Fig. 8, although by no means a precise demonstration that this is the mechanism of decay, suggest that the soft components of all three specimens are indeed due to the $K\alpha$ line of chromium. The intensities of the radiations from the three samples have been adjusted to separate the curves in the upper part of the figure for greater clarity. In the central section, the intensities of the soft components (obtained by subtraction of their gamma-rays) have been adjusted to cluster about a line drawn with a slope of that of the Cr $K\alpha$ line.

The absorption in Pb of the 310-day activity from Fe+D is given in the lower part of Fig. 8. The gamma-ray is reduced to half-value by 8.4 grams/cm² Pb, which, according to Gentner's data,[7] indicates an energy of 0.85 Mev.

Mn^{56} FROM Mn+n, Mn+D, Cr+α, Fe+n, Fe+D, Co+n: HALF-LIFE 2.59±0.02 HOURS (−)

The identification with Mn^{56} of the much-studied 2.6-hour manganese period requires no argument at this date. It was originally produced by Fermi and his associates[10] through the reactions $Mn^{55}(n,\gamma)Mn^{56}$, $Fe^{56}(n,p)Mn^{56}$, and $Co^{59}(n,\alpha)Mn^{56}$. Recently Henderson and Ridenour[4] have obtained the same activity by $Cr^{53}(\alpha,p)Mn^{56}$. We have repeated all of these transmutations and in addition have produced the disintegrations $Mn^{55}(d,p)Mn^{56}$ and $Fe^{58}(d,\alpha)Mn^{56}$. Our best value for the half-life is 2.59±0.02 hours, obtained from a sample of manganese oxide that was bombarded for 1.5 hours with 8 microamperes of 7.6 Mev deuterons. This specimen was followed for 22 half-lives; the extrapolated initial intensity of the beta- and gamma-rays was 5×10^7 times background. The decay is shown in Fig. 9, wherein the gamma-ray curve was obtained by filtering through 0.2 cm Al and 1.1 cm Pb.

[9] Alvarez, Phys. Rev. **53**, 606 (1938).

[10] Amaldi, d'Agostino, Fermi, Pontecorvo, Rasetti, Segrè, Proc. Roy. Soc. **A149**, 522 (1935).

A portion of the 2.6-hour activity observed after deuteron bombardment of iron must be ascribed to $Fe^{56}(n,p)Mn^{56}$, since the activity is found in iron sheets placed behind a thick iron target. The neutrons may come from the general background of neutrons always present during operation of the cyclotron, as well as from the $Fe(d,n)Co$ reaction.

Figure 10 exhibits the absorption curves in Al and Pb of Mn^{56}. Here again is the suggestion of a homogeneous group of electrons formed by internal conversion of a gamma-ray, since the curve for the electrons alone (obtained by subtracting the gamma-ray from the original data) is concave to the origin. The range is measured as 1.3 ± 0.1 grams per cm^2 Al, indicating a maximum energy of 2.7 ± 0.2 Mev. This is in fair agreement with the value obtained by more precise methods: cloud chamber measurements have given values of 2.8 Mev,[11] 3.2 Mev[12] and recently two groups of electrons have been reported[13, 14] at 1.2 and 2.9 Mev. These were detected by the same technique.

Our absorption data on the gamma-ray show it to be reduced to half-value by 11.4 grams per cm^2 Pb, which corresponds to an energy of 1.2 Mev by Gentner's compilation.[7] This is in only rough agreement with the value 1.65 Mev found by Mitchell and Langer,[15] who measured with coincidence counters the range of the Compton recoil electrons ejected by the gamma-ray.

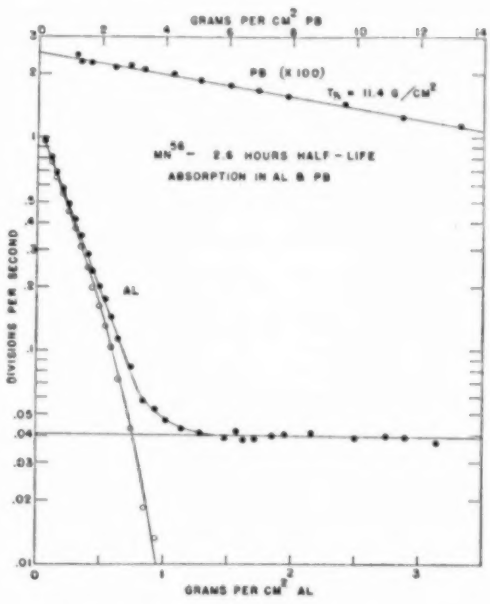

FIG. 10. Absorption curves of Mn^{56}.

TABLE I. *Transmutations and thick target yields.*

HALF-LIFE	REACTION	PROJECTILE ENERGY	PROJECTILES PER ACTIVE NUCLEUS
46 min.	$Cr^{50}(d,n)Mn^{51}$	5.5 Mev	2×10^{6}
21 min.	$Fe^{54}(d,\alpha)Mn^{52}$	5.5 Mev	1×10^{8}
6.5 days	$Fe^{54}(d,\alpha)Mn^{52}$	5.5 Mev	1×10^{8}
310 days	$Fe^{56}(d,\alpha)Mn^{54}$	5.5 Mev	2×10^{8}
310 days	$Cr^{53}(d,n)Mn^{54}$	5.5 Mev	1×10^{6}
310 days	$V^{51}(\alpha,n)Mn^{54}$	16 Mev	1×10^{5}
2.6 hours	$Mn^{55}(d,p)Mn^{56}$	5.5 Mev	1×10^{6}
2.6 hours	$Mn^{55}(d,p)Mn^{56}$	7.6 Mev	4×10^{4}

YIELDS

From the above data on bombardment time and current and initial activities, it is possible to make an estimate of the thick target yield for the different transmutations, with an approximate absolute calibration for the sensitivity of the electroscope. These computations (Table I) must be considered as only very rough, since no endeavor was made to obtain quantititative yield measurements. In the case of the 310-day activities, an estimate of the number of disintegrations was made from the ionization produced by the gamma-rays only (there were no particles present); for the other activities, the ionization due to both particles and gamma-rays was used. The yields are given as though the target element were composed entirely of the single isotope concerned.

This research has been made possible by the generous and continued support of The Research Corporation and The Chemical Foundation. The work was facilitated by W.P.A. assistance.

[11] Gaerttner, Turin and Crane, Phys. Rev. **49**, 793 (1936).
[12] Alichanian, Alichanow and Dzelepow, Nature **136**, 257 (1935).
[13] Brown and Mitchell, Phys. Rev. **50**, 593 (1936).
[14] Bacon, Grisewood and Van der Merwe, Phys. Rev. **52**, 668 (1937).
[15] Mitchell and Langer, Phys. Rev. **52**, 137 (1937).

Gamma-Rays from Fluorine Due to Proton Bombardment

E. J. Bernet, R. G. Herb, D. B. Parkinson
Department of Physics, University of Wisconsin, Madison, Wisconsin

(Received July 19, 1938)

A detailed study has been made of the resonance excitation of gamma-rays from fluorine when bombarded with high speed protons in the energy range 0.18 Mev to 2.2 Mev. Because of improvements in the high voltage generator and in the preparation of uniform thin fluorine films, the resonance peaks obtained are much narrower than in the previous work at this laboratory, and many new resonances have been discovered. For the seven resonance peaks which are best defined, estimates are given as to voltage position and half-width.

Introduction

GAMMA-RADIATION from the disintegration of fluorine by protons was first observed by McMillan[1, 2] in 1934. By the use of a cyclotron to accelerate protons, and a thick calcium fluoride target, he obtained a smoothly increasing excitation curve up to his maximum voltage of 1.15 Mev. However, the work of Hafstad and Tuve[3] and of Hafstad, Heydenburg and Tuve,[4] who used an electrostatic generator and a thick target of calcium fluoride, showed that the gamma-ray excitation curve from fluorine was not a smooth exponential increase but consisted of a number of well-defined steps in the voltage region from 100 kv to 1000 kv. Their work showed the advantages of a monochromatic beam of protons as well as steady and accurately measured generator voltages for obtaining excitation curves. The work by Herb, Kerst and McKibben[5] in 1937 was in good agreement with that of Hafstad, Heydenburg and Tuve in the lower voltage range and carried the data up to slightly over 2 Mev. Since this first work was only of an exploratory nature it seemed desirable to repeat experiments on excitation of gamma-rays from fluorine in an effort to determine widths and positions of resonances more accurately.

Apparatus

The Wisconsin electrostatic generator operating under 100 pounds air pressure has been described in a paper by Herb, Parkinson, and Kerst.[6] Recent improvements and present technique are described in a paper by Parkinson *et al.*[7] It is now possible to keep the generator voltage constant to within approximately $\frac{1}{4}$ percent over most of the time required for a measurement, with occasional fluctuations of the order of $\frac{1}{2}$ percent.

Figure 1 shows the arrangement of the target chamber and electroscope used in this work. High speed protons entering from the left pass through a defining aperture $\frac{3}{16}''$ in diameter. A thin platinum sheet was placed over the outside of the defining aperture to cut down gamma-radiation produced by protons stopped around the edge. The main chamber, containing the target, is insulated by a clear Bakelite plug and is used as a Faraday cage to measure the proton current incident on the target. The disk containing the defining aperture is grounded and the target chamber is kept at a negative potential of about 45 volts so as to prevent electrons generated at the edge of the hole from entering the chamber. Since the proton current is rather unsteady, a current integrator, which has been previously described,[5] is used to measure total charge. A recalibration of the current integrating arrangement in terms of a standard cell was made for the present work and a small correction for leakage of the input circuit as a function of time has been applied to all the data.

A Lauritsen type electroscope was used for measurement of relative gamma-ray intensities. The electroscope was tested for linearity and

[1] McMillan, Phys. Rev. **46**, 325 (1934).
[2] McMillan, Phys. Rev. **46**, 868 (1934).
[3] Hafstad and Tuve, Phys. Rev. **48**, 306 (1935).
[4] Hafstad, Heydenburg and Tuve, Phys. Rev. **50**, 504 (1936).
[5] Herb, Kerst and McKibben, Phys. Rev. **50**, 691 (1937).
[6] Herb, Parkinson and Kerst, Phys. Rev. **51**, 75 (1937).
[7] Parkinson, Herb, Bernet and McKibben, Phys. Rev. **53**, 642 (1938).

readings were always taken over the same scale divisions. It was found necessary to use lead shielding, arranged as shown in Fig. 1, to cut down background ionization by gamma-rays produced at the defining aperture and by x-radiation from the generator. The natural leak of the electroscope was found to be about 0.020 divisions per minute, and this correction has been applied uniformly to all the data.

Target Preparation

In our previous work on gamma-radiation from fluorine, thin targets were prepared by electrolyzing a piece of sheet nickel in hydrofluoric acid. As nickel fluoride is not soluble in hydrofluoric acid, the film thickness could be governed by the current and by the length of time in electrolysis. Nickel, however, was found to give considerable gamma-radiation when bombarded by protons with energies above 1 Mev and it is therefore not satisfactory as a base for a thin fluorine target. Because of this difficulty with thin targets on nickel, the use of thick targets was considered, and some work was done with thick calcium fluoride crystals. It was found, however, that a detailed analysis of a complex excitation curve is difficult to obtain with a thick target. Resonances are indicated by steps in a thick target yield curve, which in the low voltage region can be determined with fair accuracy, but a weak resonance at high voltage can easily be missed, since it appears only as a relatively small increase in an intensity which is already high. When a thin target is used, resonances appear as peaks in the yield curve, and because of the large change of relative intensity in the resonance region, more accurate measurements are possible.

The considerations outlined above showed that for a suitable target a uniform thin film of some fluorine compound must be prepared on a metal base which gives a low yield of gamma-radiation.

Platinum was found to give a very low yield of gamma-radiation (probably none) when bombarded with 2 Mev protons, but attempts to form a film of a fluorine compound on a platinum surface were not successful. A lead sheet was next examined for gamma-ray yield. A measureable intensity was observed at high voltage, but it was sufficiently low to be negligible in comparison to the fluorine yield, and it is probable that the yield observed was due to contamination. Thin films of lead fluoride were easily formed on a lead sheet by dipping the sheet into hydrofluoric acid. However, all yield curves obtained from these targets gave broad resonance peaks, and the yield at a given voltage decreased quite rapidly with time. It is quite likely that because of heat developed during bombardment, the lead fluoride film diffuses into the lead base. Pure tantalum obtained from the Fansteel Corporation was then tried as a target base, and since it was found to be very satisfactory, it was used for all the data presented in this paper.

In the preparation of a thin film on a tantalum sheet, the surface of the tantalum was first polished with very fine emery paper and was then cleaned by boiling in water and by washing in alcohol. The tantalum was next electrolyzed in concentrated hydrofluoric acid at currents of from 50 to 250 milliamperes for approximately one minute. The tantalum fluoride formed is dissolved by the hydrofluoric acid, but the electrolyzing process appeared to be necessary for additional cleansing of the metal surface. Upon removing the target from the hydrofluoric acid, a few drops of the solution were left on the surface. When these droplets dried, the tantalum fluoride gathered together in lumps and resonance peaks were observed to be broad even from a film giving very low intensity.

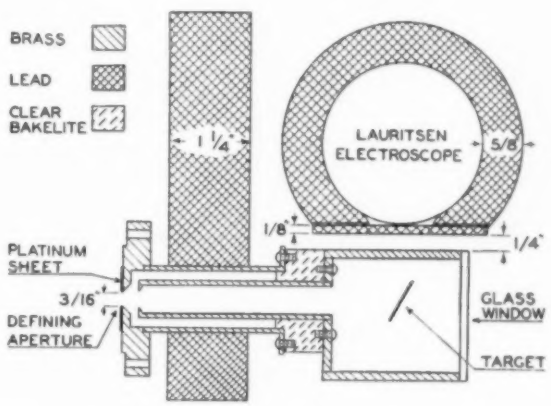

Fig. 1. Target chamber and electroscope.

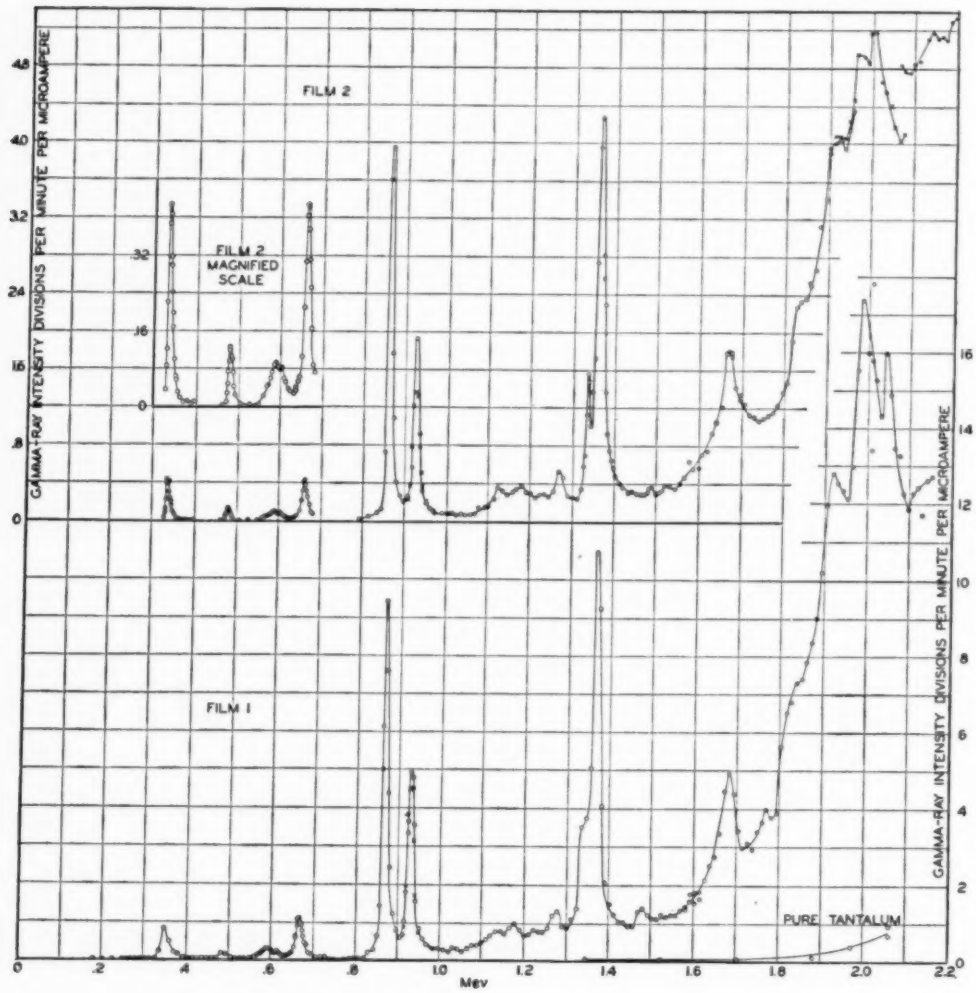

FIG. 2. Gamma-ray intensity *vs.* energy of bombarding ions.

The present technique consists of removing the target from the solution and allowing a few drops to remain on the surface just as before, but then these drops are spread out over the surface of the target by adding a few drops of alcohol which wets the surface of the tantalum uniformly. The mixture is flowed back and forth over the surface by tilting and then drained off and the target allowed to dry. With experience it is possible to control the thickness of the resulting film to some extent, but before films were used for yield curves, they were first tested for yield and uniformity by going over the two resonances at 0.862 Mev and 0.927 Mev and noting the height of peaks and more especially the extent of the drop between peaks.

RESULTS

Figure 2 shows the excitation curves obtained from two different tantalum fluoride films. A background run on a clean tantalum sheet without a fluorine film (Fig. 2) gave a very low yield, and it is probable that the intensity observed was entirely due to x-radiation from the generator.

FILM 1

The run on film 1 (Fig. 2) was begun at 0.8 Mev and carried up to 2.15 Mev. The same spot on the film was used for all the data. The doublet peaks at 0.862 Mev and 0.927 Mev which were not resolved in the previous work at this laboratory were very well resolved in this

run. One point on the prominent peak at 1.36 Mev appears to be off, but this was later shown to be due to a satellite. Although the peak at 1.67 Mev is very broad, it has never given any indication of being a doublet in subsequent work. Above 1.8 Mev the form of the yield curve indicates that in this region there are a number of intense levels too closely spaced for good resolution.

To determine the condition of the film spot after this energy range had been covered, a check run was taken on the resonance peak at 0.927 Mev (film 1, crosses). The peak appeared at the same voltage as in the previous work and yields were practically unchanged. This is a very satisfactory check both on the dependability of the generating voltmeter and on the stability of the fluorine film.

The gamma-ray intensity was next investigated below 0.8 Mev by bombardment of the same spot on film 1. In previous work at Washington, D. C.[4] and at this laboratory,[5] a very broad resonance was indicated in the region between 0.5 Mev and 0.7 Mev, and a sharp resonance was found at 0.330 Mev. The data from film 1 show sharp resonances at 0.660 Mev, 0.479 Mev, and 0.334 Mev, and a broad resonance with its peak at about 0.589 Mev. A good curve was easily obtained for the resonance at 0.660 Mev, but a great deal of time was spent on the 0.589 Mev resonance, since several yield curves indicated the possible presence of a closely spaced doublet. The resonances at 0.334 Mev and 0.479 Mev were not examined in great detail with film 1 since prolonged bombardment in the region of 0.6 Mev had damaged the film and resonances were somewhat broadened. The data in the lower voltage range were obtained by use of diatomic ions and with 50 pounds air pressure in the generator tank.

Film 2

To obtain information regarding the influence of film thickness on the half-width of the resonances obtained with film 1, another film (film 2) was prepared. At the 1.36 Mev resonance this film gave an intensity only 0.4 as high as the intensity from film 1. As with the previous film, only a single spot on film 2 was used for the complete curve. After the complete voltage range had been covered, a check run was taken on the 0.927 Mev peak to determine the condition of the film (film 2, crosses). Although the resonance peak obtained in the check run is lower in intensity than the original run, the values of the voltage position and half-width agree very well. The region below 0.5 Mev was taken in more detail with this film than with film 1, and the first four resonance peaks in the low voltage range are shown with the ordinate scale increased by a factor of five.

Additional runs were taken with film 2 on the peak at 0.589 Mev, but no better resolution was obtained than with film 1. Every yield curve obtained for this peak has indicated the presence of a close doublet, but definite resolution has not been obtained. The satellite on the low voltage side of the peak at 1.363 Mev was first resolved with film 2. Two subsequent runs on this peak with different films are shown in Fig. 3A and Fig. 3B. By a change in ordinate scale these peaks were brought to the same height for comparison of the position of the satellite. Two separate high voltage runs were taken on film 2, one from 1.9 Mev to 2.1 Mev (crosses),

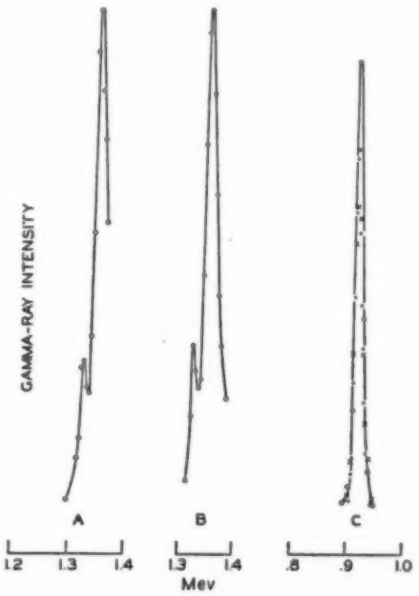

Fig. 3. (A) (B) Check runs on peak at 1.363 Mev to observe satellite. (C) Readings taken to check voltmeter. Resonance peak in fluorine, open circles are original run on film 2, crosses are the check run with protons, solid circles are the check run with diatomic ions.

and the other, taken a day later, from 2.1 Mev to 2.2 Mev (solid circles) (Fig. 2). The rise in the intensity at 2.1 Mev between the two runs is difficult to understand since it indicates that the film was thicker for the higher voltage run, which was taken last. A possible explanation can be made if it is assumed that the fluorine compound formed in preparing the target is TaF_5. This compound is a liquid above 97°C, and if the temperature of the target should rise sufficiently at some time during bombardment, there might be a rearrangement of the film.

Above 1.7 Mev the data from film 2 do not agree well with film 1 data. In general form the curves are similar, but the relative heights of peaks and the extent of drop between peaks is not consistent. The radiation in this voltage region is probably due to a number of prominent overlapping resonance levels. Thus to fix the position of a peak it is necessary to determine a rather small change in the intensity. Experimental inaccuracy due to nonuniformity of films, voltage fluctuations, and errors in electroscope readings probably account for the lack of consistency in the data.

Resonance Energies

In the energy region below 1.7 Mev ten resonance levels are quite well established. Their energy positions in Mev of bombarding protons are as follows: 0.334, 0.479, 0.589, 0.660, 0.862, 0.927, 1.26, 1.335, 1.363 and 1.67. As the levels above 1.7 Mev are not well resolved, no attempt has been made to estimate their energy positions. For the energy region from 1.0 Mev to 1.3 Mev only one resonance (1.26 Mev) is included in the list, although two more are indicated between 1.1 Mev and 1.2 Mev. The radiation in this region seems to be due to a number of weak overlapping levels. Another weak resonance is probably present at about 1.48 Mev.

Before the data on film 1 were taken, a calibration of the generating voltmeter was made at the 0.440 Mev resonance of lithium with both protons and diatomic ions (the value of 0.440 Mev for the lithium resonance was assumed as a standard for the voltage scale in this work). The data of film 1 are plotted with that calibration. Most of the data on film 2 were taken about five weeks later than the data on film 1, and the resonance peaks appeared to come at higher voltages. After the data on film 2 were complete the voltmeter was again calibrated with the 0.440 Mev resonance of lithium, and its sensitivity was found to be 1.6 percent higher than in the previous calibration. With the new voltmeter sensitivity, the voltage position of resonances of film 2 agreed with those from film 1 as closely as could be determined from the experimental curves. For the well-defined peaks, the voltage positions checked to within about 0.2 percent.

The increase in sensitivity of the voltmeter was very disturbing since it could not be explained at that time, and it indicated that the voltmeter might not be dependable unless calibrated frequently. A recent experience with another generator equipped with a similar voltmeter suggested an explanation which is probably correct. The voltmeter is mounted with the outer surface of its rotating vane approximately flush with the inner surface of the tank, and it was found that if the vanes were moved inward or outward by a small amount, the voltmeter sensitivity changed considerably. The voltmeter is supported on a flanged fitting and seats against a rubber gasket. The position of the vanes therefore depends on how much the gasket is compressed when the voltmeter is bolted to its supporting flange. When the voltmeter was taken off for oiling and remounted it is quite likely that the gasket was compressed more than before and that this change caused the observed increase in sensitivity. By a slight change in the method of mounting the voltmeter it will be possible to fix the position of the vanes much more accurately, and this source of trouble will be removed.

The linearity of the voltmeter was tested a number of times in the last two years, but as an additional check the 0.927 Mev resonance of fluorine was studied with diatomic ions for bombardment. These data together with the original data and the check run with protons are shown in Fig. 3C. The open circles are from the original run on this resonance with film 2, the crosses show the data of the check run with protons, and the solid circles are the data obtained with diatomic ions. Agreement is very

good, and it is believed that the greatest uncertainty in the voltage positions of the fluorine resonances is due to the uncertainty in the position of the lithium resonance which was assumed to be at 0.440 Mev.

Resonance Energies from CaF_2 Crystals

Several yield curves have been obtained in the region between 0.8 Mev and 1.0 Mev with thick CaF_2 crystals as targets. In the first runs with these targets the 0.862 Mev and 0.927 Mev resonances appeared at higher voltages. This shift was found to be caused by accumulation of charge on the crystals. The smallest crystal used (about 1 cm square and 1 mm thick) gave a shift of about 10 kev. Larger crystals caused a greater shift. To prevent the crystals from charging up, a fine tungsten wire was spot welded to the grounded target support and was bent so that its end pressed firmly onto the crystal at approximately the center of the region where the proton beam hit. With this arrangement the resonance voltages agreed with those determined from the thin films on tantalum. It is probable that the crystal becomes conducting over the area being bombarded, and that charge easily leaks off to a lead touching this area.

A second method of preventing accumulation of charge was also tried, and was found to be satisfactory. Fine mesh gauze (about 100 mesh) was etched with acid until it gave a transmission of over $\frac{1}{2}$. This was stretched over the crystal and was spot welded to the grounded target support. The gauze probably made contact with the crystal at only two or three places, and in some cases probably did not make contact where the proton beam hit. It is probable however that contact was not essential since protons hitting the gauze generate secondary electrons and this source of electrons should be sufficient to neutralize any charge on the crystal. All crystals with which this method was tried gave fairly consistent results.

Table I. *Half-widths of resonance peaks.*

Resonance Voltage Mev	Experimental Half-width kev		Corrected Half-width kev	
	Film 1	Film 2	Film 1	Film 2
0.334		9.8		8.0
0.479		12.1		10.5
0.660		15.7		14.4
0.862	13.4	12.1	9.8	10.9
0.927	18.8	15.7	15.5	14.6
1.335		9.2		8.3
1.363	23.3	20.6	20.8	19.8

Widths of Resonance Levels

The well-defined resonance peaks were plotted carefully to a large scale and their half-widths were determined. Table I gives these values in the columns showing experimental half-widths. Factors tending to increase the values of the observed widths over the true widths of the nuclear levels are (1) film thickness, (2) inhomogeneity of the proton beam, (3) voltage fluctuations.

If it is assumed that the thin films consist of TaF_5, film thickness can be determined by utilizing thick target yields. If a film is thin compared to the width of the nuclear resonance level, the area under a resonance peak is given by

$$A = IN' \int\int g(E-E')f(E_0-E')dEdE', \quad (1)$$

where

E_0 = resonance voltage,
I = proton current,
N' = number of fluorine atoms per cm^2,
E = generator voltage,
E' = voltage or energy of incident protons,

$g(E-E')$ gives the energy distribution of incident protons when the generator-voltage is held as close as possible to E. [The ratio of the number of incident protons with energy between E' and $E'+dE'$ to the total number of protons is equal to $g(E-E')dE'$.] The disintegration cross section for protons of energy E' is equal to $f(E_0-E')$. Since $\int g(E-E')dE = \int g(E-E')dE' = 1$ we have $A = IN' \int f(E_0-E')dE'$.

Therefore the area is independent of the homogeneity of the proton beam or voltage fluctuations providing they do not change while measurements are being made on a particular resonance peak.

The total contribution of a resonance level to a thick target yield curve (height of step) is given by

$$Y = IN \int\int g\{(E-ax)-E'\}f(E_0-E')dE'dx, \quad (2)$$

where x measures distance into the target,

a = stopping power of target material,
N = number of fluorine atoms per cm³,
E' = the energy of protons at distance x in the target,
E, I, E_0, g, and f have the same meaning as in (1).

Since

$$\int g\{(E-ax)-E'\}d(ax)=1,$$

we have $$Y=\frac{IN}{a}\int f(E_0-E')dE'$$

and $$\frac{A}{Y}=\frac{N'}{N}a.$$

Thus the area under a thin target resonance peak divided by the height of the resonance step from a thick target curve gives the absorption thickness of the thin film regardless of the homogeneity of the proton beam.

From a yield curve taken with a CaF_2 crystal as a target the 0.862 Mev and 0.927 Mev resonances were found to contribute, respectively, 49 divisions per minute per microampere and 24 divisions per minute per microampere. Yields from CaF_2 were converted to yields from TaF_5 under the approximate rule that atomic stopping power varies with the square root of atomic weight. Thus yields from a thick target of TaF_5 should be 1.07 times as great as yields from CaF_2.

Areas under the 0.862 Mev and 0.927 Mev resonance peaks were determined for both film 1 and film 2, and the values found for film thicknesses are as follows: For film 1, with the 0.862 Mev resonance, the absorption thickness was found to be 3.59 kev and from the 0.927 resonance an absorption thickness of 4.01 kev was determined. For film 2, the two values were 1.21 kev from the 0.862 Mev resonance and 1.39 kev from the 0.927 Mev resonance.

The absorption thickness of a film should decrease with increasing voltage, yet the values determined are greater at the higher voltage resonance. This discrepancy is probably due to an inaccurate determination of the relative contribution of the two resonance levels to the thick target yield. The values of film thickness determined from the 0.862 Mev level are probably more accurate than those from the weaker 0.927 Mev level. Thus in correcting the experimental half-widths for film thickness, the values were assumed to be 3.6 kev for the absorption thickness of film 1 at 0.862 Mev and 1.2 kev for film 2 at 0.862 Mev. These values probably set a fairly accurate lower limit to film thickness. If other compounds of fluorine, such as lower fluorides of tantalum, were present in the films, absorption would be increased. Nonuniformity of the films or diffusion of the fluorine compound into the tantalum would also increase the absorption thickness of the films. In computing the absorption thickness of the films at other resonances, stopping power was assumed to vary inversely as the square root of the voltage. Experimental half-widths of the resonances, corrected for absorption thickness of the film, are given in Table I under the heading "corrected half-widths."

If thick target yield curves are used to determine resonance widths, the effect of film thickness does not enter. As several yield curves had been taken on CaF_2 crystals at the 0.862 Mev resonance and the 0.927 Mev resonance, they were examined for resonance widths. Following a suggestion by Professor Breit, we used expressions of the form

$$Y=A\left\{\tan^{-1}\frac{E-E_0}{\Delta E}+\frac{\pi}{2}\right\},$$

where ΔE is resonance half-width, for fitting the yield curves. These expressions did not fit the curves very well, but since they set reasonably close limits to the half-widths, better formulae were not developed. As closely as could be determined, the thick target resonance widths agreed with the thin film determinations.

The effect of voltage fluctuations and inhomogeneity of the proton beam on observed resonance widths is difficult to estimate, but the excellent resolution of the satellite at 1.33 Mev indicates that these factors are not giving large contributions to the widths of the broader levels.

An attempt was made to fit the thin target resonance peaks with dispersion terms of the form

$$Y=\frac{A}{(E-E_0)^2+(\Delta E)^2}.$$

The levels at 0.862 Mev and 0.927 Mev could be fitted fairly well, but a sum of two such expressions could not be made to fit the 1.363 Mev level and its satellite. Finally, to obtain an estimate of the half-width of the satellite, a dispersion formula was chosen to fit the intense 1.363 Mev level in the region above the satellite. This curve was subtracted from the experimental curve and a remainder was obtained which was assumed to be due to the satellite. The half-width determined for the satellite (9.2 kev) did not depend critically upon the form of the curve chosen for the main resonance peak.

Discussion of the Fluorine-Proton Reaction

The nature of the nuclear reaction responsible for the gamma-radiation from fluorine is as yet poorly understood. Several investigations have been made of the energy of gamma-rays from fluorine excited by protons at fairly low voltages. McMillan bombarded fluorine with 1.15 Mev protons, and from absorption measurements concluded that the radiation is monochromatic with an energy of 5.4 Mev. Delsasso, Fowler, and Lauritsen[8] recently measured the energy of the fluorine gamma-radiation with a cloud chamber and concluded that the radiation is monochromatic with an energy of 6.0 Mev. They used 0.750 Mev protons and were therefore obtaining radiation from the first four resonance levels. Gaerttner and Crane[9] made a recent study of the fluorine gamma-radiation with a cloud chamber, and they obtained two gamma-ray lines—at 4.0 Mev and 5.7 Mev. They used 0.40 Mev protons in their first work, but then repeated the measurements with 0.75 Mev protons, and obtained the same gamma-ray lines. These results indicate that there is no difference in the character of the radiation from the first four resonances of fluorine. Practically nothing is known, however, regarding the energy of radiation from the high voltage resonances.

Henderson, Livingston, and Lawrence[10] obtained alpha-particles with a range of 6 cm from fluorine bombarded by 0.675 Mev protons. This range corresponds to an energy of 7.08 Mev. The alpha-particles were observed, at a right angle from the proton beam, and when a correction is applied for the energy of the incident protons, a good energy balance is obtained with the reaction $F^{19}+H^1 \rightarrow O^{16}+He^4$. It therefore appears that there can be no gamma-radiation accompanying the 6.0 cm alpha-particles. If the gamma-radiation is due to the reaction giving $O^{16}+He^4$, short range alpha-particles should be emitted. Although no short range alpha-particles have been observed, it is possible that they have been missed.

Another possible reaction, $F^{19}+H^1 \rightarrow Ne^{20}$, is exothermic by 12.9 Mev exclusive of the energy due to the incident protons. The emission of two successive gamma-rays may be assumed, but with either the results of Delsasso, Fowler, and Lauritsen, or the results of Gaerttner and Crane, the energy balance is not good.

Discussions of the probable reaction responsible for gamma-ray emission from fluorine are given in the papers by Fowler and Lauritsen,[8] and by Gaerttner and Crane.[9]

Tentative Interpretation of Results*

The sharpness of the resonance levels observed in these experiments is surprising at first sight and indicates that there are selection rules which separate the energy levels of the Ne^{20} nucleus into at least two almost mutually isolated systems. Qualitatively the existence of a selection rule can be inferred from the failure of the Ne^{20} compound nucleus to disintegrate into O^{16} and He^4 in normal states. There is available for this at least 8.2 Mev which is more than sufficient to overcome the effect of the Coulomb barrier. In the absence of selection rules the mean life of a virtual Ne^{20} level would be expected to be short and the width of the levels would be expected to be comparable with that of the excited state of Be^8 which according to Dee and Gilbert is ~ 1 Mev. According to the indeterminacy relation this corresponds in order of magnitude to the time necessary for a particle with velocity $c/30$ to traverse a distance 6×10^{-13} cm. The width of the levels according to observation is

[8] Delsasso, Fowler and Lauritsen, Phys. Rev. **51**, 527 (1937).
[9] Gaerttner and Crane, Phys. Rev. **52**, 582 (1937).
[10] Henderson, Livingston and Lawrence, Phys. Rev. **46**, 38 (1934).

* This discussion is due to Professor G. Breit.

~ 10 kev and it may be less for some of the levels. It is necessary to explain the sharpening of the levels by a factor of at least 100 in comparison with the width expected on the one-body picture.

The necessity for reducing the probability of decay into O^{16} and He^4 in normal states exists independently of the actual process of γ-ray emission. It is immaterial for the present whether the γ-rays are emitted by an excited O^{16} nucleus or by cascade transitions in the Ne^{20}. The general situation is similar to that discussed by Oppenheimer and Serber for the bombardment of B^{11} with H^1.

It has been pointed out by Bethe[11] that the even parity and zero spin of O^{16} and He^4 offer a particularly simple possibility for ruling out the disintegration into normal O^{16} and He^4. The levels of Ne^{20} that have odd total angular momentum and even parity or even total angular momentum and odd parity are completely unable to dissociate into $O^{16}+He^4$. In this explanation of Bethe's one deals with a rigorous selection rule and it offers perhaps the most likely explanation of the sharpness of the γ-rays.

It should be observed, that in addition the disintegration into $(O^{16})^*+He^4$ must be made sufficiently improbable. It is unlikely that all $(O^{16})^*$ with an energy lower than $F^{19}+H^1-He^4$ have zero total angular momentum. It is, therefore, necessary to assume in addition that either all these $(O^{16})^*$ have zero angular momentum or else that the energy difference $(O^{16})^*-O^{16}$ is sufficiently high to make the alpha-particle energy low in comparison with the Coulomb barrier. The high intensity of the γ-rays indicates that the γ-ray emission occurs at least partly through $(O^{16})^*+He^4$ because otherwise it has to compete with proton escape which is appreciable at the higher energies. The observed γ-ray energy of 6 Mev indicates that $(O^{16})^*-O^{16}$ is at least 6 Mev and that the alpha-particle energy varies between 2.2 and 4.2 Mev in the experiments. For low energy protons there is no difficulty in making the broadening of the levels due to dissociation into $(O^{16})^*+He^4$ unobservably small and it is conceivable that some of the resonances at low proton energies have to do with γ-ray emissions in Ne^{20} as has been proposed by Bethe.[11] One would expect, however, that even at low proton energies there will be some γ-rays due to the $(O^{16})+He^4$ process and it is apparently impossible to infer the existence of a Ne^{20} level from these experiments.

For this explanation it is essential to have odd levels of even parity or even levels of odd parity in the observed energy range. In addition there is the possibility of using approximate selection rules for ordinary and isotopic spin.

It appears to be too difficult to make a direct calculation of the level systems in Ne^{20} at this stage. But something can be learned by comparing the above results with other experiments. This will be made first with the 440 kev resonance of Li^7+H^1. The half-value width of this resonance has been measured by Hafstad, Heydenburg and Tuve[4] and was found to be ~ 11 kev. It is probable[12] that all of this width is due to proton escape, the alpha-particle disintegration of the compound nucleus is probably ruled out by the rigorous parity selection rule. On this view the protons in the reaction have angular momentum $L=0$. By use of the one-body picture the half-width can be expected to be[13] $\sim 2E/\int \bar{G}^2 d\rho$. Here $\bar{G}$ is r times the radial wave function for resonance normalized so as to have unit amplitude at $r=\infty$, $\rho=2\pi r/\Lambda$, $\Lambda=$proton wave-length. At resonance the function G outside the nuclear well is the irregular Coulomb function[14] G. For $r=3\times 10^{-13}$ cm, $G^2\sim 4.7$, $\rho\sim 0.38$. The above formula gives with these values[12] a half-width ~ 100 kev. Such a large value means essentially that the Coulomb barrier has little to do with the problem and that the resonance width in the one-body model depends considerably on the parameters of the model.[15] If 100 kev is taken for the resonance half-width on the one-body model there must be a further reduction by a factor 10 in the width due to the difference between the actual nucleus and the one-body

[11] H. A. Bethe, Rev. Mod. Phys. **9**, 69 (1937); see p. 232.
[12] Pages 510–512 of reference 4.
[13] G. Breit and F. L. Yost, Phys. Rev. **48**, 203 (1935). A more accurate formula is Eq. (32) in G. Breit and E. Wigner, Phys. Rev. **49**, 519 (1936).
[14] F. L. Yost, J. A. Wheeler and G. Breit, Phys. Rev. **49**, 174 (1936).
[15] By use of a different method, Bethe, Rev. Mod. Phys. **9**, 69 (1937), see p. 206, estimates a factor 10 for the effect of the barrier. Neither Bethe's estimate nor the present one nor the still higher estimates for 1,2 can pretend to be more than guesses at orders of magnitude.

model. This factor may be thought of as due to the necessity of a rearrangement in the Be^8 nucleus so as to liberate the proton. Neglecting the Coulomb barriers for $Ne^{20} \rightarrow O^{16}+He^4$ one would expect a width of ~ 3 Mev. On the assumption that the rearrangement factor is ~ 10 the expected width is ~ 300 kev. The observed widths of ~ 10 kev$\rightarrow$1 kev leave a factor of $\sim 30 \rightarrow 300$ to be accounted for. This type of estimate is somewhat arbitrary since it has been supposed that the rearrangement factor is the same for proton and alpha-particle emission.

It has been pointed out by Oppenheimer and Serber[16] that the approximate conservation of ordinary and isotopic spin may be expected to serve as an approximate selection rule. A factor of the order of 100 for each of these spins may be expected. Because of the operation of one of these selection rules one may expect widths ~ 3 kev and because of the simultaneous operation of both one might get even smaller widths ~ 0.03 kev.

As has been emphasized by Bohr,[17] the many-body aspect of nuclei may be expected to lead to a great complexity of levels for the heavier nuclei and the same point has been brought out with less emphasis by Wigner and the writer.[18] Bethe's and Placzek's analysis of experimental material has shown that there is an important qualitative difference between heavy and light nuclei and that the number of nuclear levels as well as their sharpness increases with atomic weight. It is difficult to distinguish between a general increase in the complexity of internal motions and the operation of specific selection rules. The number of levels has to do only with nuclear complexity and could serve as a criterion if the calculation of the level density could be made reliably.

At 1.5 Mev incident energy the Coulomb barrier effects become small for protons. At the higher energies broadening due to proton escape may be expected to come in. It may be that lack of resolution of resonances between 1.8 and 2.2 Mev is due partly to this cause.

In addition to the sharp levels that have been detected in the gamma-ray experiments there may be present also other levels in the same energy range of the continuum. Experiment shows that from 0.3 Mev to 0.4 Mev there are practically no gamma-rays emitted in regions between resonance peaks. It must be concluded that the broader levels do not lead to as strong γ-ray emission as the narrow levels or else that there are no broad levels in this region. For this energy range one may neglect proton escape as a cause of broadening and the width due to radiative transitions in Ne^{20} is also negligible. One may consider as causes for the width the possible dissociations into normal $O^{16}+He^4$ or else into $(O^{16})^*+He^4$ or finally into $O^{16}+(He^4)^*$. The observed energy of the γ-rays makes the latter possibility unlikely.

Levels having a large width due to dissociation into normal $O^{16}+He^4$ will not give rise to an observable background if their width is large enough. For such levels the competition with the process responsible for γ-ray emission will be too severe. Thus if there were a level present in this energy region with a width of 300 kev the γ-ray intensity due to it would be less than that in the observed peaks in the ratio 1 : 30. In this energy region such an intensity is too difficult to observe. The background from 1.0 Mev to 1.3 Mev has a definite structure and produces the impression of having a rising continuation from 1.5 Mev to 1.8 Mev. It is impossible to tell whether it is partly built up of diffuse levels. It may be partly due to levels that dissociate into normal $O^{16}+He^4$ with an intermediate probability and which, therefore, emit weaker γ-rays.

The dissociation into $(O^{16})^*+He^4$ should give a cause of broadening that varies strongly with the energy available for dissociation. By use of the atomic masses of Bethe and Livingston the energy available (Q value) is found to be 8.2 Mev. If we attribute 6 Mev to the γ-ray, the alpha-particle energy is found to vary from 2.2 Mev to 4.2 Mev in the experiments, which corresponds roughly to a factor 50 in the penetration through the barrier. There may be important effects due to the character of the nuclear levels besides.

[16] J. R. Oppenheimer and R. Serber, Phys. Rev. **53**, 636 (1938).
[17] N. Bohr, Nature **137**, 344 (1936).
[18] G. Breit and E. Wigner, Phys. Rev. **49**, 519 (1936). See pp. 528, 530.

The small intensity at energies close to the first resonance must be due partly at least to the large barrier effect on the proton. The large yield of γ-rays at high energies indicates successful competition with dissociation into $O^{16}+He^4$. It suggests the origin of these γ-rays as due to $(O^{16})^*\rightarrow O^{16}+h\nu$. The apparently diffuse structure of the levels at the highest energies may be caused partly by the increased width due to dissociation into $(O^{16})^*+He^4$ as well as the broadening due to proton escape.

In conclusion it must be emphasized that the above considerations are speculative.

The authors are indebted to Professor G. Breit, Professor H. B. Wahlin, and Professor L. R. Ingersoll for advice and support, and to the Wisconsin Alumni Research Foundation for financial assistance.

SEPTEMBER 15, 1938 PHYSICAL REVIEW VOLUME 54

The Transmutation of Titanium by Th C′ Alpha-Particles

W. L. DAVIDSON, JR. AND ERNEST POLLARD
Sloane Physics Laboratory, Yale University, New Haven, Connecticut

(Received June 30, 1938)

Protons have been observed from the bombardment of titanium by Th C′ alpha-particles. They are probably due to the reaction $Ti^{48}+He^4\rightarrow V^{51}+H^1$. Three groups of protons are found corresponding to nuclear energy change $[Q]$ values of $+1.10$, 0.00 and -3.63 Mev. The separation of the last two groups is abnormally great. Combined with Dempster's value for the mass of Ti^{48}, the results lead to a mass of 50.9598 for V^{51}.

INTRODUCTION

TITANIUM, under bombardment by high energy alpha-particles, has been found to give a considerable yield of protons. The magnitude of the yield seems to require that the following reaction is responsible:

$$Ti^{48}+He^4\rightarrow V^{51}+H^1+[Q]$$

where $[Q]$ represents the nuclear energy change which takes place in the process.

We have investigated the transmutation protons arising from this reaction. Two different geometrical arrangements were used; first, an arrangement whereby the protons ejected at 90° to the incident alpha-particle are detected; and second, one in which the emergent proton and incident alpha-particle are in the same direction. Absorption curves have been obtained for both arrangements. Any definite "steps" in such a curve may be interpreted as representing energy levels in the residual nucleus, and by finding the nuclear energy change [Q value] corresponding to each group of protons, the spacing of these energy levels can be found. The recent publication by Dempster of a value for the mass of Ti^{48}, combined with the Q value corresponding to the limiting energy of the protons, should enable us to use this reaction to calculate the mass of V^{51}. The reaction is of additional interest since vanadium has an excess of five neutrons over protons in its nucleus. No other element studied has such a high excess of neutrons and hence any anomalies found might be considered significant.

APPARATUS

The apparatus used has been described in earlier papers.[1,2] A few minor additions have been made, which tend to make the apparatus more nearly automatic in operation. In its present state, an all night run, involving ten changes of absorption foils, may be carried through with no attention required after it is started. The proportional counter was filled with argon at one atmosphere of pressure and operated

[1] C. J. Brasefield and E. Pollard, Phys. Rev. **50**, 296 (1936).
[2] E. Pollard and C. J. Brasefield, Phys. Rev. **50**, 890 (1936).

at a case potential of 2600 volts. This arrangement proved entirely satisfactory throughout the whole experiment, which involved a total counting time of more than 400 hours.

Figure 1 gives the details of the two arrangements. A $\frac{1}{8}$-inch layer of titanium metal filings cemented to a copper backing served as a target for the so-called "right angle" scheme. For "forward" observation it was necessary that the layer be thin enough to allow the protons to get through to the counter. It proved inconvenient to obtain a layer of the metal sufficiently thin for our purpose. Hence a layer was prepared by brushing an alcoholic suspension of TiO_2 onto a thin gold foil, and an attempt made to obtain a uniform layer of the oxide over the whole bombardment surface.

The solid angle subtended between source and counter is normally greater in the "forward" method. However, because of the reduced effective area of the "forward" layer since oxygen is present, the yield from both arrangements was very nearly the same. The "forward" method is not open to use at ranges of less than 40 cm on account of the masking effect due to natural protons from the source in this region. Hence the "right angle" method is superior to the "forward" arrangement for the complete analysis of an element.

Experimental Procedure and Results

A straightforward procedure was employed. Protons ejected from the target under bombardment by alpha-particles from a Th C′ source were detected by the counter after passing through various thicknesses of aluminum foil. The strength of the sources used varied from day to day but averaged around half a millicurie. This necessitated long runs at each absorption point in order to obtain data of reasonable statistical weight. Our counter background was never greater than 12 counts per hour, and the actual background was subtracted in every case from the total yield. Between 200 and 1000 particles were counted at each point on the "right angle" curve. The "forward" curve represents a somewhat smaller number of counts.

Figures 2 and 3 depict the absorption curves obtained. The number of protons ejected per minute per millicurie is plotted as ordinate against the range R of the protons in centimeters air equivalent.

From Fig. 2 it is evident that there are three proton groups present, corresponding to ranges of 26 cm, 73 cm, and 98 cm. These two latter groups are verified in Fig. 3, which shows ranges of 92 cm and 112 cm. Q values for each group are tabulated in Table I. It is clear that the values for corresponding groups from both arrangements agree to within the experimental error.

It is seen that the energy levels are for the most part widely separated. This is contrary to the trend one would expect in elements of increasing atomic weight. Perhaps the high neutron excess in vanadium may be the underlying cause of this phenomenon.

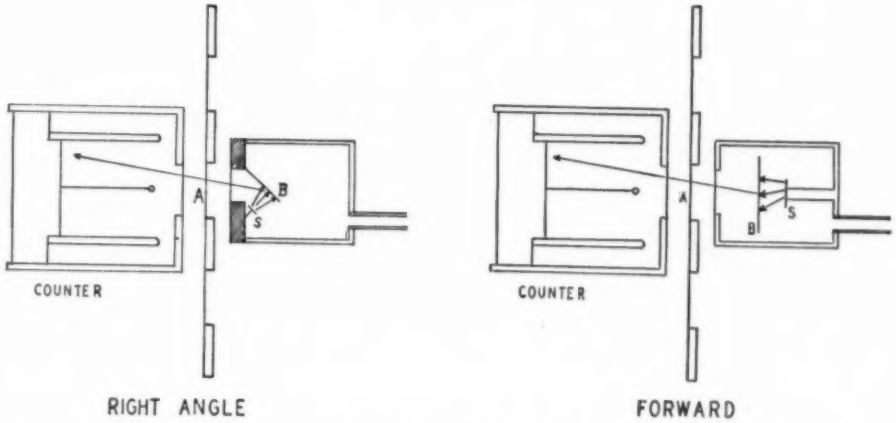

Fig. 1. Schematic arrangement of source (S), target (B), and screens (A) in "right angle" and "forward" methods of bombardment and detection.

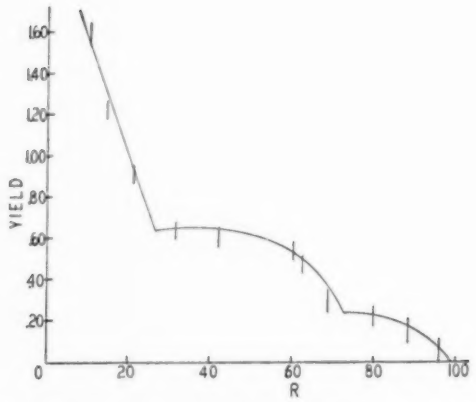

FIG. 2. Absorption curve for the protons ejected in the "right angle" direction. Three groups of protons of ranges 26, 73 and 98 cm are present.

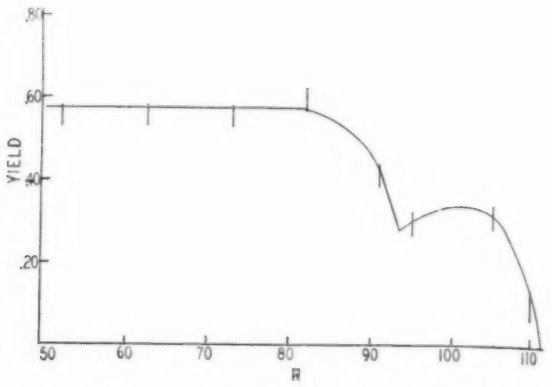

FIG. 3. Absorption curve for the protons ejected in the same direction as the incident alpha-particles. Two groups are present, of range 92 and 112 cm, whose "Q" values agree with those of the two most penetrating groups of Fig. 2.

Expressing the energy change for the longest range proton group in terms of mass units and adopting Dempster's recent value for the mass of Ti^{48} [3] we have:

TABLE I. *Value of Q in the* Ti^{48}–He^4 *reaction for the various groups of ejected protons.*

	Right Angle		Forward		Average
Group	Range cm	"Q" Mev	Range cm	"Q" Mev	"Q" Mev
1	26	−3.63			−3.63
2	73	−0.19	92	+0.19 Mev	0.00
3	98	+1.20	112	+1.00 Mev	+1.10

$$Ti^{48}+He^4 \rightarrow V^{51}+H^1+[Q],$$
$$47.9651+4.0039=V^{51}+1.0081+0.0011$$

and we derive the value 50.9598 for the mass of the stable vanadium nucleus.

We wish to thank Professor A. F. Kovarik for his interest in this work.

[3] A. J. Dempster, Phys. Rev. **53**, 64 (1938).

The Transmutation of Scandium by Th C′ Alpha-Particles

ERNEST POLLARD
Sloane Physics Laboratory, Yale University, New Haven, Connecticut
(Received July 11, 1938)

The emission of protons from scandium under bombardment by Th C′ alpha-particles has been observed according to the reaction $Sc^{45}+He^4 \rightarrow Ti^{48}+H^1$. Three groups of protons are found corresponding to nuclear energy changes -0.3, -1.4 and -2.6 Mev. With Dempster's value for the mass of Ti^{48} the mass of Sc^{45} is deduced to be 44.9599.

INTRODUCTION

WHEN bombarded by Th C′ alpha-particles a target of scandium oxide was found to emit a rather small yield of protons. As scandium has only one stable isotope these must correspond to the reaction

$$Sc^{45}+He^4 \rightarrow Ti^{48}+H^1,$$

in which a stable isotope of titanium is formed. The protons are found to be emitted in several groups and there is some interest in the analysis of these groups into their appropriate Q values since relatively little information is available regarding the excited states of nuclei as heavy as the resulting Ti^{48}. Measurement of the maximum energy of the protons enables the mass of Sc^{45} to be deduced from Dempster's recent value for the mass of Ti^{48}.

EXPERIMENTAL ARRANGEMENT AND RESULTS

The experimental arrangement and procedure was precisely as described in previous papers.[1] The targets used were layers of Sc_2O_3 either squeezed onto a fiber backing or, for layers transparent to protons, painted onto a gold foil from an alcoholic suspension. All experiments were carried out with "thick" layers, although the fact that only the more energetic alpha-particles are effective in causing transmutation reduces the overlapping of groups considerably. The protons were detected by means of a proportional counter and amplifier and were observed by the so-called "right angle" and "forward" methods; absorption curves were plotted in each case in the usual way. Sources varied between 0.5 and 1.0 mC.

The results are shown in Fig. 1 which gives two graphs of yield *versus* absorption. The lower curve was obtained by the forward method with a rather high bias on the thyratron recorder (this is rendered necessary by the unsteadiness of the background due to gamma-radiation) so that protons of residual range exceeding fifteen centimeters are not counted. It can be seen that three groups are present of ranges 49, 66 and 87 cm. Considerable time was spent in establishing the reality of the low point at 66 cm, which is the only evidence for this group, and a total of five hundred particles per point were counted in twenty all-night runs taken at ten values of absorption. All experiments of this kind are open to statistical uncertainty but it is felt to be reasonably sure that this group is real. The yield is roughly one-third of the background count at 66 cm absorption. The upper curve was taken by the right angle method and shows the presence

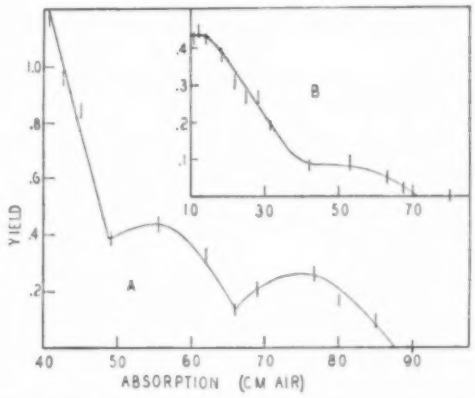

FIG. 1. Absorption curves for protons emitted, A in forward and B in right angle directions. Three groups are present, one of which is not resolved in graph B because of the small yield. Consistent Q values for the shortest and longest range groups are obtained from the two graphs.

[1] C. J. Brasefield and E. Pollard, Phys. Rev. **50**, 296 (1936); E. Pollard and C. J. Brasefield, Phys. Rev. **50**, 890 (1936); W. L. Davidson, Jr. and E. Pollard, Phys. Rev. **54**, 408 (1938).

TABLE I. *Values of Q for the three groups.*

	Right Angle		Forward		Average
Group	Range cm	"Q" Mev	Range cm	"Q" Mev	"Q" Mev
1	40	−2.7	49	−2.5	−2.6
2	not resolved		66	−1.4	−1.4
3	71	−0.5	87	−0.2	−0.3

of two groups of ranges 40 cm and 71 cm. The third group found in the other curve should occur at 58 cm. The yield in this region is so small that it is not possible to resolve groups and no attempt was made to do so. There appears to be a flattening of the graph for absorption less than 15 cm.

Discussion

The values for the nuclear energy change [Q values] derived from the above data are given in Table I. It will be seen that there is reasonable agreement between the values found by the two methods of observation for groups 1 and 3. As the yield of protons is low, the error should be taken as ± 0.3 Mev, which corresponds to an uncertainty in range of roughly 5 cm.

The various Q values correspond to excited states of the product nucleus Ti^{48}. There is as yet no known simple method of classifying nuclei to exhibit regularities of properties; however the excess of neutrons over protons is often referred to in theoretical calculations. In Table II is collected the average spacing of all the known levels of nuclei from Ne^{22} to V^{51}, grouped according to this manner. It can be seen that there is no significant trend in level spacing as the neutron excess increases beyond two.

TABLE II.[2] *Average spacing of levels for various elements arranged according to their excess of neutrons over protons.*

Excess of Neutrons Over Protons	Element	Average Spacing of Levels Mev
1	Al^{27}	0.90
	P^{31}	0.80
	Cl^{35}	0.70
2	Ne^{22}	1.54
	Na^{24}	3.20
	Mg^{26}	1.67
	Al^{29}	1.10
	Si^{30}	1.56
	S^{34}	1.42
	A^{38}	2.00
	Ca^{42}	1.35
4	Ti^{48}	1.15
5	V^{51}	2.37

[2] These values are collected from the following papers: O. Haxel, Physik. Zeits. **36**, 804 (1935); A. N. May and R. Vaidyanathan, Proc. Roy. Soc. **A155**, 519 (1936); E. McMillan and E. O. Lawrence, Phys. Rev. **47**, 343 (1935); E. O. Lawrence, Phys. Rev. **47**, 17 (1935) and papers in reference 1.

The drop in proton yield for absorptions less than 15 cm is consistent with the fact that the potential barrier to emergent protons will greatly diminish the chance of escape of a proton which has sufficient energy to do so, but yet has to penetrate the barrier. Calculations show that a proton of 15 cm range has a 20 percent chance of traversing the barrier while one of 10 cm range has only one-fourth the chance. This would thus indicate that the lifetime of the composite V^{49} nucleus is very short, of the order of 10^{-22} sec.

From Dempster's[3] value for the mass of Ti^{48} we have

$$Sc^{45}+He^{4}\rightarrow Ti^{48}+H^{1}[+Q]$$
$$Sc^{45}+4.0039=47.9561+1.0081-0.0004,$$

which gives the value 44.9599 for the isotopic weight of Sc^{45}.

The author wishes to thank Mr. W. L. Davidson, Jr. for helping him to complete the observations in spite of the competition of constructing a cyclotron, and Professor A. F. Kovarik for his interest in the work.

[3] A. J. Dempster, Phys. Rev. **53**, 64 (1938).

The Disintegration Constant of Thorium and the Branching Ratio of Thorium C

ALOIS F. KOVARIK AND NORMAN I. ADAMS, JR.
Sloane Physics Laboratory, Yale University, New Haven, Connecticut
(Received June 30, 1938)

In age determinations of minerals in which thorium predominates, some inconsistencies have appeared when the value used for the disintegration constant of thorium is that adopted by the International Radium-Standard Commission (1930). This value differs from the original Geiger-Rutherford value by 30 percent. The present research was undertaken to determine the disintegration constant of thorium by the method of counting alpha-particles. Easily weighed sources were used. The material was obtained from a thorite from the same lot that was used by Geiger and Rutherford. The thorite contained only a small amount of uranium and correction for the ionium present was made. Various checks on the counting are given. The half-value period of thorium was found to be $1.39(10)^{10}$ years and the branching ratio, thorium C′ to thorium (C+C′), is 0.663. A method of impounding the thoron, yet permitting alpha-particles to escape, is described.

INTRODUCTION

THE determination of the age of radioactive minerals demands several constants but mainly the constants of disintegration of uranium and of thorium. Radioactive minerals from the same locality should yield the same age determination whether the minerals are those containing chiefly thorium, e.g. the monazites, or are those having uranium in predominance, e.g. the uraninites. Considerable disagreement, however, is found when the value of the disintegration constant of thorium used is that corresponding to the half-value period of $1.8(10)^{10}$ years, which is the value adopted by the International Radium-Standard Commission in their report of 1930.[1] The first determination of the disintegration constant of thorium was made by Geiger and Rutherford[2] with a value corresponding to $T=1.3(10)^{10}$ years, the use of which value gives better age agreement but it differs from the accepted value above by 30 percent. The disagreement in age determinations is not due to the uranium constant.

Geiger and Rutherford obtained their material as thorium oxide from a thorite and counted scintillations of the order of 3000. They began counting about five weeks after the material was chemically separated from the mineral and, therefore, in their material there was nearly a practical radioactive equilibrium between thorium and its isotope, radiothorium. Mesothorium was separated. Because the chemical analysis showed a very small amount of uranium, no correction was attempted for the isotope ionium. Other older determinations[3] were made by McCoy ($T=1.8(10)^{10}$ yr.), Heimann ($T=1.5(10)^{10}$ yr.), and by Meitner ($T=2.3(10)^{10}$ yr.) who used chemically purified thorium oxide and studied the ionization produced by the radiations. The original source of the material is not stated nor the condition of radioactive equilibrium and no correction is made for ionium.

The value of the constant adopted by the International Commission is based on the deductions of Kirsch,[4] who used the data of a chemical analysis of a certain Ceylon thorianite, by Hönigschmid,[5] in which the atomic weight of the lead was found to be 207.21, i.e., that of ordinary lead. It can be shown[6] on the assumption that the original quantities changed in no other way than by radioactive disintegration of the radioactive substances present that, approximately, $\lambda_{Th} : \lambda_u = \text{Th D/Th} : \text{Ra G/U}$ and

[1] J. de phys. et rad. **2**, 273–289 (1931); Physik. Zeits. **32**, 569–581 (1931); Phil. Mag. (7) **12**, 609–632 (1931).
[2] H. Geiger and E. Rutherford, Phil. Mag. (6) **20**, 691–698 (1910).
[3] H. N. McCoy, Phys. Rev. **1**, 401–403 (1913); Bertha Heimann, Wien. Ber. IIa, **123**, 1369–1372 (1914); L. Meitner, Physik. Zeits. **19**, 257–263 (1918).
[4] G. Kirsch, Wien. Ber. IIa **131**, 551 (1922); Naturwiss. **11**, 372 (1923); Physik. Zeits. **31**, 1017–18 (1930); Naturwiss. **18**, 1054 (1930).
[5] O. Hönigschmid, Zeits. f. Electrochem. **25**, 91–97 (1919).
[6] *The Age of the Earth. Physics of the Earth.* Vol. 4, N.R.C. Bull. 80 (1931).

λ_{Th} can be obtained in terms of λ_u and the various data. A critique of this question has been given by one of us in *The Age of the Earth*[6] and it need be here only pointed out that the Ceylon thorianites, found in geological river beds, are very uncertain as to the condition of remaining "unaltered primary minerals." It is very doubtful that the accurately obtained chemical data may be used in the above approximate relation to obtain an accurate value for the disintegration constant of thorium.

A more recent value has been obtained by Fesefeldt[7] ($T=1.3(10)^{10}$ yr.) by using the Geiger-Müller counter in counting alpha-particles from quite small sources of thorium oxide obtained from monazite sand.

In view of the variations in the values of the constant by different observers, the difficulties in the check on the age determinations of monazites and uraninites from the same locality and the fact that ionium correction has not been made in any of the determinations of the disintegration constant of thorium, we have undertaken this task, at the request of the National Research Council's committee, to consider all corrections and possible checks and to determine the constant by counting the alpha-particles. The final results from thorite material give the half-value period of thorium, $T=1.39(10)^{10}$ yr. and also the branching ratio of thorium C as 0.663.

Material

It is essential, for several reasons, that a complete history of the material used be known. Thorium is obtained from minerals in which it is in radioactive equilibrium with all its disintegration products. In the chemical separation of thorium not only thorium is separated but also its isotopes radiothorium and ionium—the latter, if any uranium is also present in the mineral. The amount of ionium depends on the uranium content and is in equilibrium with all the products of uranium. The radiothorium is in equilibrium with the thorium at the time of the chemical separation of both from the mineral but since it disintegrates to half-value in 1.9 years and is also formed from thorium through the disintegration of mesothorium whose half-value period is 6.7 years, the actual amount of radiothorium (and all subsequent products of the series) will decrease with time and reach a minimum (see curves, Fig. 2) relative to the amount of thorium, in 4.8 years, after which it increases again and becomes 50 percent of the thorium equilibrium amount in 9.0 years, 75 percent in 16.8 years, etc. If it is not known when the thorium was chemically separated from the mineral one does not know the contribution due to the radiothorium unless the experiments are so refined that a differentiation based on the ranges of the alpha-particles can be made.

The ionium correction can be made if the uranium content of the mineral is known, or, more accurately, if the radium content is measured by the radon method against some radium standard solution.

It is therefore essential to start with a mineral and, preferably, with one having a small uranium content. This was done by Rutherford and Geiger and by Fesefeldt. Our mineral was thorite and came from the same lot that Geiger and Rutherford used.[8] The chemical work was done by Dr. Jeanne Henry Cornet of Brussels while sojourning in New Haven. Special care was taken to separate out quantitatively the thorium, uranium and radium. The thorium was then changed to thorium oxide and samples of this were tested for the molecular weight which showed the thorium oxide to be pure. The radium was dissolved and several samples were made to measure the amount of radium by the radon method. The radium-standard solution of the laboratory was previously prepared by careful gamma-ray measurements and was checked against a solution from the Reichsantalt (Berlin). The radium (mineral) activity is also the activity of the ionium. The analysis of the thorite gave for the important constituents as follows, in percent: thorium 42.21, uranium 0.52, iron 2.64, silicon 27.38.

The specimens used in the experiments were prepared on aluminum disks 8 cm in diameter in the form of quite uniform layers but varying in thickness for the different samples. The pro-

[7] Hans Fesefeldt, Zeits. f. Physik **86**, 605–610 (1933).

[8] Two samples were given to one of us by Geiger in 1910 from a lot collected by B. B. Boltwood. Although we are not certain, we believe that they were Norwegian thorite specimens.

cedure was as follows. The oxide was ground to fine powder in an agate mortar wet with a small amount of chloroform. It was then transferred to a test tube containing about 20 cm^3 of chloroform and after shaking it was decanted into a second test tube where it left behind a small quantity of oxide in larger granules. It was found unnecessary to repeat with a third test tube but by further shaking all thorium oxide was found to be held in suspension before pouring it over the aluminum disk. A special circular metal vessel was made with inner walls curved and with a recess in the base for the aluminum disk so that the surface of the disk and the bottom surface of the vessel formed a plane. A weight with three legs having needle-point feet, which came on the disk near its circumference, held the disk in place. Enough chloroform was placed in the dish to cover the disk about 1 mm before the oxide from the test tube was poured over. In this manner waves were diminished, striations ordinarily found in the deposited layer were obviated and very uniform layers were obtained. The material was then left undisturbed, protected from dust, etc., until the chloroform evaporated and then the metal dish, cleaned of its contents in the meanwhile, was heated and the disk with the layer of thorium oxide was placed in it on a suitable ring to evaporate any small quantity of liquids that might still remain in the oxide. The specimen was then weighed to determine its surface density, the aluminum disk, cleaned and dried by warming, had been previously weighed. A suitable cylinder with a knife-edge end was placed centrally on the material and disk and the outside rim of oxide was carefully removed. After warming the specimen it was weighed again. Several such performances, with decreasing but known size of the cylinder, were done for the purpose of obtaining data on the uniformity of the density of the layer and for obtaining a size suitable for the number of channels to be used in a grid which geometrically reduced the total number of alpha-particles counted to the desired amount. The mean surface densities (mg of oxide per cm^2) obtained were plotted against the distance from the center to get a curve for a slight correction in the last mean density obtained for the material of an area corresponding as nearly as possible to that part of the grid to be used in the experiment.

Since thoron gas is one of the products of the material a method had to be devised to impound it by a covering thin enough to allow the alpha-particles to emerge. Various substances were tried but the best results were obtained with celluloid and varnish. Fesefeldt used celluloid alone but somewhat thicker than we desired. We found that very thin films were very pervious to thoron. However a thin layer of varnish on a double layer of thin celluloid gave satisfactory results in nearly all cases. The films were produced as follows: 1 g of celluloid was dissolved in 200 cm^3 of amylacetate. A quantity varying between 0.1 and 0.2 cm^3 of this solution was dropped on the surface of distilled water (20 cm diameter) on which the celluloid film formed. A wire frame of appropriate size and shape was brought under the film and by cutting the film with amylacetate it could be folded and placed on an aluminum rim whose external diameter corresponded to that of the thorium oxide disk. After it was thoroughly dried it was dipped into a very dilute solution of waterproof (water-lite spar) varnish, 20 cm^3 in turpentine 300 cm^3 and by careful manipulation, and the use of centrifugal force, the excess varnish was moved to the outer edge of the aluminum rim where it was wiped off. It was then dried for several days and dipped in varnish again. The double celluloid film had a stopping power for alpha-particles of polonium of a fraction of a millimeter of air and when doubly varnished its stopping power corresponded to 2 or 3 mm air as was found by direct test with an auxiliary apparatus with a Geiger point counter. The inner edge of the rim was carefully attached to the prepared film by the use of undiluted varnish to prevent leaks at this place and the rim itself was similarly sealed to the aluminum disk with the inner circle of the thorium oxide under the film. Tests for thoron leak were immediately carried out in the regular apparatus and leaks of 1 atom of thoron per minute were easily detected. Generally no leak was observed. In some cases a big leak, due to damage to the film, occurred and the specimen was discarded. In two cases small leaks were observed but counts were taken after an appropriate study of the natural back-

ground count was made to correct the counts made in the experiment.

For the determination of the disintegration constant of thorium, as reported in this paper, *only* thorium oxide from the *thorite* was used. For purposes of checks and also for further data on the branching ratio, thorium oxide was also prepared from two commercial re-purified materials, both of which had been used by the late B. B. Boltwood in some of his experiments. One source was thorium nitrate (Welsbach) used by Boltwood as early as 1907 and the other an oxide (Eimer and Amend) obtained prior to 1918. Results from these materials will be discussed later.

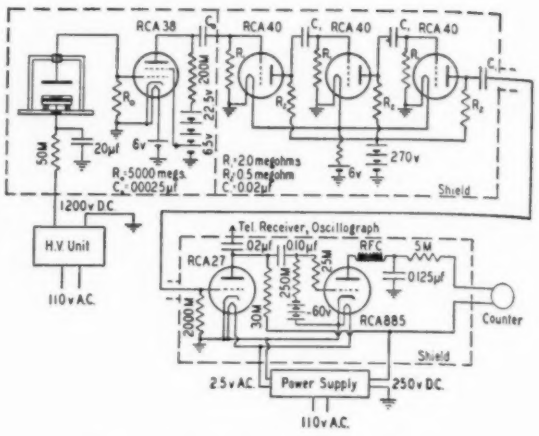

FIG. 1. Amplifier and counter circuit.

APPARATUS

Except for slight improvements the apparatus employed to count and record the alpha-particles was the same as that used in the earlier determination of the disintegration constant of uranium.[9] The alpha-particles from a specimen of thorium oxide placed in an ionization chamber passed upward through cylindrical channels in an accurately machined brass plate and produced ions in the air above. The negative ions were collected on an electrode placed about 2.0 cm from the drilled plate, since a potential difference of 1200 volts was maintained between the two. The number of ions due to each alpha-particle was sufficient to change the potential of the collecting electrode momentarily by approximately $2.5(10)^{-4}$ volt. This voltage pulse was communicated to the input of a vacuum tube amplifier whose details are shown in Fig. 1. The relay mechanism used in the uranium experiments to actuate the Cenco counter was replaced by a thyratron circuit of conventional design. This change together with the introduction of a short time-constant (pulse sharpening) coupling circuit between the first and second stages of amplification materially improved the resolution of close counts and increased the possible counting rate. Various tests indicated that counting rates as high as 150 per minute could be used safely. The accuracy of recording was checked periodically by means of a telephone receiver or an oscillograph, connected as shown in the figure.

The original drilled plate or grid (G_1) used in the uranium experiments was remeasured and found to have changed slightly in thickness, because of polishing and cleaning. With the new value of the thickness (5.110 mm) and the unchanged value of hole radius (1.962 mm) calculation showed that the number of alpha-particles emerging per channel was $N_0(0.36951)$, where N_0 is the total number of alpha-particles emitted from a square millimeter of the source. The method of calculation is given in the paper on uranium.[9] In addition to G_1 another grid, G_2, having a larger number of smaller channels, was prepared in order to check the results obtained with G_1. The second grid whose thickness was 5.084 mm had 308 channels of mean radius 0.9978 mm. The latter value is the average of direct measurement (0.9980 mm) as in the case of G_1 and calculation based on amount of metal removed by drilling (0.9976 mm). The calculated number of alpha-particles emerging per channel of G_2 was $N_0(0.02852)$. Hence the ratio of the number of alpha-particles per channel of G_2 to the number per channel of G_1 for any given source was by calculation 0.07717. The average of a large number of experimental determinations of this ratio gave 0.07708, a very satisfactory agreement.

The background or natural count of the apparatus was determined usually by placing an aluminum plate over the grid in such a way as to prevent alpha-particles from reaching the ioniza-

[9] A. F. Kovarik and N. I. Adams, Jr., Phys. Rev. **40**, 718 (1932).

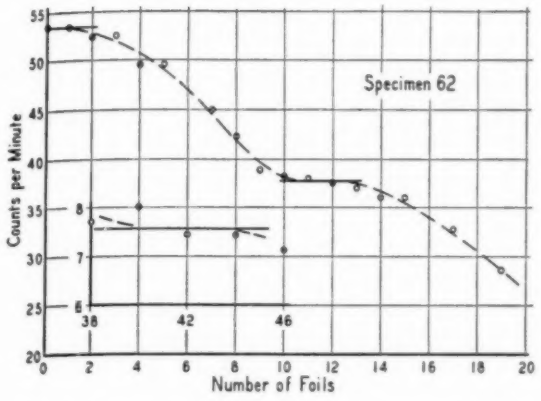

FIG. 2. Counts of particles through aluminum foils.

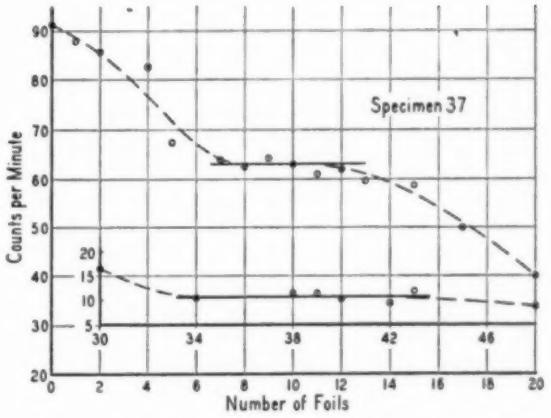

FIG. 3. Counts of particles through aluminum foils.

tion space. However, in the case of some specimens which had a slight leak of thoron it was necessary to make additional observations with the specimen removed.

METHOD OF PROCEDURE

The specimen, after reaching radioactive equilibrium, was fitted into a recess in the base of the counting chamber. One of the two grids used with a predetermined number and arrangement of channels was placed in a definite position on top of the specimen. A certain number of positions of the grid relative to the material were required to give opportunity for every part of the source to emit alpha-particles through the open channels. For grid G_2, having 308 small size channels, only two positions were required. For the grid G_1 the number varied from 4 to 18, depending on the arrangement of the selected channels. The naturals were counted at the beginning and the end and many times in between, in each series of counts, so that they were well distributed relative to other counts taken and in total had a long time count. The natural or background count depends, in case of alpha-particle counting, mainly on laboratory and electrical circuit disturbances and on the sensitivity of the apparatus. Since the latter was sometimes made fairly high, the records for the naturals show some variation. Of course, thoron leak brings in a variation which may change with conditions of the experiment.

The emerging alpha-particles belong to thorium, ionium, radiothorium, thorium X, thoron, thorium A, thorium C and thorium C′. Counts were obtained with the channels open and in the various positions of the grid over the specimen. If aluminum foils of moderate stopping power (2–3 mm air) are placed over the grid and successively increased in number, then at first the count will remain unchanged, but ultimately the shortest range alpha-particles will not be counted and in fact the straggling alpha-particles will first be eliminated. Because thorium and ionium alpha-particles (2.6 cm; 3.0 cm) have ranges with overlapping stragglers and because the next longer range alpha-particles, namely, those from radiothorium (4.0 cm) differ in range from those of thorium and ionium by nearly a centimeter of air, the counts for a certain number of aluminum foils will be again constant and form another horizontal step in the curve (Figs. 2, 3, 4) giving counts against number of aluminum foils. Were it not for straggling and for imperfect collimation due to size of the channels the drop in counts from one step to the next would be vertical and there would be as many steps as there are ranges of alpha-particles. Where two different ranges are close together so that the stragglers of one overlap with those of the other, differentiation between them is not possible.

In the present experiments we are interested in three steps, namely, the initial step in which all alpha-particles are counted and this will be referred to as the open step, the next following step, after eliminating alpha-particles of thorium and ionium, referred to as the first step, and

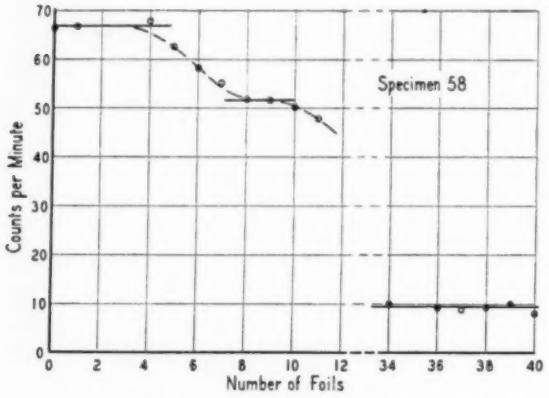

FIG. 4. Counts of particles through aluminum foils.

finally the step, referred to as the second step, when all the alpha-particles are eliminated except those of thorium C′ (8.6 cm). The count difference between the open step and the first step gives the count for the number of alpha-particles from thorium plus ionium. The net count of the second step represents the alpha-particles from thorium C′, which, with those from thorium C, would represent one-fifth of the particles given by the net count of the first step (Ra Th, Th X, Tn, Th A, Th(C+C′)).

The difference, open step less first step, when corrected for the ionium, gives the count of disintegrating thorium atoms, counted as restricted by the geometry of the grid. With the knowledge of this and the mass of the thorium involved we can obtain the value of the disintegration constant. The ratio of the net second step count to one-fifth of the net first step count gives us the branching ratio of Th C, i.e., Th C′ : Th(C+C′). The ratio of the net first step count to net open step count, when corrected for the ionium contribution, would be 5 : 6 if radiothorium were in equilibrium with thorium, as it actually is in the mineral. It will be a smaller ratio when the counts are made some time after the chemical separation of the thorium from the mineral. (See Fig. 5.)

It is, therefore, important to establish the three steps and obtain a sufficiently large count for each step and for the various positions of the grid to use all parts of the material. It is also important to have the mean date of such counts and the date of the chemical preparation, from the mineral, of the material used. Our material was prepared May 30, 1930. Because it was impossible to begin the experiments until much later it was decided to carry them on long enough to be able to check the theoretical curve through the minimum. This check is shown in curve labeled ratio r in Fig. 5. The curve drawn is the theoretical curve representing the ratio of the activity of the radiothorium and subsequent alpha-ray products, which are all in transient equilibrium, to the activity of thorium plus

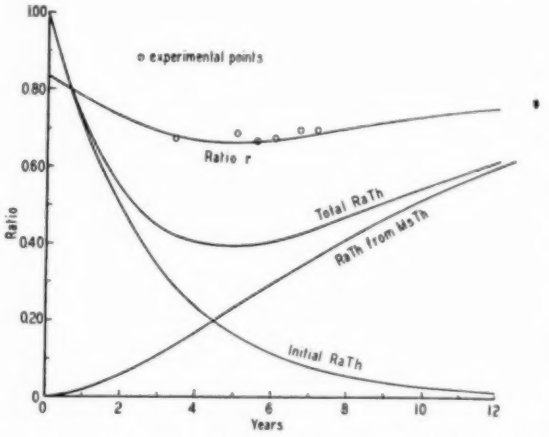

FIG. 5. Ratio of activity of radiothorium and subsequent alpha-ray products.

radiothorium and the other products. Experimentally, this ratio is the net first step count to the net open step corrected for the ionium.

RESULTS AND CALCULATIONS

The data needed for the calculation are given in Table I. The mean date of the counting is given in the second column so that the age of the material used may be obtained for the calculation of the ratio $r=5\rho/(5\rho+1)$, where ρ=the activity of radiothorium on that date relative to the activity of thorium or to its own equilibrium activity on May 30, 1930 when it was separated with the thorium from the mineral. The third column indicates the grid and number of channels used. The fourth column gives the mean surface density of the thorium oxide. The fifth column gives the gross count and time for each of the three important steps and the [ ] figure, where given, represents the weight assigned. The last column gives the natural or background count per minute. Generally the

counts for the various positions of the grid were nearly alike and in such cases the total was obtained by adding the counts and the periods, respectively, for the various positions. In cases of largely differing counts per position, the positions were weighted alike, irrespective of actual counts.

Table II gives the data reduced to the number of alpha-particles counted per minute, per channel of the grid G_1 and per surface density of 1 mg ThO_2/cm^2. Where grid G_2 was used the calculated ratio of the number of emerging alpha-particles per one channel of G_2 and G_1, respectively, is used to make the reduction as indicated. The last column gives our estimated weight for the value in the case of each specimen. This was arrived at, on the basis of 10, considering the total counts, open and first steps, the number of positions of the grid over the specimen, the constancy of the surface density as the area was reduced and the absence (or presence) of thoron leak. Specimens 35 and 59 had leaks and special efforts were made to study the background counts to make a proper correction. Specimen 36, as its surface density indicates, was thick and some of the straggling alpha-particles did not emerge. Specimen 37 had a thick varnished celluloid film and the open count was likewise deficient so that the open step could not be obtained (see Fig. 3). In both of these cases the count for thorium was obtained from the first step averaged with the second step for which the branching ratio 0.663 was used to get the first step result. The mean value was used to obtain the open count (thorium alone) by the use of the calculated ratio r.

The ionium correction is expressed as 3.39 percent of the experimental net open count and was obtained by the radon method of measuring the radium in the thorite. After having determined the thorium plus ionium count for several specimens a preliminary determination of the thorium was obtained and the radium (=ionium) activity was expressed as percent of the combined thorium plus ionium count.

The mean weighted result for one channel of grid G_1, therefore, becomes the important figure for calculation. Other values of constants used

TABLE I. *Data used in counting alpha-particles.*

SPEC.	DATE (MEAN)	CHANNELS GRID	DENSITY $MgThO_2/cm^2$	STEP	GROSS COUNT : MINUTES	NATURAL PER MIN.
17	X·6·1933	$11G_1$	0.886	open	83351 : 3100	2.666
				1st	81672 : 4320	2.666
				2nd	1195 : 285	2.055
36	XII·9·1934	$11G_1$	3.65	open	layer too thick	
				1st	181526 : 2610[18]	2.60
		$4G_1$	3.65	1st	7976 : 300[1]	2.60
		$7G_1$	3.65	1st	16502 : 350[1]	2.60
		$11G_1$	3.65	2nd	54734 : 4843	2.60
34	III·9·1935	$22G_1$	2.656	open	88212 : 575	2.43
				1st	108993 : 1145[3]	2.43
				1st	68475 : 710[2]	3.45
				2nd	18260 : 1248[2]	2.43
		$33G_1$	2.656	open	31601 : 150	2.43
				1st	70904 : 500	2.43
				2nd	9054 : 425[1]	2.43
35*	XII·1·1935	$19G_1$	1.230	open	128598 : 2000	6.644
				1st	102865 : 2300	6.644
				2nd	33008 : 2800	6.644
37	III·12·1936	$27G_1$	1.36	(open	128722 : 1415)	2.534
				1st	100035 : 1590	2.534
				2nd	23429 : 2200	2.534
53	VII·5·1936	$36G_1$	0.352	open	42099 : 1255	2.108
				1st	38515 : 1650	2.348
62	III·4·1937	$308G_2$	0.818	open (a)	53430 : 1000[1]	2.781
				open (b)	16968 : 300[1]	2.781
				1st (a)	56427 : 1500[1]	2.781
				1st (b)	15934 : 400[1]	2.781
				2nd (total)	9081 : 1200	2.781
59*	VII·25·1937	$308G_2$	1.031	open	78798 : 1060	9.77
				1st	38638 : 730	8.87
				2nd	7337 : 640	5.85

TABLE II. *Number of alpha-particles per min. per channel.*

Spec.	open − 1st step Th + Io	3.39% (Th + Io) Ionium	Th/min/1 hole/σ $=\frac{1\text{ mg ThO}_2}{\text{cm}^2}$		Wt.
			G_2	G_1	
17	7.982	0.271		0.7912	10
34	47.70	1.617		0.7802	8
35*	19.575	0.664		0.8092	8
53	10.443	0.354		0.7962	8
36	Deduced from 1st and 2nd steps			0.8430	4
37	" " " " "			0.8185	8
62	15.764	0.534	$\frac{0.06045}{0.077169}$	=0.7833	10
59*	20.51	0.70	$\frac{0.062384}{0.077169}$	=0.8084	6
		Weighted mean = 0.8000			

TABLE III. *Branching ratio:* Th C′/Th(C+C′).

Spec.	$\frac{\text{net 2nd step}}{\frac{1}{8}\text{ (net 1st step)}}$	Weight
17	0.6580	10
36	0.6488	10
34	0.6636	8
35*	0.6756	8
37	0.6721	10
62	0.6685	10
59*	0.6643	6
58 commercial	0.6558	10
	Weighted mean = 0.663	

are indicated. Avogadro's number used is the recent value by S. v. Friesen[10] and 232.12 is used for the atomic weight of thorium.

The calculation of the number of alpha-particles emitted by a gram of thorium is made as follows:

0.8000 = alpha-particle per minute per 1 channel, G_1, per 1 mg ThO_2/cm^2,

$0.87884 = Th/ThO_2$,

$N \equiv$ number of alpha-particles emerging from 1 channel, G_1, per second,

$N_0 \equiv$ number of alpha-particles emitted from 1 mm^2 source per second,

$$N = N_0(0.3695),$$

$$\therefore\quad N_0 = \frac{0.8000/\text{min.}}{0.3695} \times \frac{1\text{ min.}}{60\text{ sec.}} \times \frac{1}{0.87884} \times \frac{10^5}{\text{gTh}}$$

$$= 4.1058(10)^3 \frac{\alpha}{\text{sec.}}/\text{gTh.}$$

The number of atoms in a gram of thorium is given by

$$\frac{6.028 \times (10)^{23}}{232.12} = 2.597(10)^{21}\text{ Th atoms per gTh}$$

and hence

$$\lambda = 4.1058(10)^3 : 2.597(10)^{21} = 1.58(10)^{-18}\text{ sec.}^{-1}$$
$$= 4.99(10)^{-11}\text{ year}^{-1}.$$

The corresponding half-value period is $T = 1.389(10)^{10}$ years. Table III gives the values of the branching ratio of thorium C for the various specimens. The last one, number 58, was a commercial (Welsbach nitrate) material. The mean weighted value of this ratio is 0.663.

DISCUSSION AND CONCLUSION

The history of the material from the thorite is completely known for purposes of checking up on the relative activity of radiothorium and its subsequent products. The experiments were carried on through the minimum value $\rho = 0.3919$ which occurred at 4.8 years and the experimentally obtained ratio $r = 5\rho/(5\rho+1)$ for various periods; i.e., the mean dates of the counting on each specimen, lie close to the curve calculated with the half-value periods of MsTh and RaTh as 6.7 years and 1.9 years, respectively. The disintegration constant is smaller than that of Geiger and Rutherford or that of Fesefeldt by 6.8 percent of their value. Since our thorite came from the same lot as Geiger and Rutherford's, it is probable that the ionium content was nearly the same in both sets of samples. If our ionium percent correction is applied to the Geiger and Rutherford half-value period ($T = 1.3(10)^{10}$ yr.) it becomes nearly $1.34(10)^{10}$ years which differs by only $3\frac{1}{2}$ percent from our value—a discrepancy easily accounted for by the relatively small count they made of the alpha-particles. The analysis of our thorite gave thorium and uranium content 42.21 percent and 0.52 percent, respectively. The uranium in the thorite, in grams per gram of thorium, is, therefore, 0.0123. The radium associated with this amount of uranium is $4.18(10)^{-9}$ g. The radium separated from the thorite, measured by the radon method, was found to be $4.11(10)^{-9}$ g of

[10] S. v. Friesen, Proc. Roy. Soc. **A160**, 424–440 (1937).

radium associated in the thorite with 1 g thorium, which is a very good check on the chemical analysis.

The method used in these experiments makes it possible to determine the count for thorium and ionium. The ionium correction has a check from the uranium content obtained by chemical analysis. The thorium count can also be obtained from first step data when the ratio $r=5\rho/(5\rho+1)$ is calculated with the knowledge of the age of the material and also from the second step with the additional knowledge of the branching ratio. This was indicated for the specimens 36 and 37. In the remaining specimens these facts were used to check the theoretical curve for the ratio r and to obtain the branching ratio. The original branching ratio was determined by Marsden and Barratt[11] as 0.65 by counting scintillations. More recently Meitner and Freitag,[12] who used the cloud chamber, obtained 0.657. Our experiments yield the value 0.663.

We also carried out long counts on two different commercial materials formerly used by Boltwood. One was Welsbach nitrate which was changed to oxide and from which radium (and mesothorium) were separated in 1930 and the other was Eimer and Amend oxide similarly treated. The radium was measured by the radon method. The complete history is not known but Boltwood's records indicate that he used some of the material in 1917 and in 1925 and may have used the Welsbach nitrate in 1905–07. Consequently, it is not known whether the radium measured was grown in some short period from the ionium or whether it was wholly or partially separated at the time of extraction from the mineral. If one assumes in the case of Eimer and Amend material that it was about 20 years old and that, when produced, the mesothorium and radium were removed, then the radium found by the radon method is the radium grown from ionium in those 20 years application of such a correction for ionium to the thorium plus ionium count gives 0.808 as against 0.8000 for the thorite material (column 4, Table II). The Welsbach nitrate material required the assumption that the radium measured actually represented the equilibrium amount in the mineral from which the material was obtained in order to give a reasonable check on the thorium count. This may be true since the material may be from monazite sand for which the radium content is of the order we measured. Under this assumption, the Welsbach material yields as a mean from two specimens 0.7939 (cf. thorite, Table II). Both materials would give fairly correct results if the assumptions made are correct. These experiments were done specifically to point out the difficulties encountered when the history of the material is incompletely known.

We used sources large enough for precise weighing. This required proper reduction of the alpha-particle count, for accuracy, which was accomplished geometrically with the channelized grid. Two grids whose channels differed widely were used. The ratio of calculated number of alpha-particles, from a given source, emerging from the two channels, respectively, received an excellent check experimentally and also the thorium count in the experiments (Table II) gives satisfactory agreement among the results obtained.

It seems to us that none of the important phases of the problem has been overlooked. Considering all the possible errors, we have concluded that the possible error in the final result for the disintegration constant is not greater than two percent and that it is smaller for the branching ratio determination.

In conclusion, we desire to express our thanks to L. Hurwitz who assisted us in some of the work, and to Dr. Jeanne Henry Cornet for the preparation of the original material as well as later preparation of some of the commercial material used for checks.

[11] E. Marsden and T. Barratt, Proc. Phys. Soc. London **24**, 50 (1911).

[12] L. Meitner and K. Freitag, Zeits. f. Physik **37**, 481–517 (1926).

Variational Theory of the Alpha-Particle

H. Margenau and Warren A. Tyrrell, Jr.
Sloane Physics Laboratory, Yale University, New Haven, Connecticut
(Received June 23, 1938)

The energy of the normal state of the alpha-particle is calculated with the use of an elaborate variational method, in which a fixed set of nuclear constants in the general symmetric Hamiltonian has been adopted. The result agrees well with an earlier, independent calculation, and allows the convergence limit to be determined with considerable precision. Comparison with previous work on H^3 indicates that the binding energies of both H^3 and He^4 can be very nearly accounted for with the use of a single set of constants satisfying the conditions imposed by the triplet state of H^2; but the value of g (ratio of Heisenberg to Majorana forces) required is lower than usually supposed, and will give somewhat too low an energy for the singlet state of H^2. The same methods are employed to calculate the excited singlet and triplet states of the alpha-particle, and yield the results which have already been stated. No excited state is stable. A virtual excited state is shown to exist near the energy of dissociation into four particles.

ALL attempts at gaining detailed knowledge of nuclear forces rely heavily upon the binding energies of light nuclei. These are known from experiments with considerable accuracy, but the theoretical methods which link them to the postulated laws of nuclear force are very uncertain indeed. Endeavors of refining these methods are therefore desirable.

Unfortunately, the nuclear four-body problem can only be solved by successive approximations. Of the method used it must be required that the energy calculated by it should converge to the true value, and preferably converge rapidly. Two general techniques are available: Schrödinger perturbation theory[1] and the variational method. As to perturbation theory it is well known that, within a given order, it does not converge to the correct energy, although the odd orders do furnish upper bounds. Hence a safe perturbational procedure must at least include the third order—the first-order result is in general poor. But the third-order perturbation is almost as difficult to calculate as the variational energy which always respresents an upper limit. Hence the variational method is employed for the most part in this paper, although occasional comparison with perturbational results is made.

The method of linear variation functions converges if the functions form a complete set, it converges rapidly if that set is chosen judiciously. But the selection of function sets is strongly limited by the practical demand of tractability. This dictates in effect that all functions shall be products of exponentially decreasing functions and polynomials. Despite this severe limitation there is some latitude inasmuch as the kind of coordinates to be adopted is not prescribed. The choice of polynomials does not affect the convergence;[2] in this work the Hermite type of polynomial is used.

Hermite functions of particle coordinates measured from a fixed fictitious center have an analytic behavior quite different from the same functions with relative coordinates as arguments. This permits two independent calculations to be made with variation functions which superficially appear identical. The use of relative and center of mass coordinates is more adapted to the nature of the problem, since it conforms in a simple way to the existence of nuclear particle groups.[3] For this reason one would expect a variation calculation in these coordinates to converge more rapidly than the other scheme which is essentially an extended Hartree method. Another advantage of the method of relative coordinates is seen in the fact that it necessitates no correction of the kinetic energy which is automatically referred to the center of mass. The price paid for these advantages is the greater labor which the method entails.

For H^3 both calculations have been made,[4] and the result is the expected one. The "Hartree method" gave an energy of -6.84 Mev with the

[1] E. Feenberg and S. S. Share, Phys. Rev. **50**, 253 (1936); D. R. Inglis, Phys. Rev. **51**, 531 (1937).

[2] The whole calculation could be carried through with equal facility and identical results if spherical harmonics with the same radial exponential function were chosen.

[3] J. A. Wheeler, Phys. Rev. **52**, 1083 (1937).

[4] H. Margenau and D. T. Warren, Phys. Rev. **52**, 790 (1937).

use of 21 functions, the relative coordinate method yielded −7.21 Mev with only 13 functions; the same nuclear parameters were employed in both computations. In the same paper, the ground state of the alpha-particle was treated, but only in individual particle coordinates. The first part of this communication deals with the same problem and yields results which are in a sense complementary to those previously published. Besides confirming them it shows again the superiority of the relative coordinate method which, with the use of 11 functions, yields an answer better than that of the other method involving 14 rather more complicated functions. In view of this double evidence we may now estimate the true energy of the He^4 problem, and also that of H^3, more accurately than has been done before, and more definite conclusions can be drawn regarding the consistency of present assumptions about nuclear force constants.

It is generally hoped that, aside from relativity effects,[5] the binding energies of all nuclei can be fitted by a single set of nuclear force parameters. There even appears to be considerable evidence that this can be achieved by employing a Hamiltonian operator which is symmetrical in all particles[6] except for Coulomb forces. This prevailing optimism has been disturbed somewhat by the results of variational calculations on H^3 and He^4, made by Rarita and Present.[7] The present work shows, as did the former paper,[4] that a discrepancy exists, but it is not as alarming as appeared from Rarita and Present's work.

The later sections of this paper are devoted to the excited states of the alpha-particle.[8] Several estimates of the energies of these states have been made,[9] all of a very approximative character. Whereas other authors were led to believe that the P states were probably stable, our calculations, made with a more recent Hamiltonian, decide fairly definitely against their stability. Considerable effort has been made to locate the excited S state of the alpha-particle; it is found to be virtual and to lie at about 1.3 Mev above the dissociation limit.

Throughout the present work the assumption of perfect symmetry of nuclear forces, without distinction between neutrons and protons, has been made.

The Ground State

In central, individual particle coordinates, the potential interaction for all pairs of particles may be written in the general form:

$$V_{ij}=-AJ_{ij}(w+mP_{ij}+bQ_{ij}+hP_{ij}Q_{ij}), \quad (1)$$

where P_{ij} acts on coordinates, Q_{ij} on spins, and w, m, b, and h are the relative strengths of Wigner, Majorana, Bartlett, and Heisenberg forces, respectively. If the coordinate part of the variation functions is chosen symmetric in like particles, a summation over spins leads to an interaction:[10]

$$\begin{aligned}(V_{ij})_1&=-AJ_{ij}[(w+\tfrac{1}{2}b)+(m+\tfrac{1}{2}h)P_{ij}],\\ (V_{ij})_2&=-AJ_{ij}[(w-b)+(m-h)P_{ij}],\end{aligned} \quad (2)$$

where the subscripts 1 and 2 refer to interactions between pairs of unlike and like particles, respectively.

As in the previous work,[4] the Gaussian form of interaction is used; thus $J_{ij}=\exp(-r_{ij}^2/a^2)$.

It has been pointed out by Breit and Feenberg[11] that the effect of the P_{ij} operators is very small inasmuch as the ground state of the alpha-particle is nearly symmetric in all particles. This will be discussed in more detail later. In the above expressions, the Majorana coefficient is predominant. Therefore it will be a good

[5] G. Breit, Phys. Rev. **53**, 153 (1938).
[6] M. A. Tuve, N. P. Heydenburg and L. R. Hafstad, Phys. Rev. **50**, 806 (1936); G. Breit, E. U. Condon, R. D. Present, Phys. Rev. **50**, 825 (1936); E. Wigner, Phys. Rev. **51**, 106 (1936).
[7] W. Rarita and R. D. Present, Phys. Rev. **51**, 788 (1937).
[8] When this manuscript was completed there appeared a paper by S. S. Share, Phys. Rev. **53**, 875 (1938), which contains some of the results here obtained. Since our method of attack is different, a more general Hamiltonian has been used, and the excited S state has been investigated in greater detail, we are persuaded not to withdraw these sections from publication. Share's result on the excited S state of He^4 is not significant because his energy does not represent an upper limit. Our result does represent such a limit.
[9] E. Feenberg, Phys. Rev. **49**, 328 (1936); Bethe and Bacher, Rev. Mod. Phys. **8**, 82 (1936).
[10] This is obvious for like particles; for unlike particles, cf. Bethe and Bacher, Rev. Mod. Phys. **8**, 82 (1936).
[11] G. Breit and E. Feenberg, Phys. Rev. **50**, 850 (1936).

approximation to write

$$(V_{ij})_1 = -AJ_{ij}[w+m+\tfrac{1}{2}(b+h)]P_{ij} = -BJ_{ij}P_{ij},$$
$$(V_{ij})_2 = -AJ_{ij}[w+m-(b+h)]P_{ij} = -CJ_{ij}P_{ij}. \quad (3)$$

If now $b+h=g$, then $B=(1-\frac{1}{2}g)A$, $C=(1-2g)A$.

The Coulomb energy, small compared with the total energy, will be omitted from the variational calculation and taken into account afterwards. Hence the Hamiltonian in central, individual particle coordinates is

$$H=-(\hbar^2/2M)\sum_i \nabla_i^2 - B\sum_{ij}{}_1 J_{ij}P_{ij} - C\sum_{ij}{}_2 J_{ij}P_{ij}, \quad (4)$$

where $\sum_1$ is extended over pairs of unlike, and $\sum_2$ over pairs of like particles. This is the same Hamiltonian which was employed for H^3 (cf. Eq. (2), reference 4).

In order to facilitate comparison of the present work with the results for H^3, the following values of the constants have been assumed:

$$A=35.60 \text{ Mev}, \quad a=2.25\times10^{-13} \text{ cm}, \quad g=0.194$$

which give

$$B=32.10 \text{ Mev}, \quad C=21.77 \text{ Mev}.$$

The transformation to relative coordinates is:

$$\boldsymbol{\varrho}_1=(\tfrac{1}{2})^{\frac{1}{2}}(\mathbf{r}_1+\mathbf{r}_2-\mathbf{r}_3-\mathbf{r}_4);$$
$$\boldsymbol{\varrho}_2=(\tfrac{1}{2})^{\frac{1}{2}}(\mathbf{r}_1-\mathbf{r}_2); \quad \boldsymbol{\varrho}_3=(\tfrac{1}{2})^{\frac{1}{2}}(\mathbf{r}_3-\mathbf{r}_4). \quad (5)$$

Since this transformation, the interaction J_{ij}, and, as will be seen below, the form of variation function are all symmetric with respect to the Cartesian axes, attention may be confined to the scalar X component equations in much of what follows. Taking ξ_i, η_i, ζ_i to be the rectangular components of the relative vectors $\boldsymbol{\varrho}_i$, we find:

$$x_{12}=2^{\frac{1}{2}}\xi_2; \qquad x_{13}=(\tfrac{1}{2})^{\frac{1}{2}}(\xi_1+\xi_2-\xi_3)$$
$$x_{14}=(\tfrac{1}{2})^{\frac{1}{2}}(\xi_1+\xi_2+\xi_3); \quad x_{23}=(\tfrac{1}{2})^{\frac{1}{2}}(\xi_1-\xi_2-\xi_3)$$
$$x_{24}=(\tfrac{1}{2})^{\frac{1}{2}}(\xi_1-\xi_2+\xi_3); \quad x_{34}=2^{\frac{1}{2}}\xi_3.$$

This leads to Table I, which gives the effect of the permutation operators P_{ij} upon the ξ_i.

The Hamiltonian may now be written in relative coordinates. Eq. (4) becomes

$$\begin{aligned} H=&-(\hbar^2/2M)(2\nabla_1^2+\nabla_2^2+\nabla_3^2) \\ &-B\{\exp[-\tfrac{1}{2}\tau(\boldsymbol{\varrho}_1+\boldsymbol{\varrho}_2-\boldsymbol{\varrho}_3)^2]P_{13} \\ &+\exp[-\tfrac{1}{2}\tau(\boldsymbol{\varrho}_1+\boldsymbol{\varrho}_2+\boldsymbol{\varrho}_3)^2]P_{14} \\ &+\exp[-\tfrac{1}{2}\tau(\boldsymbol{\varrho}_1-\boldsymbol{\varrho}_2-\boldsymbol{\varrho}_3)^2]P_{23} \\ &+\exp[-\tfrac{1}{2}\tau(\boldsymbol{\varrho}_1-\boldsymbol{\varrho}_2+\boldsymbol{\varrho}_3)^2]P_{24}\} \\ &-C\{\exp[-2\tau\boldsymbol{\varrho}_2^2]P_{12} \\ &\qquad +\exp[-2\tau\boldsymbol{\varrho}_3^2]P_{34}\}, \end{aligned} \quad (6)$$

where $\tau=1/a^2$. Eq. (6) is symmetric with respect to an interchange of coordinates 2 and 3. This necessitates the use of variation functions symmetric in coordinates 2 and 3, because the ground state of He^4 is nondegenerate and hence possesses the same symmetry as the Hamiltonian. Furthermore, an interchange of the protons (particles 1 and 2), or of the neutrons causes a change of sign in $\boldsymbol{\varrho}_2$ or $\boldsymbol{\varrho}_3$, respectively. Therefore, all variation functions must be even functions of relative coordinates 2 and 3, in order that they may be symmetric coordinate functions.

As in the work on H^3, single harmonic oscillator functions are employed for variation functions. The notation for these functions is as follows: Single Hermite functions are written

$$\varphi_n(p^{\frac{1}{2}}x)=\varphi_n{}^p(x)=N_{n,p}\exp(-px^2/2)H_n(p^{\frac{1}{2}}x),$$

where $N_{n,p}$ is a normalizing factor, H_n is a Hermite polynomial, and x may be any of the rectangular components of $\boldsymbol{\varrho}_1$, $\boldsymbol{\varrho}_2$, $\boldsymbol{\varrho}_3$. Then we define

$$\varphi_{lmn}(i)=\varphi_l(\xi_i)\varphi_m(\eta_i)\varphi_n(\zeta_i),$$

and these functions can be symmetrized with respect to the Cartesian axes by forming

$$\phi_{lmn}=(\tfrac{1}{6})^{\frac{1}{2}}(1+\delta_{lm}+\delta_{ln}+\delta_{mn}+2\delta_{lm}\delta_{ln}\delta_{mn})^{-\frac{1}{2}}$$
$$\times(\varphi_{lmn}+\varphi_{lnm}+\varphi_{nlm}+\varphi_{mln}+\varphi_{mnl}+\varphi_{nml}). \quad (7)$$

TABLE I. *The effect of the P_{ij} operators upon the ξ_i.*

P_{ij}	$P_{ij}\xi_1$	$P_{ij}\xi_2$	$P_{ij}\xi_3$
P_{12}	ξ_1	$-\xi_2$	ξ_3
P_{13}	$-\xi_2+\xi_3$	$\frac{1}{2}(-\xi_1+\xi_2+\xi_3)$	$\frac{1}{2}(\xi_1+\xi_2+\xi_3)$
P_{14}	$-\xi_2-\xi_3$	$\frac{1}{2}(-\xi_1+\xi_2-\xi_3)$	$\frac{1}{2}(-\xi_1-\xi_2+\xi_3)$
P_{23}	$\xi_2+\xi_3$	$\frac{1}{2}(\xi_1+\xi_2-\xi_3)$	$\frac{1}{2}(\xi_1-\xi_2+\xi_3)$
P_{24}	$\xi_2-\xi_3$	$\frac{1}{2}(\xi_1+\xi_2+\xi_3)$	$\frac{1}{2}(-\xi_1+\xi_2+\xi_3)$
P_{34}	ξ_1	ξ_2	$-\xi_3$

The variation parameters p determine the classical potentials for the oscillator functions; since all variation functions are chosen symmetric in coordinates 2 and 3, two, rather than three such parameters are needed. In the work that follows, it will be implicit that p is the parameter for coordinate 1 and q for coordinates 2 and 3. To give an explicit example of the notation employed,

$$\phi_{200}(1)\phi_{000}(2)\phi_{000}(3)=(\tfrac{1}{3})^{\frac{1}{2}}[\varphi_2{}^p(\xi_1)\varphi_0{}^p(\eta_1)\varphi_0{}^p(\zeta_1)+\varphi_0{}^p(\xi_1)\varphi_2{}^p(\eta_1)\varphi_0{}^p(\zeta_1)+\varphi_0{}^p(\xi_1)\varphi_0{}^p(\eta_1)\varphi_2{}^p(\zeta_1)]\times\varphi_0{}^q(\xi_2)\varphi_0{}^q(\eta_2)\varphi_0{}^q(\zeta_2)\times\varphi_0{}^q(\xi_3)\varphi_0{}^q(\eta_3)\varphi_0{}^q(\zeta_3).$$

The single function which gives the lowest energy is $\psi_0=\phi_{000}(1)\phi_{000}(2)\phi_{000}(3)$, hereinafter designated as the ground state function. No functions have been used variationally which do not combine with the ground state function. This eliminates all functions of odd degree of excitation, and, in addition, certain functions of even degree. As can be readily shown from the nature of the integrals below, in general those functions which do not combine with ψ_0 have also vanishing matrix elements with functions combining with ψ_0. It is thus clear that functions which do not combine with the ground state are unimportant variationally.

A list of all functions of low excitation which combine with ψ_0 follows:

Ground state function:

$$\psi_0=\phi_{000}(1)\phi_{000}(2)\phi_{000}(3)$$

Doubly excited:

$$\phi_{200}(1)\phi_{000}(2)\phi_{000}(3)$$
$$(\tfrac{1}{2})^{\frac{1}{2}}\phi_{000}(1)[\phi_{200}(2)\phi_{000}(3)+\phi_{000}(2)\phi_{200}(3)].$$

Quadruply excited:

$$\phi_{400}(1)\phi_{000}(2)\phi_{000}(3)$$
$$(\tfrac{1}{2})^{\frac{1}{2}}\phi_{000}(1)[\phi_{400}(2)\phi_{000}(3)+\phi_{000}(2)\phi_{400}(3)].$$
$$\phi_{000}(1)\phi_{200}(2)\phi_{200}(3)$$
$$(\tfrac{1}{2})^{\frac{1}{2}}\phi_{200}(1)[\phi_{200}(2)\phi_{000}(3)+\phi_{000}(2)\phi_{200}(3)]$$
$$\phi_{000}(1)\phi_{110}(2)\phi_{110}(3)$$
$$(\tfrac{1}{2})^{\frac{1}{2}}\phi_{110}(1)[\phi_{110}(2)\phi_{000}(3)+\phi_{000}(2)\phi_{110}(3)]$$
$$\phi_{220}(1)\phi_{000}(2)\phi_{000}(3)$$
$$(\tfrac{1}{2})^{\frac{1}{2}}\phi_{000}(1)[\phi_{220}(2)\phi_{000}(3)+\phi_{000}(2)\phi_{220}(3)].$$

Sextuply excited:

$$\phi_{200}(1)\phi_{200}(2)\phi_{200}(3)$$
$$\phi_{600}(1)\phi_{000}(2)\phi_{000}(3)$$
$$(\tfrac{1}{2})^{\frac{1}{2}}\phi_{000}(1)[\phi_{600}(2)\phi_{000}(3)+\phi_{000}(2)\phi_{600}(3)]$$
$$(\tfrac{1}{2})^{\frac{1}{2}}\phi_{400}(1)[\phi_{200}(2)\phi_{000}(3)+\phi_{000}(2)\phi_{200}(3)]$$
$$(\tfrac{1}{2})^{\frac{1}{2}}\phi_{200}(1)[\phi_{400}(2)\phi_{000}(3)+\phi_{000}(2)\phi_{400}(3)]$$
$$(\tfrac{1}{2})^{\frac{1}{2}}\phi_{000}(1)[\phi_{400}(2)\phi_{200}(3)+\phi_{200}(2)\phi_{400}(3)]$$
$$(\tfrac{1}{2})^{\frac{1}{2}}\phi_{220}(1)[\phi_{200}(2)\phi_{000}(3)+\phi_{000}(2)\phi_{200}(3)]$$
$$(\tfrac{1}{2})^{\frac{1}{2}}\phi_{200}(1)[\phi_{220}(2)\phi_{000}(3)+\phi_{000}(2)\phi_{220}(3)]$$
$$(\tfrac{1}{2})^{\frac{1}{2}}\phi_{000}(1)[\phi_{220}(2)\phi_{200}(3)+\phi_{200}(2)\phi_{220}(3)]$$
$$\phi_{200}(1)\phi_{110}(2)\phi_{110}(3)$$
$$(\tfrac{1}{2})^{\frac{1}{2}}\phi_{110}(1)[\phi_{200}(2)\phi_{110}(3)+\phi_{110}(2)\phi_{200}(3)]$$
$$(\tfrac{1}{2})^{\frac{1}{2}}\phi_{310}(1)[\phi_{110}(2)\phi_{000}(3)+\phi_{000}(2)\phi_{110}(3)]$$
$$(\tfrac{1}{2})^{\frac{1}{2}}\phi_{110}(1)[\phi_{310}(2)\phi_{000}(3)+\phi_{000}(2)\phi_{310}(3)]$$
$$(\tfrac{1}{2})^{\frac{1}{2}}\phi_{000}(1)[\phi_{310}(2)\phi_{110}(3)+\phi_{110}(2)\phi_{310}(3)]$$
$$\phi_{222}(1)\phi_{000}(2)\phi_{000}(3)$$
$$(\tfrac{1}{2})^{\frac{1}{2}}\phi_{000}(1)[\phi_{222}(2)\phi_{000}(3)+\phi_{000}(2)\phi_{222}(3)]$$
$$\phi_{420}(1)\phi_{000}(2)\phi_{000}(3)$$
$$(\tfrac{1}{2})^{\frac{1}{2}}\phi_{000}(1)[\phi_{420}(2)\phi_{000}(3)+\phi_{000}(2)\phi_{420}(3)]$$
$$\phi_{110}(1)\phi_{110}(2)\phi_{110}(3)$$
$$(\tfrac{1}{2})^{\frac{1}{2}}\phi_{211}(1)[\phi_{110}(2)\phi_{000}(3)+\phi_{000}(2)\phi_{110}(3)]$$
$$(\tfrac{1}{2})^{\frac{1}{2}}\phi_{110}(1)[\phi_{211}(2)\phi_{000}(3)+\phi_{000}(2)\phi_{211}(3)]$$
$$(\tfrac{1}{2})^{\frac{1}{2}}\phi_{000}(1)[\phi_{211}(2)\phi_{110}(3)+\phi_{110}(2)\phi_{211}(3)].$$

There are 61 octuply excited functions which could be added to the list. The importance of these and higher excited functions will be discussed later.

The evaluation of the matrix element $H_{ij}=\int\psi_i H\psi_j d\tau$ divides into three parts: the evaluation of the kinetic energy, the unlike particle interaction, and the like particle interaction.

To find the kinetic energy, it is to be noted that the function

$$\psi=\varphi_{n_{\xi_1}}(p^{\frac{1}{2}}\xi_1)\varphi_{n_{\eta_1}}(p^{\frac{1}{2}}\eta_1)\varphi_{n_{\zeta_1}}(p^{\frac{1}{2}}\zeta_1)\times\varphi_{n_{\xi_2}}(q^{\frac{1}{2}}\xi_2)\cdots\varphi_{n_{\zeta_3}}(q^{\frac{1}{2}}\zeta_3)$$

satisfies the equation

$$(h^2/2M)\{-(2\nabla_1{}^2+\nabla_2{}^2+\nabla_3{}^2)+[2p^2\rho_1{}^2+q^2(\rho_2{}^2+\rho_3{}^2)]\}\psi=E\psi,$$

and the eigenvalues are

$$E(n_{\xi_1}\cdots n_{\zeta_3}) = (\hbar^2/M)[(\sum_{\xi\eta\zeta} n_1 + \tfrac{3}{2})2p + \tfrac{1}{2}\sum_{\xi\eta\zeta}(n_2+n_3)+3\tfrac{1}{2}q]. \quad (8)$$

Hence

$$(E_{\text{kin}})_{ij} = \int \psi_i[-(\hbar^2/2M)(2\nabla_1^2+\nabla_2^2+\nabla_3^2)]\psi_j d\tau$$

$$= E\delta_{ij} - (\hbar^2/2M)\int \psi_i[2p^2\rho_1^2 + q^2(\rho_2^2+\rho_3^2)]\psi_j d\tau, \quad (9)$$

since the functions are orthogonal and normalized. Moreover, the last part of Eq. (9),

$$2p\int \psi_i p\rho_1^2\psi_j d\tau + q\int \psi_i q\rho_2^2\psi_j d\tau + q\int \psi_i q\rho_3^2\psi_j d\tau,$$

breaks up into integrals of the form

$$\int \varphi_i{}^p(\xi) p\xi^2 \varphi_j{}^p(\xi) d\xi \equiv \lambda_{ij} = (i+\tfrac{1}{2})\delta_{ij} + \tfrac{1}{2}[(i+1)(i+2)]^{\frac{1}{2}}\delta_{j,\,i+2},$$

so that the matrix elements of the kinetic energy can be written as sums of various λ_{ij}.

If we set

$$R_{ij} \equiv \int \psi_i \exp[-\tfrac{1}{2}\tau(\varrho_1+\varrho_2+\varrho_3)^2]P_{14}\psi_j d\tau,$$

$$S_{ij} \equiv \int \psi_i \exp[-\tfrac{1}{2}\tau(\varrho_1+\varrho_2-\varrho_3)^2]P_{13}\psi_j d\tau,$$

$$T_{ij} \equiv \int \psi_i \exp[-\tfrac{1}{2}\tau(\varrho_1-\varrho_2-\varrho_3)^2]P_{23}\psi_j d\tau,$$

$$U_{ij} \equiv \int \psi_i \exp[-\tfrac{1}{2}\tau(\varrho_1-\varrho_2+\varrho_3)^2]P_{24}\psi_j d\tau,$$

then the unlike particle interaction part of H_{ij} is

$$-B(R_{ij}+S_{ij}+T_{ij}+U_{ij}).$$

R_{ij} may be written as the product of three integrals, one for each rectangular component. Replacing $(\psi_i)_x$ and $(\psi_j)_x$ by ϕ_{lmn} functions, we see that the basic integral is

$$r_{ijk,\,lmn} = \int \varphi_i{}^p(\xi_1)\varphi_j{}^q(\xi_2)\varphi_k{}^q(\xi_3) \times \exp[-\tfrac{1}{2}\tau(\xi_1+\xi_2+\xi_3)^2]P_{14}\varphi_l{}^p(\xi_1) \times \varphi_m{}^q(\xi_2)\varphi_n{}^q(\xi_3)d\xi_1 d\xi_2 d\xi_3$$

and that then R_{ij} is expressible as a sum of products of three $r_{ijk,\,lmn}$. To facilitate integration, a transformation

$$\xi_1 = s; \quad \xi_2 = \tfrac{1}{2}(u+t); \quad \xi_3 = \tfrac{1}{2}(u-t) \quad (10)$$

is made; Table II gives the effect of the P_{ij} operators upon ξ_i in terms of u, s, t.

The effect of the P_{ij} operators upon $\varphi_l\varphi_m\varphi_n$ can be expressed by their effect upon the arguments of these functions; hence

$$r_{ijk,\,lmn} = \int \varphi_i{}^p(s)\varphi_j{}^q\left(\frac{u+t}{2}\right)\varphi_k{}^q\left(\frac{u-t}{2}\right) \times \exp(-\tfrac{1}{2}\tau(s+u)^2)\varphi_l{}^p(-u) \times \varphi_m{}^q\left(\frac{t-s}{2}\right)\varphi_n{}^q\left(\frac{-t-s}{2}\right)dsdtdu,$$

$$= \tfrac{1}{2}\int H_i(p^{\frac{1}{2}}s)\cdots H_l(-p^{\frac{1}{2}}u)\cdots I ds dt du,$$

where

$$I \equiv \varphi_0{}^p(s)\varphi_0{}^q\left(\frac{u+t}{2}\right)\varphi_0{}^q\left(\frac{u-t}{2}\right)\varphi_0{}^p(-u) \times \varphi_0{}^q\left(\frac{t-s}{2}\right)\varphi_0{}^q\left(\frac{-t-s}{2}\right)\exp(-\tfrac{1}{2}\tau(s+u)^2),$$

and $\frac{1}{2}$ is the Jacobian of the transformation. From the form of I, it may be seen that $r_{ijk,\,lmn}$ vanishes unless $i+j+k$ is of the same parity as $l+m+n$.

A similar procedure is carried through for S_{ij}, T_{ij}, U_{ij}, which gives basic integrals $s_{ijk,\,lmn}$, $t_{ijk,\,lmn}$, $u_{ijk,\,lmn}$, respectively, which the reader can easily construct with the aid of Table II.

In the integrand of $s_{ijk,\,lmn}$, u and t may be interchanged. This makes $s_{ijk,\,lmn}$ identical with $r_{ijk,\,lmn}$, except that the arguments of φ_k and φ_n are reversed in sign. Hence

$$s_{ijk,\,lmn} = (-1)^{k+n} r_{ijk,\,lmn}. \quad (11a)$$

TABLE II. *The effect of P_{ij} upon ξ_i in terms of u, s, t.*

P_{ij}	$P_{ij}\xi_1$	$P_{ij}\xi_2$	$P_{ij}\xi_3$
P_{12}	s	$-\frac{1}{2}(u+t)$	$\frac{1}{2}(u-t)$
P_{13}	$-t$	$\frac{1}{2}(-s+u)$	$\frac{1}{2}(s+u)$
P_{14}	$-u$	$\frac{1}{2}(-s+t)$	$-\frac{1}{2}(s+t)$
P_{23}	u	$\frac{1}{2}(s+t)$	$\frac{1}{2}(s-t)$
P_{24}	t	$\frac{1}{2}(s+u)$	$\frac{1}{2}(-s+u)$
P_{34}	s	$\frac{1}{2}(u+t)$	$\frac{1}{2}(t-u)$

In the integrand of $t_{ijk,\ lmn}$, a change of the signs of t and u throughout yields

$$t_{ijk,\ lmn}=(-1)^{i+k+m+n}r_{ijk,\ lmn}, \tag{11b}$$

and by similar reasoning we find

$$u_{ijk,\ lmn}=(-1)^{i+m}r_{ijk,\ lmn}. \tag{11c}$$

It will be noted that

$$-B(R_{ij}+S_{ij}+T_{ij}+U_{ij})=-4BR_{ij} \text{ or } 0, \tag{11d}$$

depending upon the values of j, k, m, n in the basic integrals encountered. These rules make it easy to pick out functions which combine with each other. Lists of over 100 of the various $r_{ijk,\ lmn}$ have been prepared, but will not be reproduced here.

If we put

$$V_{ij}\equiv\int\psi_i\exp[-2\tau\rho_2^2]P_{12}\psi_j d\tau$$

$$W_{ij}\equiv\int\psi_i\exp[-2\tau\rho_3^2]P_{34}\psi_j d\tau,$$

then the like particle interaction part of H_{ij} is

$$-C(V_{ij}+W_{ij}).$$

V_{ij} is the product of three integrals, one for each rectangular axis; and it is necessary to consider only one of them. P_{12} leaves ξ_1 and ξ_3 unchanged (cf. Table I); integration over ξ_1 and ξ_3 yields unity. Now let

$$v_{ij}\equiv\int\varphi_i{}^q(\xi_2)\exp[-2\tau\xi_2^2]P_{12}\varphi_j{}^q(\xi_2)d\xi_2$$

$$=\int H_i(q^{\frac{1}{2}}\xi_2)H_j(-q^{\frac{1}{2}}\xi_2)$$

$$\times[\varphi_0{}^q(\xi_2)\varphi_0{}^q(-\xi_2)\exp(-2\tau\xi_2^2)]d\xi_2.$$

Then V_{ij} will be expressible as a sum of products of three v_{ij}. From the form of the bracketed expression, it may be proved that v_{ij} vanishes unless i is of the same parity as j. Only eight different v_{ij} appear in V_{ij} for all the doubly and quadruply excited variation functions listed above.

Furthermore, $W_{ij}=V_{ij}$ because all functions ψ_i are symmetric in relative coordinates 2 and 3.

When Wigner forces are introduced, integrals of the types above without exchange operators are needed. These can of course be calculated in a similar manner, or more directly without the use of the transformation (10). In the following, integrals will be understood to refer to Majorana forces if no further designation is given. When the necessity for distinction arises, integrals involving Wigner and Majorana forces will be labeled by superscripts W and M, respectively. It is to be noted here that the relations (11) hold for Wigner terms also.

In order to obtain the variational energy, we must solve for the lowest root E_1 of the determinantal equation $|H_{ij}-\delta_{ij}E|=0$. It is obviously too laborious to retain p and q as variation parameters throughout the solution. However, the minimum of H_{00} occurs at $2p=q=0.5135$, and H_{00} accounts for most of the binding energy. Therefore the values of p and q which minimize E_1 will not differ appreciably from these values, and it is safe to evaluate H_{ij} at the minimum of H_{00}, before insertion in the determinant. This procedure has been followed here; the numerical method of solving the secular equation has been outlined elsewhere.[4]

Since the numerical values of H_{0i} are available from the variational calculation, it is very simple also to make a second order Schrödinger perturbation calculation by use of the same functions. In this scheme, the additional energy is

$$E^{(2)}=\sum_i{}'\frac{H_{0i}{}^2}{E_0-E_i}$$

and it is clear from Eq. (8) that

$$E_0-E_i=-\frac{\hbar^2}{M}\sum\{(n_i)_\xi+(n_i)_\eta+(n_i)_\zeta\}q,$$

if $q=2p$. Thus the denominator will be the same for all functions of the same degree of excitation.

TABLE III. *Results of variational and perturbational calculations for the ground state of* He^4 *(in Mev).*

No. of Functions	E_1	E_1-H_{00}	$E^{(2)}$	$\frac{E_1-H_{00}}{E^{(2)}}$
4	−26.29	−0.60	−0.50	1.20
5	−26.41	−0.72	−0.59	1.22
8	−26.52	−0.83	−0.74	1.12
11	−26.76	−1.07	−0.81	1.32
33			−0.93	

Table III lists the results of the variational and perturbational calculations. The most elaborate variational calculation has been made with the ground state function and all the doubly and quadruply excited functions, a total of 11 variation functions. The result is in excellent agreement with a former calculation[4] by an entirely independent scheme (individual particles coordinates) which gave −26.67 Mev.

It will be seen that the variation method gives a lowering of the total energy slightly greater than that of second order perturbation theory with the same set of functions. The ratio between the contributions varies somewhat irregularly for different stages of the calculation; after inclusion of all the quadruply excited functions, it is 1.32. By adjusting the perturbational energy for all the sextuply excited functions, we feel that a close estimate of the variational energy due to these functions (in relative coordinates) may be obtained; multiplication of 0.12 by 1.32 yields 0.16 Mev for this estimate.

The division of functions into classes of various degrees of excitation is quite dependent upon the type of coordinates employed; in relative coordinates, the set of sextuply excited functions is equivalent to some of the sextuply excited, and many of the octuply excited functions in individual particle coordinates. Hence 0.16 Mev also represents a *rough* estimate of the effect of octuply excited functions in individual particle coordinates. We may at least say, then, that octuply excited states make a very small contribution to the total energy of the alpha-particle. This is not true in the deuteron problem.[12]

Perturbational results show that functions higher than octuply excited have a negligible effect upon the ground state. Thus, allowing a contribution of −0.33 Mev for the effect of sextuply and octuply excited states, we obtain −27.09 Mev as a fairly close estimate for the convergence limit of the variational energy. The Coulomb energy is +0.82 Mev; therefore the final figure for the energy of the ground state of He^4 is −26.27 Mev.

As already mentioned, the foregoing results involve the approximation of treating the Wigner part of (2) as though it were a Majorana operator. The effect of this approximation may be easily traced through the first-order calculation leading to H_{00}. Since it is small in H_{00}, it will be completely neglected in the higher contributions.

Let H be the operator (4), used in this work, and $\mathfrak{H}$ the same operator, but without the P_{ij}'s. Then H_{00} and $\mathfrak{H}_{00}$ will in general have separate minima.[13] If $B=C$, the two minima coincide and occur at $\lambda=1$. In that case no correction at all is necessary. For the values of B and C adopted in this paper, this coincidence is not quite present. But it is seen from Fig. 1, where both H_{00} and $\mathfrak{H}_{00}$ are plotted as functions of λ at the minimum with respect to σ, that the correction is small indeed. To give an idea of the correction required in the worst possible case ($C=0$) we have plotted similar curves representing that situation in the lower part of Fig. 1. It is seen that even there the two minima differ by less than $\frac{1}{2}$ Mev in energy. Hence it is clear that the effect of ignoring the "ordinary" constituent of the nuclear forces is quite inappreciable in dealing with the ground state of He^4. The same is true for H^3.

It is now possible to test the adequacy of the symmetrical Hamiltonian in reference to the two important problems: H^3 and He^4. The present results and those obtained previously[4] are gained with the same nuclear constants, and by the same method. We feel that the value of the binding energy of He^4 here derived probably represents a closer estimate than that for H^3. On the other hand, further experience with the present method has led us to believe that the margin of uncertainty in its convergence for H^3

[12] D. T. Warren and H. Margenau, Phys. Rev. **52**, 1027 (1937).

[13] Algebraic expressions for H_{00} and $\mathfrak{H}_{00}$ may be found in the papers of Wigner, Phys. Rev. **43**, 252 (1933), Feenberg, Phys. Rev. **47**, 850 (1935) and others. For the definition of the variation parameters λ and σ see Eq. (13).

is far smaller than was judged by Margenau and Warren. We prefer to assume that the result for the binding energy of H^3 is 7.3 Mev (7.21 being actually obtained variationally). If it is *greater*, the discrepancy (Eqs. (12)) to which this analysis leads, will be *less* pronounced.[14]

Slight adjustments in the constants B and C will not change the contributions of the higher variation functions appreciably. We shall therefore inquire what changes in B and C are necessary so that H_{00}, computed with the adjusted values of these parameters, plus the uncorrected higher contributions, shall equal the observed binding energies for both H^3 and He^4. Table IV shows the procedure. The last row shows the energy to be accounted for by the ground state function ψ_0.* Working with the minimizing values of λ and σ we then determine B and C from the equations for H_{00}.

$$\left.\begin{aligned} H^3: &\quad -7.20 = 22.09 - 0.669B - 0.314C \\ He^4: &\quad -27.0 = 47.37 - 1.70B - 0.850C \end{aligned}\right\}.$$

They yield:

$$\begin{aligned} H^3: &\quad B = 32.6 \text{ Mev}, \quad C = 23.8 \text{ Mev}, \\ He^4: &\quad B = 32.4 \text{ Mev}, \quad C = 22.0 \text{ Mev}, \end{aligned}$$

which reveal a slight inconsistency. Remembering that $B = (1 - \frac{1}{2}g)A$, $C = (1 - 2g)A$, we find

$$H^3: \quad g = 0.167, \quad He^4: \quad g = 0.181. \qquad (12)$$

It is to be noted first that these values of g are considerably smaller than that usually derived from the $^1S - {}^3S$ energy spacing of the deuteron states.

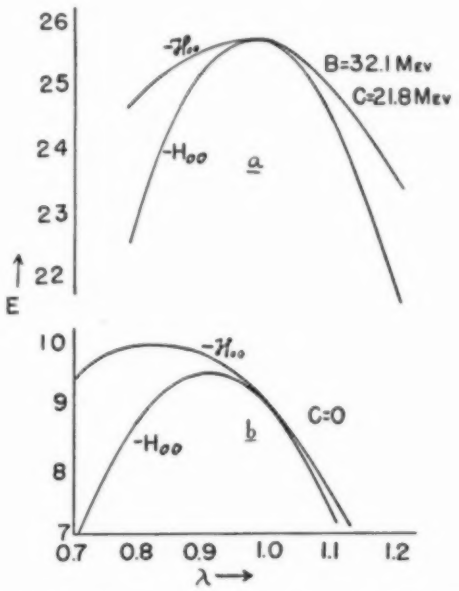

FIG. 1. Variational binding energy of He^4 in *zeroth* approximation with (H_{00}) and without ($\mathfrak{H}_{00}$) exchange forces: (a) $B = 32.1$ Mev, $C = 21.77$ Mev; (b) $B = 32.1$ Mev, $C = 0$.

The significance of the discrepancy inherent in (12) is best seen by computing the binding energies of H^3 and He^4 with an artificial *mean* value of g, equal to 0.174. This yields 8.1 Mev and 28.3 Mev, which differ from the experimental results by -0.2 and $+0.7$ Mev, respectively. The discrepancy has the same sense as that found by Rarita and Present, but is less severe. It is to be noted, however, that this improved agreement involves the use of a value of g which differs considerably from that of Rarita and Present (0.215), and one which leads to a stable singlet state of the deuteron. We may thus say: The strong discrepancy in the binding energy of light nuclei emphasized by Rarita and Present may be made much less pronounced by choosing a smaller value of the ratio of Heisenberg to Majorana forces. In fact, by taking g as small as 0.174 the discrepancy almost vanishes. While it is unlikely that such a value is compatible with

TABLE IV. *Computation of* H_{00}.

	H^3	He^4
Experimental energy	−8.3	−27.6
Coulomb energy	0	+ 0.8
Contributions from functions other than ψ_0	−1.1	− 1.4
H_{00}	−7.2	−27.0

[14] In his review article Breit (Rev. Sci. Inst. 9, 63 (1939)) mentions the existence of a disagreement between the results of Rarita and Present and those of Margenau and Warren. We fear that excessive caution on the part of the latter authors in estimating the convergence limit of their method is responsible for this impression. The numerical results certainly show no contradiction, for, with the adopted set of constants Margenau and Warren obtained binding energies of 7.21 for H^3 and 25.85 for He^4. If these had been taken at face value the same qualitative conclusion as that drawn by Rarita and Present would have resulted, as was stated. Whether one method converges faster than the other is at present unknown, and all estimates of convergence limits must be regarded as plausible subjective judgments. A direct quantitative comparison of the results of the two papers in question is not feasible because of the different form of the potentials adopted.

* We are neglecting (a) the effect of states in which the spins are distributed differently among the particles; (b) relativity corrections. (a) is of the same magnitude as the estimated error in the convergence limit; (b) is probably appreciable but at present impossible to calculate uniquely.

scattering data, a compromise value around 0.19 might bring the discrepancy within the range of errors caused by the neglect of relativity and other corrections.

Excited S State

We are concerned here with an excited state possessing the same symmetry as the ground state. An upper bound to the position of the state may therefore be obtained by solving $|H_{ij}-\delta_{ij}E|=0$ for E_2, the next highest root above E_1. It is not possible, however, to find any one variation function for which H_{ii} is a *good* approximation to E_2. Hence we cannot use the minimization procedure which was followed in locating E_1; instead, it is necessary to minimize E_2 directly with respect to one or both of the variation parameters.

Careful study was made with the following set of functions in relative coordinates:

$$\psi_0=\phi_{000}(1)\phi_{000}(2)\phi_{000}(3)$$

$$\psi_1=(\tfrac{1}{2})^{\frac{1}{2}}\phi_{000}(1)[\phi_{200}(2)\phi_{000}(3)+\phi_{000}(2)\phi_{200}(3)]$$

$$\psi_2=\phi_{200}(1)\phi_{000}(2)\phi_{000}(3)$$

$$\psi_3=(\tfrac{1}{2})^{\frac{1}{2}}\phi_{000}(1)[\phi_{400}(2)\phi_{000}(3)+\phi_{000}(2)\phi_{400}(3)].$$

The Hamiltonian given by Eq. (6) was used; the matrix elements may then be evaluated by the technique developed for the ground state. Instead of the variation parameters p and q, it is more convenient to write

$$p=(2-\lambda)\sigma\tau;\quad q=2\lambda\sigma\tau. \tag{13}$$

Of the ten matrix elements involving the foregoing functions, we shall give here only the three diagonal ones which seem of principal interest, and omit the others because of their length.

Let

$$r\equiv r_{000,\,000}=\lambda^{\frac{1}{2}}(2-\lambda)^{\frac{1}{2}}\left(\frac{\sigma}{\sigma+1}\right)^{\frac{1}{2}}$$
$$v\equiv v_{00}=\left(\frac{\lambda\sigma}{\lambda\sigma+1}\right)^{\frac{1}{2}}. \tag{14}$$

Then:

$$H_{00}=3(2+\lambda)(4.05)\sigma-4Br^3-2Cv^3,$$

$$H_{11}=(6+7\lambda)(4.05)\sigma-4B\left[\frac{5}{4}-\frac{3}{2}\lambda\left(\frac{\sigma+\frac{1}{2}}{\sigma+1}\right)+\frac{3}{4}\lambda^2\frac{\sigma^2+\sigma+5/12}{(\sigma+1)^2}\right]r^3-2C\left[\frac{\lambda^2\sigma^2+\lambda\sigma+5/4}{(\lambda\sigma+1)^2}\right]v^3$$

$$H_{22}=(14-\lambda)(4.05)\sigma-4B\left[\frac{3}{2}-3(2-\lambda)\left(\frac{\sigma+\frac{1}{2}}{\sigma+1}\right)+\frac{3}{2}(2-\lambda)^2\frac{\sigma^2+\sigma+5/12}{(\sigma+1)^2}\right]r^3-2Cv^3,$$

where 4.05 Mev has been put for $\hbar^2\tau/2M$.

A preliminary investigation showed that ψ_1 contributes the most to the excited S state, since H_{11} lies lower than any other H_{ii} except H_{00}. In fact, it possesses a minimum, which, however, is not to be interpreted as an excited state, for H_{11} is quite different from the second root, E_2. The position of the latter results from a compromise between the tendency of ψ_0 to raise H_{11}, and that of the higher functions to depress it.

The lowest curve for H_{11} *vs.* σ is obtained by putting $\lambda=\frac{2}{3}$ (which corresponds to $p=q$). Accordingly, all matrix elements in the secular equation are evaluated at $\lambda=\frac{2}{3}$; it then becomes necessary to find E_2 as a function of σ. It is possible, of course, that E_2 has a groove for a somewhat different value of λ, but a detailed study of this matter has not seemed to us worth while.

Figure 2 shows the dependence of H_{11} and E_2 upon σ. It is seen that E_2 shows a shallow minimum at about $\sigma=0.425$, and the value of E_2 is 1.3 Mev at this minimum. We believe that the inclusion of further functions in the variational calculation would not lower this minimum appreciably; it is questionable that it would be pushed into the discrete spectrum at all.

This state is not stable against disintegration into H^3+p, or into He^3+n, or into two deuterons. If virtual, the level is not even stable against disintegration into four particles. However, $1/\sigma^{\frac{1}{2}}$ is a measure of the mean distance of separation of the particles in units a: Fig. 2 is equivalent to a plot of total energy *vs.* distance. Hence, as we bring the particles together, there is a shallow

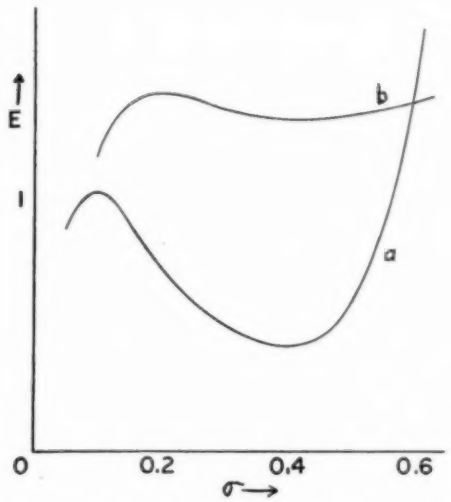

FIG. 2. Energy of excited S state in Mev for $\lambda=\frac{3}{4}$. a: H_{11}; b: Second root, E_2.

minimum in which they may vibrate. The minimizing value of σ for the ground state is 1.3; thus, for the excited S state, the mean distance of separation of the particles is about 1.75 times as great as for the ground state.

The existence of this theoretically predicted excited state is, of course, of no importance in nuclear statics; but it should give rise to a resonance peak in certain scattering and disintegration processes, as, for example, in the deuteron-deuteron reaction.

SINGLET P STATE

P states are odd in one coordinate and do not combine with the ground state of the alpha-particle. Therefore in determining the energy of the lowest P state, the variational method is just as easy to apply as in working for the ground state; it is merely necessary to select functions of the proper symmetry and to solve for the lowest root of the determinantal equation. It is not quite proper to use the Hamiltonian in the simple form (3). Nevertheless, this will be done at present; the result will then be subject to corrections which, as we shall show, are small.

Two classes of ${}^1P$ states are to be considered: (1) those in which the center of mass of the two neutrons moves with a unit of angular momentum relative to the center of mass of the two protons; (2) the states in which one pair of particles is unexcited while the other is in a P state. A representative of the first class is the function

$$\psi_1=\phi_{100}(1)\phi_{000}(2)\phi_{000}(3)$$

while

$$\psi_1'=(\tfrac{1}{2})^{\frac{1}{2}}\phi_{000}(1)[\phi_{100}(2)\phi_{000}(3)+\phi_{000}(2)\phi_{100}(3)]$$

refers to the latter class.[15] Since we are still dealing with singlet states, the spin functions are the same as in the previous work. ψ_1 and ψ_1' do not combine, nor do the variation functions which improve the one, combine with the other. ψ_1 leads to the variational energy

$$H_{11}=\int\psi_1 H\psi_1 d\tau=4.05(10+\lambda)\sigma-4B\left[1-\frac{\lambda}{2(\sigma+1)}\right]r^3-2Cv^3.$$

ψ_1' gives

$$H_{11}'=4.05(6+5\lambda)\sigma-2B\left[1+\frac{\lambda}{4(\sigma+1)}\right]r^3-C\left(\frac{1}{\lambda\sigma+1}\right)v^3.$$

The factor 4.05 here is again simply the value of $\hbar^2\tau/2M$ in Mev, and r and v are defined in (14). Both of these expressions are quite similar in dependence on λ and σ; in particular, neither goes below zero for any permitted value of the variation parameters. There is, to be sure, a groove, but no basin in $\lambda-\sigma$ space. Because of this similarity of behavior, ψ_1' was at this point dismissed from further investigation, and attention was concentrated on the changes which would occur in H_{11} if a greater number of functions were included in the variational calculation. The following were chosen for this purpose:

$$\psi_2=(\tfrac{1}{2})^{\frac{1}{2}}\phi_{100}(1)[\phi_{200}(2)\phi_{000}(3)+\phi_{000}(2)\phi_{200}(3)],$$

$$\psi_3=(\tfrac{1}{2})^{\frac{1}{2}}\phi_{100}(1)[\phi_{110}(2)\phi_{000}(3)+\phi_{000}(2)\phi_{110}(3)].$$

To minimize the energy obtained with the use of these functions with respect to both λ and σ independently would entail a great amount of labor; we have therefore permitted ourselves the following plausible short cut. The greatest contribution to the variational energy comes from ψ_1, which has a minimum with respect to λ ("groove") at $\lambda=1$. The position of this mini-

[15] The symmetrization of ϕ_{100}, as indicated by (7), is here quite unnecessary, but harmless. It was used in this work because the formulae involving these symmetrized functions were already available. Thus ψ_1 really represents a superposition of 3 degenerate P states.

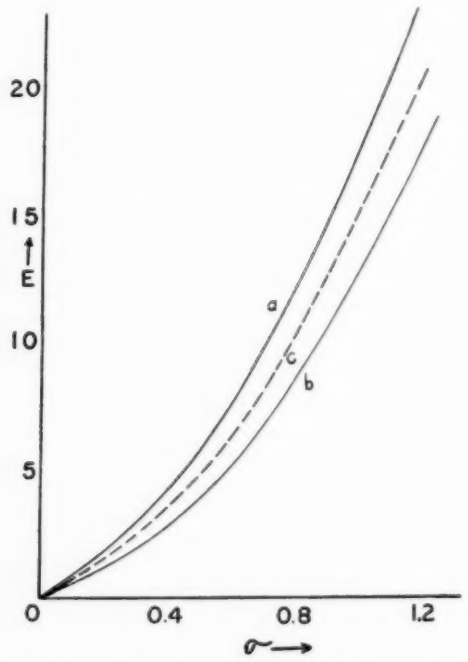

FIG. 3. Energy of ^1P state in Mev, for $\lambda=1$ (groove). *a*: Variational energy with one function: H_{11}; *b*: Lowest root of secular equation; *c*: H_{11} with general Hamiltonian.

mum is not likely to be changed very much by the inclusion of ψ_2 and ψ_3. In the numerical work we shall therefore limit ourselves to this particular value of λ.

The integrations leading to the algebraic form of the matrix elements proceed as before, except that a new set of $r_{ijk,\,lmn}$ has to be calculated. We find

$$H_{22}=4.05(10+5\lambda)\sigma - \frac{5}{2}B\frac{2-\lambda}{\sigma+1}\left[1-2\frac{\sigma+\frac{1}{2}}{\sigma+1}+\frac{\lambda^2}{6}\frac{10\sigma^2+10\sigma+3.5}{(\sigma+1)^2}\right]r^3 - 2C\left[\frac{\lambda^2\sigma^2+\lambda\sigma+5/4}{(\lambda\sigma+1)^2}\right]v^3,$$

$$H_{33}=4.05(10+5\lambda)\sigma - B\frac{2-\lambda}{\sigma+1}\left[1+\frac{4}{3}\lambda^2\frac{\sigma^2+\sigma+11/16}{(\sigma+1)^2}\right]r^3 - 2C\left[\frac{\lambda^2\sigma^2+\lambda\sigma+\frac{1}{2}}{(\lambda\sigma+1)^2}\right]v^3,$$

$$H_{12}=-3^{\frac{1}{2}}\left\{8.10\lambda\sigma-B\frac{2-\lambda}{\sigma+1}\left[1-\frac{5}{3}\lambda\frac{\sigma+\frac{1}{2}}{\sigma+1}\right]r^3 - C\frac{v^3}{\lambda\sigma+1}\right\},$$

$$H_{13}=-4(\tfrac{1}{6})^{\frac{1}{2}}B(2-\lambda)\frac{\sigma+\frac{1}{2}}{(\sigma+1)^2}r^3,$$

$$H_{23}=-2^{\frac{1}{2}}B\frac{\lambda(2-\lambda)}{\sigma+1}\left[\frac{\sigma+\frac{1}{2}}{\sigma+1}-\frac{\lambda}{3}\frac{5\sigma^2+5\sigma+7/4}{(\sigma+1)^2}\right]r^3.$$

Figure 3 shows H_{11} (upper curve), plotted against σ for the fixed minimizing value of λ. The lower curve represents the root of $\det|H_{ij}-E\delta_{ij}|=0$, calculated for different values of σ with the elements given above. Clearly, there is no tendency for the curve to dip below the zero axis, which means that the P state has an energy greater than that of the four dissociated particles composing He^4. It is hardly to be expected that the use of a greater number of functions would change this fact. Such an extension would, however, distort the monotone behavior of the root and presumably produce a minimum somewhere, which would then correspond to the energy of the unstable P state. But it seemed unwise to pursue this matter at present.

The question now arises as to the modification of these results induced by the more general form of the symmetric Hamiltonian. So far, the work was done with the potential energy operator

$$-A\sum_1[w+m+\tfrac{1}{2}(b+h)]J_{ij}P_{ij} - A\sum_2(w+m-b-h)J_{ij}P_{ij} \quad (15)$$

instead of the correct operator, given by a summation over (1). Since singlet states are symmetric in like particles, the P_{ij} in the second part of (15) are ineffective, so that a correction arises only from the first part. It is thus necessary only to calculate the matrix elements of

$$-A\sum_1(w+\tfrac{1}{2}b)J_{ij}(1-P_{ij}) \quad (16)$$

and to add them to those found previously. There still exists considerable latitude in the choice of w and b; we will take $w=-2/15$, $b=7/15$. The reason for this selection will be discussed later. The smallness of $(w+b/2)A$ makes it worth while only to compute the effect of (16) on H_{11}, and to neglect it in the secondary contributions to the energy. Now

$$\int\psi_1[\textstyle\sum_1 J_{ij}(1-P_{ij})]\psi_1 d\tau=4(R_{11}{}^W-R_{11}{}^M), \quad (17)$$

where

$$R_{11}^{W}=\frac{(\lambda\sigma+\frac{1}{2})(2-\lambda)}{\lambda(2-\lambda)\sigma+1}\left[\frac{\lambda(2-\lambda)\sigma}{\lambda(2-\lambda)\sigma+1}\right]^{\frac{1}{2}},$$

$$R_{11}^{M}=\frac{2-\lambda}{2(\sigma+1)}\left[\frac{\lambda(2-\lambda)\sigma}{\sigma+1}\right]^{\frac{1}{2}}.$$

For $\lambda=1$, (17) is simply $4[\sigma/(\sigma+1)]^{5/2}$, so that the diagonal element of (16) becomes $14.2[\sigma/(\sigma+1)]^{5/2}$. Its addition changes H_{11} of Fig. 3 into the dotted curve drawn below it. The former conclusions are evidently unaltered.

Except for the correction due to (16), the results of this section have already been stated.[16] It was also pointed out in that connection how and why they differ from those obtained by Feenberg[9] and by Bethe and Bacher.[9]

Triplet P States

The energy of the triplet states depends rather critically on the detailed form of the Hamiltonian. Hence it is advantageous to start with (1) instead of the approximation represented by (3). A triplet function is one in which the spin coordinates of either the two neutrons or the two protons appear symmetrically; hence the coordinate part is antisymmetrical in the chosen pair. In the problem under consideration, the three components of a triplet term coincide because the Hamiltonian here used ignores spin-orbit coupling. We may therefore restrict our investigation for convenience to the state in which $S_z=1$. There will, however, be a doubling of this energy due to neutron-proton symmetry. This appears in Eq. (24).

There are four possible spin functions corresponding to a total spin of one unit along the z-axis. They may be written with an obvious symbolism as follows:

$$\begin{aligned} S_1&=(+++-), \quad S_2=(++-+),\\ S_3&=(+-++), \quad S_4=(-+++). \end{aligned} \tag{18}$$

From these, two linear combinations can be formed which are symmetric in one pair and antisymmetric in the other. They are, after normalization,

$$(\tfrac{1}{2})^{\frac{1}{2}}(S_3-S_4) \quad \text{and} \quad (\tfrac{1}{2})^{\frac{1}{2}}(S_1-S_2). \tag{19}$$

(1 and 2, 3 and 4 constitute protons and neutrons respectively, and the signs in the S functions are understood to refer to the particles in this order.)

Now let u be a function of the coordinates, symmetric in 1 and 2, antisymmetric in 3 and 4; and let v be a similar function, but antisymmetric in 1 and 2, symmetric in 3 and 4. A triplet function satisfying the Pauli principle may be written in terms of these as follows:

$$=(\tfrac{1}{2})^{\frac{1}{2}}[au(S_3-S_4)+bv(S_1-S_2)], \tag{20}$$

where the parameters a and b, which satisfy $a^2+b^2=1$, are to be adjusted for minimum energy.

From (20) we calculate and then minimize

$$\sum_{\sigma}\int\psi H\psi d\tau.$$

The first step is again a summation over the spins, σ. In carrying this out it is to be observed that the only parts of H, Eq. (1), which operate on the spin functions are the Q's, and that these interchange the S functions. Thus, for instance, Q_{12} leaves S_1 and S_2 unchanged, but permutes S_3 and S_4. After the indicated summation we are left with a spin free Hamiltonian, and the problem of minimization affects only the coordinate functions; in fact

$$\sum_{\sigma}\int\psi H\psi d\tau=a^2\int uH_1ud\tau+b^2\int vH_2vd\tau$$
$$+\tfrac{1}{2}ab\left[\int uH_3vd\tau+\int vH_3ud\tau\right]. \tag{21}$$

The three spin free triplet operators have the form:

$$\begin{aligned} H_1&=E_{\text{kin}}-A\textstyle\sum_1[(w+\frac{1}{2}b)+(m+\frac{1}{2}h)P_{ij}]J_{ij}\\ &\quad -A[w-b+(m-h)P_{12}]J_{12}\\ &\quad\quad -A[w+b+(m+h)P_{34}]J_{34},\\ H_2&=E_{\text{kin}}-A\textstyle\sum_1[(w+\frac{1}{2}b)+(m+\frac{1}{2}h)P_{ij}]J_{ij}\\ &\quad -A[w+b+(m+h)P_{12}]J_{12}\\ &\quad\quad -A[w-b+(m-h)P_{34}]J_{34},\\ H_3&=-A\{(b+hP_{13})J_{13}-(b+hP_{14})J_{14}\\ &\quad +(b+hP_{24})J_{24}-(b+hP_{23})J_{23}\}. \end{aligned} \tag{22}$$

[16] H. Margenau, Phys. Rev. **53**, 198 (1938).

It is seen at once that these operators satisfy the relations

$$H_2=P_{13}P_{24}H_1; \quad P_{13}P_{24}H_3=H_3. \tag{23}$$

This inherent symmetry shows that the best possible choice which can be made for v is

$$v=P_{13}P_{24}u.$$

From this and Eq. (23) one may deduce:

$$\int vH_2vd\tau=\int (P_{13}P_{24}u)\cdot(P_{13}P_{24}H_1)$$

$$\cdot(P_{13}P_{24}u)d\tau=\int uH_1ud\tau;$$

and similarly

$$\int vH_3ud\tau=\int uH_3vd\tau.$$

If these relations are used, and E is written for the variational energy calculated from (20), Eq. (21) takes the form

$$(a^2+b^2)E=(a^2+b^2)(H_1)_{uu}+ab(H_3)_{uv}.$$

Minimization of E with respect to a and b separately yields the two equations

$$a[(H_1)_{uu}-E]+\tfrac{1}{2}b(H_3)_{uv}=0$$
$$\tfrac{1}{2}a(H_3)_{uv}+b[(H_1)_{uu}-E]=0,$$

which permit nonvanishing solutions for a and b only if the determinant

$$\begin{vmatrix}(H_1)_{uu}-E & \tfrac{1}{2}(H_3)_{uv}\\ \tfrac{1}{2}(H_3)_{uv} & (H_1)_{uu}-E\end{vmatrix}=0.$$

This leads to the energy of the triplet state

$$E=(H_1)_{uu}\pm\tfrac{1}{2}(H_3)_{uv}. \tag{24}$$

In nuclear problems, where present evidence indicates that the spin forces are subordinate to ordinary and Majorana exchange forces, the second term in (24) may be treated as a perturbation. Thus we shall first concentrate our effort upon the problem of choosing a function u which will minimize H_1 regardless of the term $(H_3)_{uv}$.

In line with the general method of this paper, u is taken to be a linear combination of functions of the type $\phi(l_1m_1n_1, 1)\phi(l_2m_2n_2, 2)\phi(l_3m_3n_3, 3)$. The symmetry with respect to permutations of particles required in u may easily be seen to demand that $l_3+m_3+n_3$ be odd, and that the corresponding sums with subscripts 1 and 2 be even. Of course none of the triplet functions combine with the ground state in the present approximation, so that we are again confronted with the problem of finding the lowest possible energy within a given class of variation functions. We must thus look for the lowest root of the resulting secular equation. Since no stable state is likely to result, only two functions have been used in constructing u:

$$\psi_1=\phi_{000}(1)\phi_{000}(2)\phi_{100}(3)$$
$$\psi_2=\phi_{200}(1)\phi_{000}(2)\phi_{100}(3).$$

In view of the symmetry of these functions with respect to P_{12}, and their antisymmetry with respect to P_{34}, or may write, by using (22) and the notation R, S, T, U, V, W previously developed,

$$H_1=E_{\text{kin}}+A\{(m+\tfrac{1}{2}h)(R+S+T+U)^M$$
$$+(w+\tfrac{1}{2}b)(R+S+T+U)^W$$
$$+(m+w-b-h)V^M+(m+h-w-b)W^M\}.$$

The matrix elements for R, S, T, and U are equal; there results, on calculation of R_{11}, V_{11} and W_{11}, the following expression for the diagonal element of H_1 with ψ_1:

$$(H_1)_{11}=4.05(6+5\lambda)\sigma$$
$$+2A\left\{(m+\tfrac{1}{2}h)\left[1+\frac{\lambda}{\sigma+1}\right](r^M)^3\right.$$
$$\left.+(w+\tfrac{1}{2}b)\left[1+\lambda\frac{\lambda\sigma+\frac{1}{2}}{\lambda(2-\lambda)\sigma+1}\right](r^W)^3\right\}$$
$$+A\left\{(m+w-b-h)\right.$$
$$\left.+(m+h-w-b)\frac{\lambda\sigma}{\lambda\sigma+1}\right\}v^3. \tag{25}$$

To carry through the numerical work it becomes necessary to adopt a set of nuclear constants. They may be fixed with a minimum of

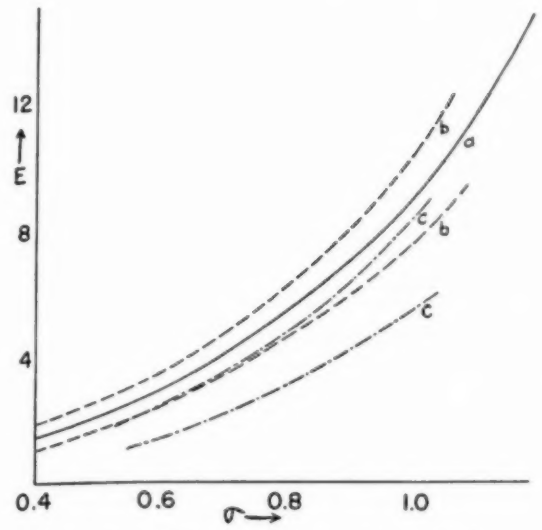

FIG. 4. Energy of ^3P state in Mev, for $\lambda=0.9$ (groove). *a*: Variational energy with one function: H_{11}; *b*: $H_{11}\pm\frac{1}{2}(H_3)uv$; *c*: Approximate locus of E with inclusion of ψ_2.

uncertainty if we utilize

(a) the fact that $b+h=g$ where g is the parameter determining the triplet-singlet separation of the deuteron levels;

(b) the Breit-Feenberg[11] inequality $m+2h\geqq 4w+2b$;

(c) the Kemmer[17] inequality $m+h\geqq 2w+2b$;

(d) the condition $w+m+b+h=1$.

The value most widely adopted for g is 0.22. We wish to point out that there is considerable uncertainty connected with this choice. As shown previously in this paper, it will not give sufficient binding energy for H^3 and the alpha-particle.[18] For the present let us take a compromise between the customary value and that deduced in an earlier section, and adopt $g=0.20$. As to the inequalities (b) and (c), it was pointed out by Inglis[1] and confirmed by more detailed calculations[19] that the best, though still quite poor, approach to the binding energy of Li^6 is obtainable by taking the equality signs to be valid. This fixes the values to be

$$w=-2/15,\quad m=14/15,\quad b=7/15,\quad h=-4/15.$$

The constant A is of course determined from the theory of the deuteron when the range of the forces is decided upon. As before, A will be taken as 35.6 Mev.

When the expression (25) is evaluated as a function of λ and σ it is found to possess a mild minimum with respect to λ, and this occurs for $\lambda\approx 0.9$. In this groove, however, it is a monotone increasing function of σ. (See Fig. 4, solid curve.) Its behavior is quite similar to that of H_{11} for the ^1P state.

Neglecting for the moment the effect of ψ_2, we investigate the term splitting due to the second part of (24). We get

$$(H_3)_{uv}=-A\{b(S+U-T-R)^W + h(S+U-T-R)^M\}_{uv}.$$

In the present case, $-S=-U=T=R$ for both Wigner and Majorana forces, so that

$$(H_3)_{uv}=\frac{28}{15}AR_{uv}{}^W-\frac{16}{15}AR_{uv}{}^M.$$

Furthermore,

$$R_{uv}{}^W=\tfrac{1}{2}\left\{\lambda\frac{\lambda\sigma+\frac{1}{2}}{\lambda(2-\lambda)\sigma+1}-1\right\}(r^W)^3$$

$$R_{uv}{}^M=\tfrac{1}{2}\left\{\frac{\lambda}{4}\frac{1}{\sigma+1}-1\right\}(r^M)^3.$$

The effect of this splitting (for $\lambda=0.9$) is shown by the dotted curves above and below $(H_1)_{11}$ in Fig. 4.

Finally, attention should be given to the effect of the function ψ_2 upon these calculations. For this purpose, $(H_1)_{12}$ has been computed for $\lambda=0.9$ and several values of σ. Only a rough estimate was made of the diagonal element $(H_1)_{22}$; but the accuracy is sufficient to justify the statement that, with the inclusion of ψ_2, the two dotted curves in Fig. 4 would be lowered to an extent indicated approximately by (c). The conclusion, then, is the same as that with regard to the ^1P state.

Changes in the form of the Hamiltonian would alter these results appreciably. It seems, however, that stability of the P states cannot be brought about by minor adjustments of w, m, b, and h. But an increase in the range of the nuclear forces would make them stable.

[17] N. Kemmer, Nature **140**, 192 (1937).

[18] The value recently adopted by Heisenberg, Naturwiss. **25**, 749 (1937), $g=0.25$, is even farther from achieving this end.

[19] K. G. Carroll and H. Margenau, Washington Meeting, April 1938, paper 36.

Coulomb Energy of Light Nuclei

H. A. BETHE
Cornell University, Ithaca, New York
(Received July 11, 1938.)

The Coulomb energy is calculated by determining the nuclear radius so that the energy difference between N^{13} and C^{13} agrees with observation. Two different assumptions are investigated: (a) that the nuclear radius is simply proportional to the cube root of the number of particles, (b) that the wave function of the last neutron or proton extends beyond the surface of the residual nucleus by an amount determined by its binding energy. The latter assumption accounts very well for the irregularities of the positron energies in the series $C^{11}N^{13}O^{15}F^{17}$, and agrees quantitatively with observation within 0.15 milli-mass-units. Theoretically and experimentally, the actual Coulomb energy should lie between the results of (*a*) and (*b*). Application of these considerations to unknown nuclei shows that C^{10} and O^{14} are highly stable, Be^{6} certainly and B^{9} almost certainly unstable, while the stability of B^{8} and N^{12} is doubtful.

IN connection with astrophysical considerations, it became desirable to decide about the stability of unknown nuclei such as Be^{6}, B^{8}, B^{9}, C^{10}, N^{12}, etc. The situation is favorable inasmuch as the "images" of all these nuclei are known, i.e., those nuclei which are obtained by interchanging neutrons and protons (He^{6}, Li^{8}, Be^{9}, Be^{10}, B^{12}). It is therefore only necessary to calculate the Coulomb energy which can be done fairly accurately even though an adequate theory of nuclear forces is still lacking. It is only necessary to estimate the nuclear radius, in particular for nuclei whose last neutron or proton is very loosely bound. In the following, simple formulae will be derived for this purpose which give, with one adjustable parameter, surprisingly good results for the Colomb energy of known isobaric pairs.

We consider a nucleus of charge $Z+1$ and radius R which consists of a "last proton" and a "residual nucleus" of charge Z. If the charges of the proton and the residual nucleus are both distributed uniformly over the sphere of radius R, the Coulomb energy is

$$C=6Ze^2/5R. \tag{1}$$

For a crude approximation, R may be assumed to be proportional to the cube root of the mass number A of the nucleus, *viz.*

$$R=r_0A^{\frac{1}{3}}. \tag{2}$$

In order to get as close an approximation to the empirical values as possible, we use the *observed* Coulomb energy for the isobaric pair $N^{13}-C^{13}$ to determine r_0. The difference between the binding energies of the last neutron in C^{13} and the last proton in N^{13} is equal to the difference between the energy evolutions in the reactions $C^{12}+H^2=C^{13}+H^1$ and $C^{12}+H^2=N^{13}+n^1$ which are 2.71 and -0.28 Mev, respectively.[1] Therefore we have for $N^{13}-C^{13}$:

$$C=2.99 \text{ Mev}=3.21 \text{ mMU}. \tag{2a}$$

This gives

$$C=1.26ZA^{-\frac{1}{3}} \text{ mMU}, \tag{3}$$
$$R=1.47\cdot10^{-13}A^{\frac{1}{3}} \text{ cm}. \tag{4}$$

The energy is given here and in the following in milli-mass-units (mMU, equal to 1/16,000 of the mass of O^{16}, 1 mMU$=0.931$ Mev$=1.83\ mc^2$). The radius is seen to extrapolate, for heavy nuclei, to Gamow's "small" radii.

The result of (3) is given in Table I under the heading "Calc. I." The agreement with the observed Coulomb energies is seen to be fair. However, (3) gives definitely too low values for the pairs $C^{11}-B^{11}$ and $O^{15}-N^{15}$. This is not surprising because (3) varies smoothly with Z whereas the observed values of the Coulomb energy do not. They are "high" for C^{11} and O^{15} and "low" for N^{13} and F^{17}.

In order to obtain such individual fluctuations of C, it appears that we must take into account the larger size of loosely bound nuclei. For a crude approximation, we consider a nucleus as composed of "the last neutron" (or proton) and "the residual nucleus of radius R_0" and assume

[1] Livingston and Bethe, Rev. Mod. Phys. **9**, 245 (1937), Table LXXII, p. 371.

that the "last particle" is completely free outside of R_0. This assumption amounts to a one-body model which may be justifiable when the residual nucleus does not possess many low excited levels (light nucleus). We should expect that our procedure gives somewhat too large radii and therefore too small Coulomb energies for nuclei with a loosely bound last particle while formula (3) will give too large Coulomb energies.

Since we assume the force on the last neutron to be exactly zero outside of R_0, the neutron wave function outside will be

$$\psi=(\alpha/r)e^{-(r-R_0)/2b} \tag{5}$$

with $$b=\hbar/2(2M\epsilon)^{\frac{1}{2}}, \tag{5a}$$

M is the neutron mass, ϵ is the binding energy of the last neutron, and α is a normalizing factor. Inside the nucleus, we assume ψ to be constant, *viz.*

$$\psi=\alpha/R_0. \tag{6}$$

Then the normalization condition is

$$\int\psi^2r^2dr=1=\alpha^2(\tfrac{1}{3}R_0+b). \tag{7}$$

If we assume a uniform charge distribution in the residual nucleus, and the same wave function for a "last proton" as for a neutron, the Coulomb energy becomes

$$C=Ze^2\left[\int_0^{R_0}\left(\frac{3}{2R_0}-\frac{r^2}{2R_0^3}\right)\psi^2r^2dr+\int_{R_0}^{\infty}\frac{1}{r}\psi^2r^2dr\right]$$

$$=Ze^2\alpha^2\left(\frac{2}{5}+\int_{R_0}^{\infty}e^{-(r-R)/b}\frac{dr}{r}\right)$$

$$\approx Ze^2\alpha^2\left(\frac{2}{5}+\frac{b}{R_0+b}\right). \tag{8}$$

By use of (7), this reduces to

$$C=\frac{6}{5}\frac{Ze^2}{R_0+b}\left(1+\frac{b}{2(R_0+3b)}\right). \tag{9}$$

The parenthesis gives only a few percent correction.

We now assume that R_0 is proportional to $A_0^{\frac{1}{3}}$, where $A_0=A-1$ is the mass number of the *residual* nucleus. To fix the coefficient, we use again the Coulomb energy of $N^{13}-C^{13}$ (3.21 mMU); we have in this case

$\epsilon=5.3$ mMU (reference 1, p. 378),
$b=1.03\cdot10^{-13}$ cm (Eq. (5a)),
$R_0=2.74\cdot10^{-13}$ cm (Eq. (9), with $Z=6$),
$r_0=1.20\cdot10^{-13}$ cm (Eq. (2), with $A_0=12$).

Inserting this value of r_0 into (9), we find

$$C=\frac{1.54Z}{A_0^{\frac{1}{3}}+(3.9/\epsilon)^{\frac{1}{2}}}\left[1+\tfrac{1}{2}\cdot\frac{(3.9/\epsilon)^{\frac{1}{2}}}{A_0^{\frac{1}{3}}+(3.9/\epsilon)^{\frac{1}{2}}}\right], \tag{10}$$

TABLE I. *Coulomb energy of light nuclei.*

Nucl. (Neutr.)	*N mMU	$A_0^{1/3}$	$(3.9/\epsilon)^{1/2}$	Z	C (mMU) Calc. I	Calc. II	Obs.	Nucl. (Prot.)	*P mMU
H^3	6.6_5	1.26	0.77	1	0.87	0.84	0.74	He^3	5.9
He^6	0.5*	1.71	2.79	2+3	3.5	1.9_5	—	Be^6	−1.3 to −0.5*
Li^7	7.6_5	1.82	0.71	3	2.0	1.99	2.02**	Be^7	5.6
Li^8	2	1.91	1.40	3+4	4.4	3.6	—	B^8	−0.3 to +0.5
Be^9	1.8_5	2.00	1.45	4	2.4	2.0	—	B^9	−0.7 to −0.3
Be^{10}	7.3	2.08	0.73	4+5	5.2	5.4	—	C^{10}	1.9*
B^{11}	12.3_5	2.15	0.56	5	2.7_5	3.0_5	3.1	C^{11}	9.3
B^{12}	>2	2.22	1.40	5+6	6.0_5	5.2	—	N^{12}	−0.9 to −0.1
	<3.3	2.22	1.09	5+6	6.0_5	5.6	—	N^{12}	0.4 to 0.8
C^{13}	5.3	2.29	0.86	6	3.21	3.21	3.21	N^{13}	2.1
C^{14}	8.9	2.35	0.66	6+7	6.8	7.1_5	—	O^{14}	5.1
N^{15}	11.6	2.41	0.58	7	3.5_5	3.8_5	3.7	O^{15}	7.9
O^{17}	4.5	2.52	0.93	8	3.9	3.9_5	3.9	F^{17}	0.6

* Binding energy of each of the *last two* neutrons or protons.
** Calculated from the observed half-life (43 days), (Roberts, Heydenburg and Locher, Phys. Rev. **53**, 1016 (1938)) on the assumption that a positron is emitted in the transition $Be^7\rightarrow Li^7$, and with the use of the Fermi theory. The experiments of Roberts, Heydenburg and Locher indicate, however, that the transition is due to K electron capture and that there is less than 1 positron in 20 K captures. This would give an upper limit of 1.94 mMU for the Coulomb energy while the actual value cannot be determined at present.

where both ϵ and C are measured in milli-mass-units.

In Table I, column "Calc. II" the Coulomb energies are calculated according to (10) for a number of light isobaric pairs. The first column of Table I gives that member of the isobaric pair which contains more neutrons; it is, in all cases listed, a known nucleus. The second column gives the binding energy of the last neutron in mMU (observed, cf. reference 1, p. 378). The next two columns give $A_0^{\frac{1}{3}}$ and $(3.9/\epsilon)^{\frac{1}{2}}$; the former quantity is proportional to the radius R_0 of the residual nucleus while the latter measures the extension of the neutron wave function beyond R_0. It is seen that for tightly bound nuclei such as Li^7, Be^{10}, B^{11}, C^{13}, etc., the latter contribution is much smaller than R_0, while for loosely bound ones, such as He^6, the neutron wave function may extend as far out as $2\frac{1}{2}R_0$. The fifth column contains the effective Z; it is simply the charge Z' of the nucleus in the first column when the two nuclei of the isobaric pair differ by one unit of charge (e.g. Li^7-Be^7), while it is $Z'+(Z'+1)$ when the charge difference is two units (e.g. Li^8-B^8). The following three columns contain the values of the Coulomb energy calculated from (3), from (10), and observed, the latter wherever the necessary data are available. Next the symbol of the isobar containing more protons is given, and finally the binding energy ϵ_P of its last proton. When the two isobars differ by one unit of charge, we have simply $\epsilon_P=\epsilon_N-C$ because then the isobars are compared with the same residual nucleus; for a charge difference of two, the relation is slightly more complicated.

The "Calc. II" column reproduces very well both the absolute values and the individual fluctuations of the Coulomb energy. C has almost the same value for the pairs $C^{11}-B^{11}$ and $N^{13}-C^{13}$, then rises sharply to $O^{15}-N^{15}$ and again stays almost the same for $F^{17}-O^{17}$. This experimentally well-known behavior thus finds its explanation in the fact that the last neutron in C^{13} and O^{17} is relatively loosely bound to the very stable residual nucleus (C^{12} and O^{16}) while the binding in B^{11} and N^{15} is much stronger. These latter nuclei are therefore smaller in size and have a larger Coulomb energy.

Actually, our calculation II over-corrects for the effect of loose binding, and gives too high a value for C for $O^{15}-N^{15}$. This might be expected from the "one-body" character of our considerations. That our formula is as good as it is, may be due largely to the fact that in the cases of loosely bound last particles (C^{13}, O^{17}) the residual nucleus (C^{12}, O^{16}) is particularly stable and therefore has particularly few low excited states. This makes the one-body model for nuclei like C^{13}, N^{13}, O^{17}, F^{17} (and also Be^9, B^9) better than usual.

In all cases, the observed value of C falls in between (or very close to) the values predicted by our two formulas, (3) and (10). This was expected from their derivation, since (3) corresponds to an extreme "compound model" and does not take into account the strength of binding of the last particle at all, whereas (10) corresponds to a "one-body model" and overemphasizes the importance of the last particle. Thus we can be confident that generally the actual value of the Coulomb energy will lie between the limits given by the two calculations. In the last column of Table I, we have therefore given the limits of the proton binding energy according to the two calculations; where these limits agreed closely, the mean was given (for C^{10} and O^{14}), where observations were available, the observed value.

For the stability of unknown nuclei we find then:

C^{10} and O^{14} are certainly highly stable, O^{14} with 5.1 mMU against $N^{13}+H$, and C^{10} with 3.8 mMU against disintegration into $2\,He^4+2\,H$. (The stability of Be^{10} is given against Be^9+n^1.)

Be^6 is certainly unstable, being between 1 and 2.6 mMU heavier than $He^4+2\,H$.

B^9 is almost certainly unstable,[2] *viz.* between 0.3 and 0.7 mMU. The lower value seems more likely because the one-body model should be

[2] The existence of B^9 was claimed in a short note by Meitner, Naturwiss. **22**, 420 (1934) who reported a weak positron radioactivity from this nucleus. This result which has never been confirmed is almost certainly incorrect because a positron radioactivity of B^9 would be in definite conflict with its stability. The condition for radioactivity of B^9 is that it be heavier than Be^9 plus two electrons, i.e., (reference 1, p. 373)

$$B^9 > 9.015\,04 + 0.001\,10 = 9.016\,14. \qquad (A)$$

The condition for stability is

$$B^9 < 2He^4 + H = 9.015\,85 \qquad (B)$$

in contradiction with (A).

good for this nucleus (Be^8+H). It seems very unlikely that B^9 should be even more stable than is indicated by the one-body model; however, in view of the comparative importance[3] of B^9 for astrophysics, direct experimental evidence would be desirable, e.g. from the reaction $Be^9+H=B^9+n$ which should occur with protons of 2 Mev energy.

B^8 and N^{12} are very doubtful. B^8 is just on the limit of stability, being slightly stable according to "Calc. II," slightly unstable according to I. The stability of N^{12} depends mostly on the exact binding energy of B^{12} which is not known at present.

[3] Bethe, "Energy Production in Stars," to appear shortly in the Phys. Rev.

SEPTEMBER 15, 1938 PHYSICAL REVIEW VOLUME 54

Bands of H_2 Ending on the $2p^1\Pi$ Level

G. H. DIEKE
Johns Hopkins University, Baltimore, Maryland

(Received May 5, 1938)

New measurements make possible a much more complete analysis of the band systems ending on $2p^1\Pi$. The constants of this state can be obtained with great accuracy and the irregularities in the Λ-doubling and perturbations traced to the interaction with the higher vibrational levels of $2p^1\Sigma$. New information is obtained about some of the states which have both electrons excited.

THE strongest and most extensive band systems in the visible H_2 spectrum are the transitions from a number of three quantum electronic levels to the $2p^1\Sigma$ state.[1] The data of these band systems can be found in Richardson's book[2] or in the original papers listed there. All the upper levels of these systems should also combine with the $2p^1\Pi$ state. The resulting band systems lie chiefly in the near infra-red around 7600A. Important fragments of these bands have been given by Richardson and Chalk,[2, 3] but the measurements of Gale, Monk, and Lee on which they based their analysis contain only the strongest lines in this region. Therefore it seems desirable to publish the data on these band systems as they were obtained from a more recent analysis based on our own measurements. This re-analysis was undertaken as a preliminary study for the analysis of the corresponding bands of HD and D_2 on which I hope to report in a future paper. I am giving the results of H_2 here separately because they throw some new light on the nature of the levels with both electrons excited about the exact interpretation of which there is still a great deal of uncertainty.

The wave numbers and intensities of the transitions from the singlet $3d$ complex are given in Table I and those from the other initial states in Table II. In general it will be found that the lines which Richardson gives agree with those listed here, but there is a considerable number of discrepancies, which must be ascribed to the scantiness of the data with which Richardson had to work. A few doubtful lines are included in the tables. They are designated by a question mark. In a few bands there are undoubtedly more lines present than those given in the tables. That is indicated by the high intensity of the last listed lines. In such cases there are marked irregularities in either the initial or the final state and a prediction of the position of the line becomes too uncertain. Only when there are good combination relations can such lines be identified with any degree of certainty. In the present instances such combination relations are not always available. However there is no doubt that future reserach will eventually locate these lines.

[1] Whenever only one electron is excited it is sufficient to specify the state of this electron, and it is understood that the other electron is in the normal state $1s\sigma$. The full notation of the $2p^1\Sigma$ state would be $1s\sigma 2p\sigma\,^1\Sigma$. Only when both electrons are excited is it necessary to specify the state of both.

[2] O. W. Richardson, *Molecular Hydrogen and Its Spectrum* (New Haven, 1934).

[3] O. W. Richardson, Proc. Roy. Soc. **A126**, 487 (1930); M. L. Chalk, Proc. Roy. Soc. **A128**, 579 (1930).

TABLE I. *The transitions from the singlet 3d complex to $2p^1\Pi$.*

J	P Branch ν	I	Q Branch ν	I	R Branch ν	I
			$3d^1\Sigma \rightarrow 2p^1\Pi$			
			0→0			
1	12 660.56	0	12 654.26	7	12 675.67	3
2	529.26	00	555.35	2	617.24	8
3			439.63	5	545.50	4
4			312.78	2	467.33	7
5			181.69	3	386.23	4
6			050.17	0	{361.54	1?
					{310.35	0?
			1→0			
1			14 880.07	3	14 854.42	0?
2			773.98	1	817.85	3
3			640.20	3	720.25	1
4					615.95	1
5			330.32	2		
			1→1			
1	12 586.99*	(3)	12 574.51	4	12 588.75	1
2	455.86		474.77	1	518.63	5
3	(297.16)		350.22*	4b	431.04	5
4	117.03	00	210.18	0	341.92	7
5			068.34	1	252.90	2
6			11 926.43	00		
7			782.83	0		
			2→1			
1			14 647.34	2		
2			576.78	0c	639.27	3
3					556.34	(5)
4					447.87	2
			2→2			
1	——	—	12 475.72*	5	12 519.68	0
2	12 365.12	2	411.32	00	475.72*	5
3	252.31	0d	314.72	0	409.31	1
4	072.58	1			282.78	4
5			045.19	00		
6					967.73	0
			3→2			
1	——	—	14 219.42	3	14 245.03	0
2			136.75	00	181.27*	(8)
3			020.10	00		
			3→3			
1	——	—	12 179.19	3		
2	12 063.55	00			12 135.76	2
3			11 994.91	1dr		
			$3d^1\Pi^- \rightarrow 2p^1\Pi^+$			
			0→0			
1	——	—	12 920.82	5	12 996.78	10
2	12 800.50	2	871.79	1	999.72	9
3	694.18	6	812.37	4	995.66	10
4	579.37	2	746.45	1	986.40	9
5	460.79	4	677.91*	1	972.82	10
6	340.94	0	604.60*	2?	955.42	5
7	221.54	1			934.49	9
8					910.17	0
9					882.70	2
10					852.16	00
			1→0			
1	——	—	15 020.09	2	15 102.10	5
2	14 899.74	0	14 977.10	3	106.75	1
3	799.45*	3c	919.17*	1	099.69*	4
4	686.43	1	850.63	1c		
5	564.70	3c			056.92	1
6	436.88	3b				
7	305.67*	4d				
			1→1			
1	——	—	12 714.53	2	12 796.52	7
2	12 600.52	1	677.91	1	807.54	3
3	509.64	5			809.69	7
4	409.02	1	576.26	00	805.04	3
5	302.67	3	516.04*	2	794.88	5
6	193.37	0			780.06	2
7	083.01	00			761.10	2
8					738.50	1
9					712.43	1

J	P Branch ν	I	Q Branch ν	I	R Branch ν	I
			$3d^1\Pi^- \rightarrow 2p^1\Pi^+$			
			2→0			
1					17 046.58	4
			2→1			
1	——	—	14 656.61	6	14 741.10	6r
2	14 542.79	3	622.60	5	752.35	4
3	454.29	6	574.80	2	751.30	5
4	353.96	3	518.03	1c	739.57	3
5	244.34	3			718.42	2
6	127.92	00			688.85	3d?
7					652.11*	4
			2→2			
1	——	—	12 485.68	2	12 569.64	5
2	12 377.33	2	459.03	0	586.99*	3
3	298.04	4			595.12	5
4	209.87	1			595.54	1
5	115.39	2			589.47	3
6	016.83	00d			577.92	0
7	11 916.15	1			561.61	1
8					541.25	00
9					517.54	00
			3→1			
1	——	—			16 507.80	
2						
3					510.77	
			3→2			
1	——	—			14 336.27	
2					351.33	
3					354.48	
			3→3			
1	——	—	——	—	12 296.00	2
2	12 105.22	00?	12 180.33	0	306.48	2
3	039.50	2			329.30	3
4						
5	876.33	1??				
			$3d^1\Pi^+ \rightarrow 2p^1\Pi$			
			0→0			
1	——	—	12 984.36	6	13 130.29	10
2	12 859.39	4	13 009.89	0	195.20	10
3	822.31	3	017.63	10	243.75	8
4	768.39	3	011.02	8	263.77*	10r
5	702.52	0	12 978.08	10b	290.33	10
6			953.46	5?		
7			942.39	8?		
			1→0			
1	——	—	15 073.26	1		
2	14 948.16*	2				
3	893.79	1				
4	799.88	3				
5	676.20	1??				
			1→1			
1	——	—	12 767.61	1	12 896.18	2
2	12 648.98	6	782.10	00	927.54	7
3	604.60*	2	759.23	0	928.49*	9
4	525.86	4				
5	418.63	1?				
			2→0			
1	——	—				
2	16 957.86	2				
3	889.24	0				
4	792.17	10?				
			2→1			
1	——	—			14 920.11	0d
2	14 658.88	3c				
3	599.96	3			906.22	0
4	518.53	6r				
			2→2			
1	——	—			12 720.54	0
2	12 495.32	2			756.55	1
3	453.15	1	12 595.54*	1		
4	353.34	2			741.78	1
5			504.30	0		

J	P Branch ν	I	Q Branch ν	I	R Branch ν	I
			$3d^1\Pi^+ \rightarrow 2p^1\Pi$			
			3→3			
1	——	—	12 272.01	00		
2	12 136.36	1			12 355.47	1
3						
4	11 995.20	1				
			$3d^1\Delta^- \rightarrow 2p^1\Pi$			
			0→0			
1	——	—	——	—	13 375.10	9
2	——	—	13 250.12	10	471.21	2
3	13 072.48	10	283.60	10	564.94	10
4	050.79	10r	315.69	10	653.85	4
5	030.09	10	345.34	2	736.43	5
6	008.43	1	368.79	2	811.73	1
7	985.14	8	385.47	2	878.65	2?
			1→0			
1	——	—	——	—	15 567.38	5
2	——	—	15 442.42	4	642.48*	7
3	15 264.80	0	454.44*	4		
4	221.95	1d	463.96	2		
5	178.29	1				
			1→1			
1	——	—	——	—	13 261.88	10r
2	——	—	13 143.25	10	342.92	4
3	12 974.98	10	165.35	9	423.29	4
4	944.50	6	189.96	10	500.21	1
5	916.31	7	211.47	9br		
6	888.51	0				
			2→1			
1	——	—	——	—	15 330.95	6
2	——	—	15 212.41*	2	391.63	0
3	15 059.37*	1			448.34	1
4	14 993.14	0				
5	941.40	0				
			2→2			
1	——	—	——	—	13 159.41	10
2	——	—	13 048.76	10	226.20	9
3	12 887.80	(1)	066.97	10r?	292.13	10
4	849.04	2	049.97	10		
5	812.37*	9				
			3→3			
1	——	—	——	—	13 066.97*	10r
2			12 951.33	9		
3	12 809.9	?				
			$3d^1\Delta^+ \rightarrow 2p^1\Pi$			
			0→0			
1	——	—	——	—	13 384.68	5
2	——	—	13 264.38	9	498.77	4
3	13 076.83*	10r	321.11	10	618.21	5
4	071.93	10	385.47*	2		
5	076.83*	10r	427.16	2		
6	060.64	10?				
			1→0			
1	——	—	——	—	15 569.40	3
2	——	—	15 449.06	2	647.63	2
3	15 261.52	0	470.05	2		
4	221.95*	1d	510.83	6		
			1→1			
1	——	—	——	—	13 263.77	10r
2	——	—	13 149.84	8	348.47	6
3	12 972.25	4	180.22	10	432.36	3
4	946.87	9	211.47	9r		

The intensities are eye estimates. Apparent irregularities in the intensities are not necessarily real, as the sensitivity of the various photographic plates may change very rapidly in this region. Quantitative intensity measurements carried out by Dr. N. Ginsburg in this laboratory are partly ready. An asterisk in the tables means that the line is a known blend.

The $2p^1\Pi$ State

The final level of our bands is also the upper level of the so-called C bands in the extreme ultraviolet of which the most accurate measurements are those of Jeppesen.[4] From the analysis of these ultraviolet bands the constants of the $2p^1\Pi$ state are known. However, the accuracy is very considerably less than that obtainable from the visible bands. If one takes this into account the results of the present paper are found to be in good agreement with Jeppesen's values (see below) except in one or two cases where there is a considerable perturbation.

All the rotational levels of the $2p^1\Pi$ state are double, and it is well known that this doubling (Λ-doubling) is due to the interaction of rotation and electronic motion. One of the components $p\Pi^-$ is uninfluenced whereas the other one $p\Pi^+$ is displaced. The magnitude of the displacement is very much influenced by the nearness of other levels with the same symmetry and the same value of J. If such levels are very close we have a typical perturbation. We know that the higher vibrational levels of $2p^1\Sigma$ overlap with the $2p^1\Pi$ state so that there is ample opportunity for the production of irregular Λ-doublings and real perturbations. Therefore it would be meaningless to calculate the constants of the $2p^1\Pi^+$ state.

The $2p\Pi^-$ levels cannot be subject to such interactions as there cannot be any Σ^- or Π^-

[4] C. R. Jeppesen, Phys. Rev. **44**, 165 (1933).

TABLE II. *The transitions from the doubly excited levels to* $2p^1\Pi$.

$^1K \rightarrow 2p^1\Pi$

	P Branch		Q Branch		R Branch	
J	ν	I	ν	I	ν	I
			0→0			
1	12 476.79	00	12 499.43	1	12 541.61	00
2	374.44	0	421.34	0	484.09*	1
3			306.48	1	385.26	00
4	057.16	00	152.55	00		
5	11 844.30	00d?				
			1→0			
1			14 728.46	3	14 768.33	1
2	14 603.55	0	647.99	0	711.71	00
3			534.28	3d		
			1→1			
1			12 422.99	3	12 462.69	0
2	12 304.46	00	348.67	0	412.55	
3			244.49*	(9)		
			2→1			
1			14 575.35	4	14 589.50	(6)
2	14 456.77	00	475.77	0	513.75	2
3	258.14	(6)	345.48	3	402.42	00
4	111.87	00			265.90	4
			13 982.05*	0?		
			2→2			
1			12 403.79	3	12 418.63*	1
2	12 293.22	00	310.35	0	350.22	4b
3			189.20	2	255.58	0
4	11 946.99	00	037.52	00	090.79	00
5			853.14	00		

$^1L \rightarrow 2p^1\Pi$

	P Branch		Q Branch		R Branch	
J	ν	I	ν	I	ν	I
			1→1			
1			11 821.27	4		
2	11 702.80	0	745.04	00		
3			635.07	1		

$^1L \rightarrow 2p^1\Pi$

	P Branch		Q Branch		R Branch	
J	ν	I	ν	I	ν	I
			2→2			
1	13 286.62	2b	13 304.01	2		
2	193.43	1			13 277.71	2
3						
4	874.57	0				

$^1M \rightarrow 2p^1\Pi$

	P Branch		Q Branch		R Branch	
J	ν	I	ν	I	ν	I
			1→1			
1			11 962.49	1d	12 013.00	00
2	11 843.83	1d			11 975.38	0
3			807.11	1	913.31	0
4					795.87	0
			2→2			
1			11 949.87	0		
2						
3			754.45	00		

$^1N \rightarrow 2p^1\Pi$

	P Branch		Q Branch		R Branch	
J	ν	I	ν	I	ν	I
			1→1			
1	13 642.25*	10	13 680.39	8	13 749.75	2
2	561.75	5	635.77	5	735.05	4
3	458.16	3	566.80	8	701.11	2
4	333.38	10				
			1→2			
1	11 471.22	1r	11 508.90	1	11 578.69	00
2	398.32	1	470.40	3	571.57	1
3			410.58	7		
4			336.17	1		
5			266.92*	0		
			2→2			
1	13 452.76*	3	13 478.62	3		
2	368.07	5	419.44	0	13 493.60	1
3	368.07	5	332.59	3	444.49	1
4	260.27	3	226.20	(9)	378.91	1
5	090.44	5	141.32	3		

$^1O \rightarrow 2p^1\Pi$

	P Branch		Q Branch		R Branch	
J	ν	I	ν	I	ν	I
			0→0			
1	13 805.50	6	13 865.88	2	13 982.05	0
2	740.91	10	861.72	1	14 027.60	1
3	674.13	7	850.00	2		
4	600.81*	6				
			0→1			
1			11 560.25*	0		
2	11 441.74	0b				
3			560.25*	0		
4	326.90	00				
			1→1			
1			13 840.60	3		
2	13 721.96	4	822.27	0	13 970.01	0
3	644.86	2	801.70	8		
4	568.30*	10				
			1→2			
1			11 669.02	2		
2			656.89	00		
			2→2			
1	13 668.42	2	13 710.66	7		
2	600.29	(10)	718.34	(10b)	13 851.82	0
3	559.78	0	690.80	9		
4	448.62	2	645.15	6		
5			620.29	6		

$U \rightarrow 2p^1\Pi$

	P Branch		Q Branch		R Branch	
J	ν	I	ν	I	ν	I
			1→1			
1						
2					13 061.21	3
3	12 816.83	00	12 892.92	1	036.28	2
4	659.53	0	815.36	0	028.23	9
5			754.61	2		

TABLE III. *Rotational differences of* $2p^1\Pi^-$.
$F(J+1)-F(J-1)$

	$V=0$	UV	1	UV	2	UV	3	UV
2	302.60	302.53	286.90	287.7	271.60	271.98	256.52	257.46
3	420.36	420.68	398.49	399.35	377.14	377.96		355.41
4	534.87	536.25	507.01	509.95	479.74	481.05		453.45
4	645.44		611.67		578.71			
5	751.28		711.87		673.32			

state which might influence it anywhere near. Therefore the rotational levels of the $2p^1\Pi^-$ state should be regular and the constants calculated from them in the usual way have the theoretical meaning attributed to them in the elementary theory of band spectra. The average values of the rotational differences $F(J+1)-F(J-1)$ are given in Table III. The values in small print marked UV are those which Jeppesen derived from the ultraviolet bands. The discrepancy with our values gives an idea of the accuracy of the ultraviolet data. It is curious to see that all Jeppesen's values except one are higher than ours, which cannot be accounted for by accidental errors of measurement. The cause is probably in the somewhat roundabout way which Jeppesen had to use to extract the values in the tables from the observational data.

As usual we represent the rotational levels by the formula

$$F(J)=B_VJ(J+1)-D_VJ^2(J+1)^2+\cdots \quad (1)$$

and calculate the constants B_V and D_V from the first three differences in each column. For $V=3$ the data are not quite sufficient to do this. The use of more differences for the calculation of the rotational constants would not increase their accuracy as the expression (1) is a very poor approximation for all but the lowest values of J. The values obtained in this way are listed in Table IV. The values in small print are those derived by Jeppesen and from them the constants in the expression

$$B_V=B_e-\alpha(V+\tfrac{1}{2})+\beta(V+\tfrac{1}{2})^2 \quad (2)$$

are found to be

$$B_e=31.340, \quad \alpha=1.626, \quad \beta=0.022.$$

The vibrational differences between successive vibrational states with $J=1$ are given in the second column of Table V.

The rotational part in the energy level for $J=1$ is $2B_V$.[5] If we therefore add $2(B_V-B_{V+1})$ to the values of the second column of Table V we get the true vibrational differences which are given in the third column. From the first two differences the constants in the formula

$$\omega(V+\tfrac{1}{2})-x(V+\tfrac{1}{2})^2+\cdots \quad (3)$$

for the vibrational energy are found to be

$$\omega=2442.74, \quad x=67.03.$$

The discrepancy of these values with 2468 and 88.93 which are the values which Jeppesen derived for these constants from his data is chiefly due to the different manner in which the constants were determined. Jeppesen used two more terms in formula (3). Whereas for most molecules that would give a much better approximation, for H_2, as I have pointed out before, usually no increase in accuracy can be expected. For it is necessary to use terms with higher vibrational quantum numbers for the calculation of the constants in the more extended formula and for these the convergence of (3) which is poor even for the lowest values of V becomes so bad as to render the formula practically useless. Therefore it cannot be expected that the values of the constants derived from the more complete

TABLE IV. *Constants used to determine rotational levels.*

V	0	1	2	3
B_V	30.532	28.949	27.411	25.895
	(30.539)	(29.113)	(27.485)	(25.931)
D_V	0.0195	0.0186	0.0181	*
	(0.0205)	(0.0198)	(0.0189)	

* As the data are very scarce for $V=3$ the value for D_3 was obtained by extrapolation from D_0 to D_2 and then the value of B_3 calculated from the single difference given in Table III.

TABLE V. *Vibrational differences of* $2p^1\Pi$.

1−0	2305.51	2308.68
2−1	2171.54	2174.62
3−2	2040.25	2043.28

[5] In general the energy of a molecule of this type is in good approximation

$$A+B[J(J+1)-2\Lambda^2+L(L+1)].$$

The part $B[L(L+1)-\Lambda^2]$ which is usually omitted comes from the interaction of rotation and electronic motion (see e.g. G. H. Dieke, Phys. Rev. **47**, 661 (1935)). A is independent of J and contains the electronic and vibrational energies. For a $p\Pi$ state $L=1$ and $\Lambda=1$ and therefore the energy becomes

$$A+BJ(J+1)$$

which for $J=1$ is $A+2B$.

TABLE VI. Λ-*doublings of the* $2p^1\Pi$ *state.*

$J \backslash V$	0	1	2	3
1	1.17	1.23	0.78	12.12
2	3.47	3.39	1.42	
3	6.51	5.93	− 3.54	
4	9.95	6.58	+27.53	
5	12.90			

formula are more accurate than those derived from just two differences, although these latter values may also be considerably different from the true ones.

Λ-Doubling and Perturbations

The positions of the $2p^1\Pi^+$ levels will be influenced by the vicinity of the higher vibrational levels of $2p^1\Sigma$. Therefore we must expect irregularities in the rotational levels of $2p^1\Pi^+$. Table VI gives the Λ-doubling, i.e., $\Pi^+(J)-\Pi^-(J)$. This can be derived directly from the observations without the help of any formula, except that the relative position of one *ortho* and one *para* level must be known. We can take for this e.g., $2p\Pi^-(1)$ and $2p\Pi^-(2)$ for $V=0$. As these levels are represented well by formula (1) we can find their relative position with any desired accuracy, and this in turn will furnish all the Λ-doublings within the errors of measurement.

Figure 1 shows the vibrational levels (for $J=2$) of the $2p^1\Sigma$ and $2p^1\Pi$ states and explains the pecularities shown by the Λ-doublings of Table VI. The vibrational levels of $2p\Sigma$ for $V>8$ have not been actually observed but are extrapolated values. $V=4$ of $2p\Pi$ was taken from Jeppesen's data.

It is well known that two rotational levels of $p\Sigma$ and $p\Pi$ with the same value of J must repel each other if they are close together. Furthermore we must remember that the spacing of successive rotational levels is much closer for $2p\Sigma$ than for $2p\Pi$. Therefore we have to pay particular attention to a $p\Pi$-level and the $p\Sigma$-level which lies immediately above it. Successive higher rotational levels of these two states will come closer and closer together which means that the $p\Pi^+$ levels will show more and more depression if the approach of the levels is at all close.

This is further illustrated in Fig. 2 which shows the distance between the rotational levels which perturb each other. ($V=0$ means $\Sigma_8(J)-\Pi_0(J)$, $V=1$: $\Sigma_{10}(J)-\Pi_1(J)$, $V=2$: $\Sigma_{12}(J)-\Pi_2(J)$). As the $p\Sigma$ levels can be obtained only by extrapolation, the actual distances might be somewhat different from those given in the figures. The good qualitative agreement between the predicted and observed perturbations shows, however, that this difference can be only very slight. For $V=0$ and small J values the $2p\Pi$ levels lie practically half way between $V=7$ and

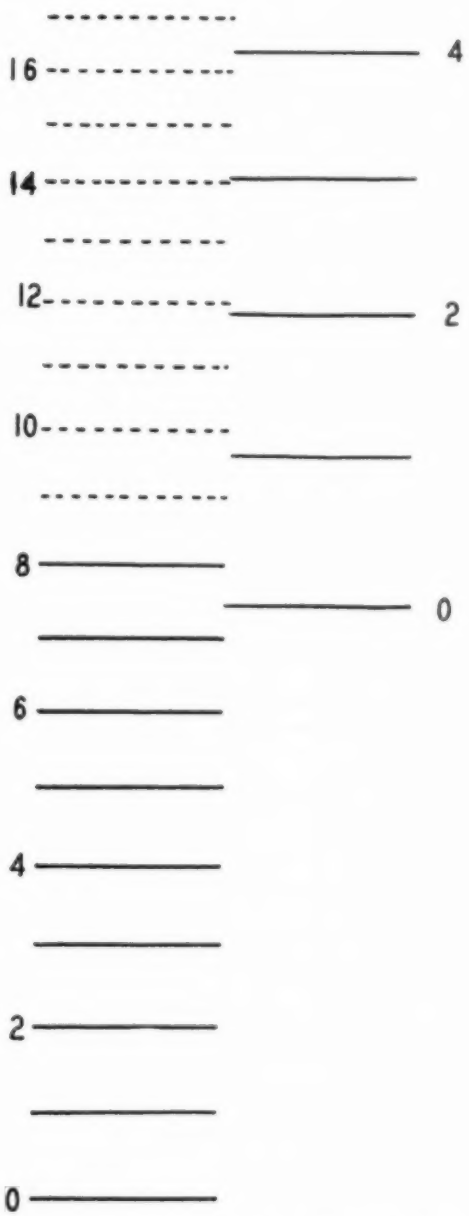

FIG. 1. Relative positions of the vibrational levels (for $J=2$) of $2p^1\Sigma$ (left) and $2p^1\Pi$ (right). The levels of $2p^1\Sigma$ with $V>8$ are extrapolated.

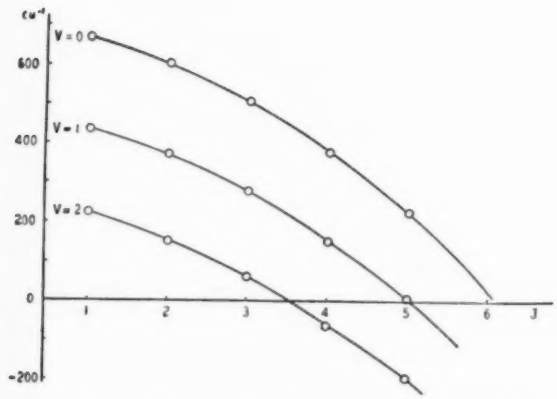

FIG. 2. Distance between the rotational levels of $2p^1\Pi$ and the closest levels of $2p^1\Sigma$ with the same J.

$V=8$ of $2p\Sigma$ and therefore the Λ-doubling shown by these levels will be very closely the normal doubling. For the highest observed J values the Λ-doubling is only slightly less than the normally expected one (which is proportional to $J(J+1)$) because the Σ_8 levels are still sufficiently far off. For $J=6$ the levels would be so close that we would have a considerable perturbation.

Figures 1 and 2 show further that the $V=1$ level of $2p\Pi$ is not very far below the $2p\Sigma_{10}$ level. For $J=1$ and 2 they are not sufficiently near to show a significant deviation from the normal Λ-doubling. However $J=3$ begins to show the influence of the nearness of the Σ_{10} levels by being appreciably depressed and $J=4$ shows this influence much stronger. $J=5$ has not been found. The extrapolated difference is only about 7 cm^{-1} which would produce a very large perturbation. It would be quite difficult to find the lines belonging to this level. $J=6$ should have an abnormally *large* Λ-doubling as the Σ_{10} level lies now *below* the Π_1 level.

This crossing over of rotational levels which gives rise to a true perturbation is actually observed for $2p\Pi_2^+$. The figure shows that this crossing over occurs between $J=3$ and $J=4$. For $J=1$ and 2 the approach is close enough so that the $2p\Pi_2^+$ levels are quite appreciably depressed. For $J=3$ the $2p\Pi_2^+$ level is so much lowered that the Λ-doubling becomes negative, whereas for $J=4$ where the Σ_{12} level lies *below* the Π_2 level the latter is shifted upwards and we obtain the large positive value 27.53 for the Λ-doubling.

For the Π_3-level the situation is slightly different. Here for $J=1$ the Σ_{14}-level lies slightly below the Π_3-level so that the abnormally large Λ-doubling 12.12 results. For increasing J-values the Σ_{14} and Π_3-levels grow apart. However their interaction, which is due to the influence of the rotation on the electronic motion, becomes larger with increasing rotation, so that nevertheless the Λ-doubling may remain roughly the same although J increases. Our data for $V=3$ are not quite sufficient to establish that. It explains however the fact mentioned by Jeppesen that for $V=3$ all the observed rotational levels show a perturbation of the approximately constant amount 10 cm^{-1}. There is no need to interpret this as a vibrational perturbation, as Jeppesen does. Vibrational perturbations between Σ and Π levels should be theoretically impossible.

The perturbations and the character of the Λ-doubling are thus completely explained qualitatively by the interaction of the $2p^1\Pi$ levels with the higher vibrational states of $2p^1\Sigma$. A further quantitative study would be possible if also these $2p\Sigma$ levels would be known empirically. The visible bands which come down on these levels are too weak for observation. The bands belonging to these levels in the ultraviolet $2p^1\Sigma \rightarrow 1s^1\Sigma$ system might be present but they have not been studied so far.

THE INITIAL STATES

There is no need to say much about the initial states of the bands discussed here, as they are well known from their combinations with the $2p^1\Sigma$ level which lie chiefly in the blue part of the spectrum. A few of the rotational levels of the initial states are new. In these cases their combinations with the $2p^1\Sigma$ states have been looked for and usually found.

However, a few significant facts about the states with both electrons excited came to light which deserve being mentioned. These states were first discovered by Richardson and given names ^1K, ^1L, ^1M, ^1N, ^1O, ^1Q. Besides there is a state which gives rise to a single progression (λ4142.8) only (here called U). There was no place for them in the scheme of the energy levels (except possibly for ^1O which was attributed by Richardson to $1s\sigma\ 3s\sigma^1\Sigma$) with only one of the two electrons excited, and therefore Weizel[6] and Richardson[2] proposed that they must be due to

[6] W. Weizel, Zeits. f. Physik **65**, 456 (1930).

states for which both the electrons are excited. This explanation seems the only possible one also in the light of further knowledge about them.

The properties of all these states are highly irregular. We know that the interaction with other states can produce such irregularities, but if they exist it is often quite difficult to know whether a given band is genuine or spurious. In most cases the evidence which Richardson gives can leave little doubt that the bands are real, but in view of the great theoretical importance which these levels have for the knowledge of the structure of the excited hydrogen molecule, additional information about them is highly desirable.

Richardson gave also some of the transitions of K and O with $2p^1\Pi$. Table II shows that now the transitions of all these states with $2p^1\Pi$ are known with the exception of Q which was regarded as very doubtful by Richardson and not included in his book. Some of the bands are very weak and consist only of a few lines, but they are always just the lines which must be expected to be strongest. We have here thus additional independent evidence that these levels must be genuine. A few more interesting facts appear from a study of the bands in Table II.

In the transitions of the $3d$ complex with $2p^1\Pi$ as well as in the corresponding triplet bands, the bands for which the vibrational quantum number does not change are much stronger than any of the bands off the main diagonal of the vibrational scheme. According to the Franck-Condon principle such a state of affairs must be expected when the moment of inertia of the initial and final states are not much different. This argument is often reversed to find the vibrational quantum numbers from the intensity distribution of a given band system. If the bands of a given diagonal are much stronger than all the other bands it is argued that this diagonal must be the main diagonal of the system, i.e. correspond to no change in the vibrational quantum number. For the L, M and N transitions with $2p^1\Pi$ we find that with Richardson's assignment of vibrational quantum numbers the strong bands would be $0\rightarrow1$ and $1\rightarrow2$. Therefore the vibrational quantum numbers of these three states were raised by one in order to make the strong bands $1\rightarrow1$ and $2\rightarrow2$.

This procedure is not free from objections. It would imply that the moment of inertia of the L, M and N states is nearly the same as that of the $2p^1\Pi$ state, which seems highly improbable. Furthermore if the lowest known vibrational levels of these states have now $V=1$ there should be lower lying levels with $V=0$. I have looked for them but have not been able to find them. However, Richardson's original assignment of vibrational quantum numbers for these states was based on a similar argument regarding the intensity distribution in the transitions to $2p^1\Sigma$, where the state of affairs is more complex. I hope that an analysis of the corresponding D_2 and HD bands on which Miss M. Lewis is working at present will clear up the situation.

The U level has the peculiarity that for the $U\rightarrow2p^1\Sigma$ bands only one branch in every band is known. It was impossible to decide whether this branch is a P, Q or R branch. However, the transitions from the U level to $2p^1\Pi$ show P, Q and R branches and it is seen immediately that the single branches of Richardson's 4142.8 progression must be P branches. Only one band of the $U\rightarrow2p^1\Pi$ system is strong enough to be found, but the existence of this one is beyond any doubt. It ends on the $V=1$ level and by the same argument which was used above we conclude that the vibrational quantum number of the U level must be one. The question whether this level is a Σ, Π, Δ, etc. level cannot be decided with absolute certainty. Richardson gives the $P3$ lines in the strongest bands as the lines with the lowest rotational quantum numbers, and from that it would seem likely that U would be a Δ-state. However, the $R1$ and $Q2$ lines of the $U\rightarrow2p^1\Pi$ band are missing, whereas the $P3$ line of this band is very weak. It is difficult to know whether the absence of these lines is significant or whether it only means that they are present but so weak that they do not register on the photographic plate. If these lines are really missing, i.e. if the $P3$ lines are spurious, the U state would have to be a Φ state.

I shall leave the discussion of possible electronic configurations for all these states to a subsequent paper.

I wish to thank Mr. W. Durding for his help with the measurements.

On the Hyperfine Structure Interval Rule in Indium

D. H. TOMBOULIAN AND R. F. BACHER
Cornell University, Ithaca, New York

(Received June 24, 1938)

Interferometric measurements on λ7182 ($5s\,6p\,{}^3P_1 \rightarrow 5s\,6s\,{}^3S_1$) and λ7276 ($5s\,6p\,{}^3P_0 \rightarrow 5s\,6s\,{}^3S_1$) of In II indicate that the separations of the state $5s\,6s\,{}^3S_1$ follow the interval rule to within the experimental error (approximately 0.05 percent). Perturbations by neighboring states are negligible and there are no effects for this state due to the known electric quadrupole moment of the nucleus. The results indicate that the assumption of a nuclear magnetic moment is very successful in accounting for the observed relative separations.

THE interval rule in hyperfine structure follows directly from the interaction of a nuclear magnetic dipole in the field of the electrons. For several years it appeared that the hyperfine structure interval rule held in all cases as well as could be determined from the various measurements. This agreement was generally taken as meaning that the form of the interaction assumed to account for the hyperfine structure, was a good one. The accuracy and extent of the experimental data on which these observations were based, was not great enough, however. More recently, numerous deviations from the interval rule have been found in the hyperfine structure separations of various elements. These may be shown to be of two types. The first is due to perturbations of the individual hyperfine levels and observed when the hyperfine separations are comparable to the distance to an adjacent state. Numerous examples of such deviations are found in the work of Paschen and Campbell[1] on In II. The second, which is sometimes found where such perturbations are expected to be negligible, is attributed to an electric quadrupole moment of the atomic nucleus. Of course, all that can really be ascertained is that the interaction term which would be introduced by the presence of such an electric quadrupole moment accounts satisfactorily for the experimentally determined separations. Evidence has been found[2] which indicates that the same element mentioned above, In, shows deviations in the interval rule which are attributed to a nuclear quadrupole moment.

Not all states of the atom are expected to be affected by a nuclear electric quadrupole moment. For an electron with orbital angular momentum $l=0$, no effect is expected. This means that a configuration of s electrons is expected to have no quadrupole effect. Such a state is the $5s\,6s\,{}^3S_1$ of In II. In addition this state has no neighboring states nearer than the ${}^1S_0$ of the same configuration which is distant 3106 cm^{-1} and would therefore produce a negligible displacement of the central hyperfine level. Hence it is interesting to see how well the interval rule is followed in the absence of the effects which usually produce deviations.

To this end, interferometric measurements on the spectral lines of In II were extended to include two lines involving the $5s\,6s\,{}^3S_1$ state, as a supplement to the excellent grating measurements of Paschen and Campbell. A Fabry-Perot interferometer was used in conjunction with a Zeiss 3-prism spectrograph and the experimental arrangements were essentially the same as for the previous measurements[2] on In II. Fig. 1 shows an enlargement of the line λ7182 ($5s\,6p\,{}^3P_1 \rightarrow 5s\,6s\,{}^3S_1$) and the neighboring line λ7276 ($5s\,6p\,{}^3P_0 \rightarrow 5s\,6s\,{}^3S_1$) which lies under the He I line λ7281. All three components of In λ7276 are visible and there is no difficulty in distinguishing them from the helium fringes which are much broader.

A pattern of the line λ7182 as well as a level diagram is shown in Fig. 2. This line should show seven components but the central component was not observed due to its extremely small intensity. Paschen and Campbell observed this weak component only in the first order in their grating work. The ${}^3S_1$ separations are ob-

[1] Paschen and Campbell, Ann. d. Physik **31**, 29 (1938).
[2] Bacher and Tomboulian, Phys. Rev. **50**, 1096 (1936); **52**, 836 (1937); Schuler and Schmidt, Zeits. f. Physik **104**, 468 (1937).

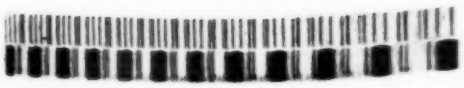

FIG. 1. Enlargement of photograph of λ7182 (above) and λ7276 taken with a 3 mm separator. The heavy fringes in the lower line are due to He λ7281.

tained directly from the differences, components (3–6) and components (2–5). The values of these separations are given in Table I as obtained from four plates taken with 3 mm separators and one with a 1 mm. The exact values of the plate separations as determined with neon standards are given in the first column of this table. For the 1 mm separator the pattern is not overlapped with that of adjacent orders but for the 3 mm separators it was. No components were superimposed, however. The *maximum* deviation from the mean is 0.0010 cm^{-1} (0.05 percent) for the larger separation and 0.0023 cm^{-1} (0.1 percent) for the smaller separation. From the same line Paschen and Campbell obtain 2.216 cm^{-1} and 1.797 cm^{-1} for the same separations. The separations of the $^3S_1$ state are checked by measurements on the line λ7276 ($5s\,6p\,^3P_0 \rightarrow 5s\,6s\,^3S_1$) which are also given in Table I. From this line Paschen and Campbell obtain 2.214 and 1.810 cm^{-1}. The present interferometric measurements show a greater consistency for the two lines as might be expected from the higher dispersion.

For a test of the interval rule the $^3S_1$ separations have been taken from the measurements of

TABLE I. *Separations of the* $5s\,6s\,^3S_1$ *state of* In II *as measured from* λ*7182 and* λ*7276.*

Separator mm	Line A	Interval 11/2−9/2 cm^{-1}	Interval 9/2−7/2 cm^{-1}	Weight
	From λ*7182* ($5s\,6p\,^3P_1 \rightarrow 5s\,6s\,^3S_1$)			
3.12265	7182	2.2089	1.8104	1
3.12265	7182	2.2091	1.8069	1
3.12265	7182	2.2078	1.8076	1
3.00148	7182	2.2089	1.8082	1
1.05530	7182	2.2095	1.8073	1
	Average	*2.2088*	*1.8081*	
	From λ*7276* ($5s\,6p\,^3P_0 \rightarrow 5s\,6s\,^3S_1$)			
3.00148	7276	2.2078	1.8091	3
3.00148	7276	2.2088	1.8109	1
	Average	*2.2081*	*1.8096*	

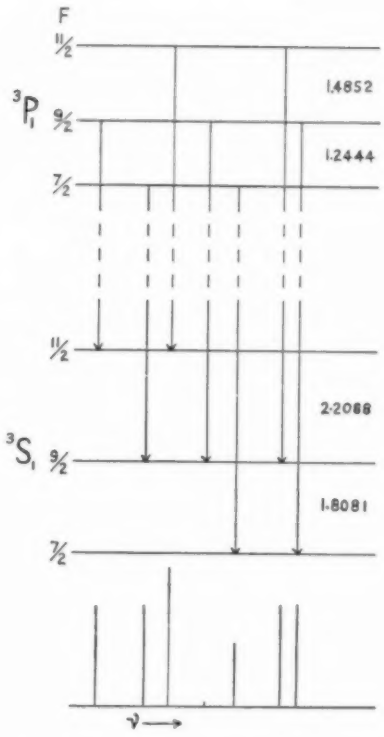

FIG. 2. Level scheme and observed structure for λ7182 ($5s\,6p\,^3P_1 \rightarrow 5s\,6s\,^3S_1$) of In II.

λ7182 since the effect of the background due to the neighboring helium line is rather hard to ascertain and might lead to some errors. The values of the separations give a ratio 1.2216 whereas if the interval rule held exactly they should be in the ratio of 11/9 or 1.2222. The difference between the ratios based on observed and calculated values is 0.05 percent which is probably within the experimental error. For the $5s\,6p\,^3P_1$ state the expected ratio on the basis of the interval rule is the same as above but the observed ratio is 1.1935. This difference is attributed to the perturbing effects of $^3P_2$ and $^3P_0$ of the same configuration.

The accuracy with which the ratio of the observed separations of $5s\,6s\,^3S_1$ agrees with the expected ratio indicates that the interval rule is followed very well in the absence of perturbations and quadrupole effects. Under these conditions the assumption of a nuclear magnetic dipole is remarkably successful in accounting for the observed relative separations.

Electron Microscope Studies of Thoriated Tungsten*

ARTHUR J. AHEARN AND JOSEPH A. BECKER
Bell Telephone Laboratories, New York, N. Y.

(Received July 21, 1938)

Many past experiments have shown that the thermionic activity of a thoriated tungsten filament is determined by the concentration of thorium on its surface. This concentration is in turn determined by the rate of arrival and rate of evaporation of thorium. Typical published values of these rates are given in Fig. 1. An electron microscope used to obtain electron images of thoriated tungsten ribbons is described. Comparison with photomicrographs shows that the active and inactive patches composing an electron image agree in size, shape and number with the exposed grains of the tungsten. The electron microscope *shows that thorium comes to the surface in "eruptions"* at a relatively small number of randomly located points. From a comparison of photomicrographs showing thoria globules and electron images of thorium eruptions, it is deduced that *all the thorium in a globule comes to the surface when an eruption occurs.* Factors such as a high temperature flash and sudden heating and cooling of the filament affect the frequency of eruptions. Thorium eruptions are the only observed manner in which thorium arrives at the filament surface. They are repeatedly observed in the early stages of thoriation. Eruptions are not observed in the later stages of thoriation where conditions are unfavorable for their observance. Electron images of a Pintsch single crystal filament reveal alternate active and inactive bands parallel to the filament axis. Thorium eruptions occur only on the active bands. With a polycrystalline ribbon the surface migration of thorium from the eruption centers is isotropic; *with a single crystal ribbon there is a strongly preferred direction of migration.* X-ray analysis shows that the surface is a (211) plane and that *the preferred direction of migration agrees with the* (111) *direction in this plane.* During the process of thoriating a filament the relative emissions from different grains change by substantial amounts; in many cases the change is so great that the relative emissions are reversed. Measurements of work function differences between grains gave values ranging up to 0.6 volt.

1. INTRODUCTION

EXTENSIVE studies have been made of the thermionic properties of thoriated tungsten and thorium on tungsten together with allied phenomena such as the reduction of thorium oxide, diffusion of thorium to the filament surface and the evaporation of thorium. In general, the thermionic activity depends on the density of thorium that can be maintained on the filament surface. This steady state thorium concentration at any given temperature is determined by the relative rates of arrival of thorium at the filament surface and evaporation therefrom.

How the steady state value of the thorium concentration varies with temperature is shown in Fig. 1 in which data published by other workers are assembled. The family of curves gives the evaporation rate as a function of temperature for various values of f.[1] This family of curves is obtained by combining results of Brattain and Becker[2] with those of Langmuir.[3] In combining the results of these two experiments the assumption has been made that at infinite temperature the evaporation rate is directly proportional to f. This assumption is relatively unimportant however in the range of temperature employed in filament work.

In addition to evaporation data, Fig. 1 contains data on the rate of arrival of thorium at the surface of thoriated tungsten as a function of temperature. Curve 1 is based on data by Langmuir[3] and curve 2 on data by Brattain and Becker.[2] Experiments by Fonda, Young and Walker[4] show that the diffusion coefficient of thorium in thoriated tungsten varies by a factor as large as 400 depending on the grain size of the filament. In the light of this, the relatively small differences in arrival rates shown by curves 1 and 2 are fully understandable.

At any given temperature the steady state value of f is obtained from the intersection of evaporation and arrival curves. In the insert in Fig. 1, curves $1A$ and $2A$, corresponding to

* Presented in part before the American Physical Society in Washington, D. C., April 1936.

[1] The quantity f is proportional to the amount of thorium on the tungsten surface, and $f=1.0$ is defined as that surface concentration of thorium which gives the optimum thermionic emission (reference 2).

[2] Brattain and Becker, Phys. Rev. **43**, 428 (1933).

[3] Langmuir, Phys. Rev. **22**, 357 (1923).

[4] Fonda, Young and Walker, Physics **4**, 1 (1933).

curves 1 and 2, respectively, give the variation of the steady state value of f with temperature. If curve 1*A* is taken as an example, the activation and deactivation of thoriated tungsten is readily understood. At a temperature of about 1900°K, $f=1.0$ is reached which by definition of f gives the optimum thermionic activity. At 2600°K f equals 0.03 or 0.04, i.e., the thermionic activity is still slightly above that of tungsten. Such curves as 1*A* and 2*A* are reversible and one can generalize as follows: As the temperature increases, the steady state value of f decreases.

In the experiments from which the data of Fig. 1 were obtained and in other work prior to the advent of the electron microscope, studies were necessarily limited to areas larger than about 1 square millimeter. Therefore, only the average value of effects that occur during the activation and deactivation of filaments could be measured and many processes could not be studied at all. When the electron microscope was adapted to thermionic studies the processes and effects that were localized on filament areas of 0.001 mm² or less could be observed.

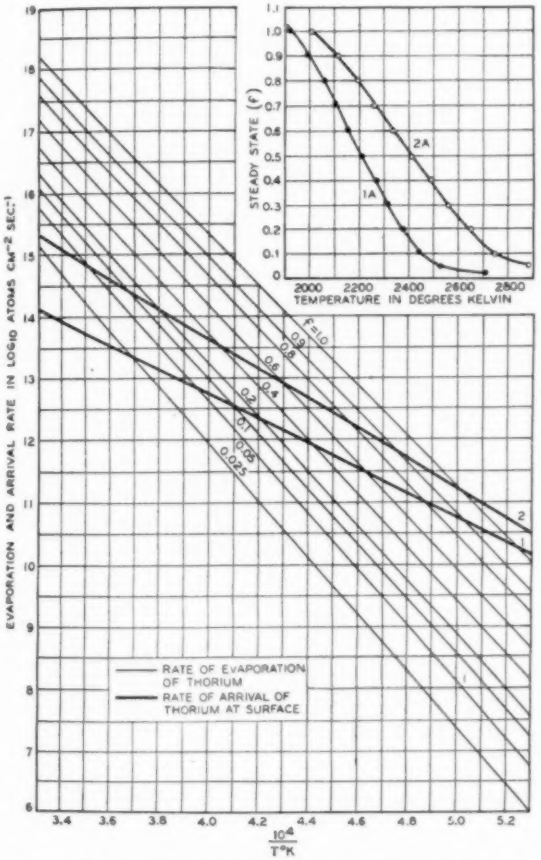

FIG. 1. Thorium arrival and evaporation rate for thoriated tungsten and the variation with temperature and amount of thorium on the surface. Curve 1, 1*A*—Langmuir data. Curve 2, 2*A*—Brattain and Becker data.

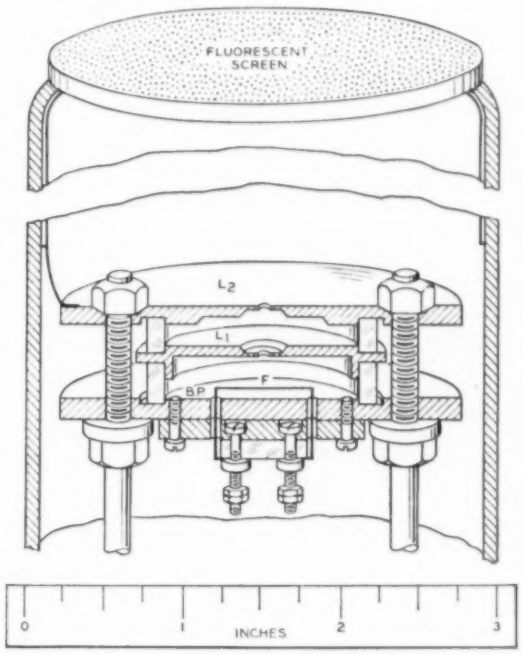

FIG. 2. Sketch of electron microscope.

The present paper describes some electron microscope studies of the details of the process of activation and deactivation of thoriated tungsten. In particular the experiments deal with the process by which the thorium arrives at the surface of the filament, the migration of thorium over the surface and the influence of the grain structure of the tungsten on these processes.

2. APPARATUS

Figure 2 is a sketch of the type of electron microscope used.[5] Four of these tubes were used in these studies. The essential parts are the filament F, the electron lenses L_1 and L_2, the backing plate *B.P.* and the fluorescent screen. The filament consists of a flat thoriated tungsten ribbon about 3 cm long, 0.038 cm wide and 0.002 cm thick.

A voltage ratio V_{L_2}/V_{L_1} of about ten is needed to form the image on the screen of this microscope. A beam voltage V_{L_2} of two or three

[5] We are indebted to Dr. C. J. Davisson of these laboratories for the design of this electron microscope.

kilovolts is usually applied. The potential of the backing plate *B.P.* is adjusted to produce parallel equipotential planes near the filament. In the electron image shown in Fig. 9 the electrical magnification is about 100; in all other cases it is about 30.

The position of the image on the screen can readily be shifted through small displacements by the introduction of small magnetic fields. Therefore to obtain well-defined photographs of the electron image, it is necessary to avoid magnetic disturbances and to heat the filament with constant direct current.

3. The Electron Image and Grain Size of Metal

Numerous comparisons of electron images and light images of metal surfaces are to be found in the literature.[6] In general, the electron images show considerable variation in emission between adjacent regions, i.e., the image is patchy. These patches have shapes and sizes which in general agree with those of the grains appearing on photomicrographs of the metal surface.

Apparently the difference in electron emissivity on various areas of a metal surface is associated with the orientation of the various crystal grains. Measurements of work function differences between faces of single crystals[7–9] yield values up to several tenths of a volt.

Figure 3 shows a comparison of electron images[10] with photomicrographs of thoriated tungsten ribbons. Both ribbons shown here are 0.038 cm wide. Pictures *c* and *g* are photomicrographs of a portion of the thoriated tungsten ribbon having relatively large grains. Pictures[11] *b*, *d*, *f* and *h* are electron images of the same portion of this filament. The large detail on the electron images agrees almost perfectly with that shown on the light images.

Pictures *a* and *e* of Fig. 3 show respectively a photomicrograph and an electron image of a small grain thoriated tungsten filament. Here again, the two kinds of images are similar; their textures are the same and in places they agree in detail.

Thus, in general, the patches on the electron image correspond to the grains of a thoriated tungsten filament. The electron image within a given grain is not entirely free from structure, however, as shown by picture *f* in Fig. 3. A granular structure in the metal surface is invariably revealed in the electron image, but of some electron image features no counterpart is found in the optical image.

4a. Thorium Eruptions

How does the thorium arrive at the surface from the interior and how does it migrate over the surface? In the early work on thoriated tungsten it was assumed that the thorium arrived at all points of the surface at approximately equal rates. However, later studies on the activation of single crystals,[12] strongly supported the thesis that thorium diffuses to the surface only along grain boundaries.

The electron images of the polycrystalline thoriated tungsten ribbon shown in Fig. 4 reveal a different phenomenon. To obtain these, the filament was first flashed at about 2600°K; between successive pictures, all made at 1490°K short time heat treatments were given at temperatures between 1500 and 1800°K. In picture "*a*" most of the filament is very inactive; nearly all of the emission comes from a few small bright spots. The succeeding pictures trace the life history of such active spots. The one at the extreme right is a good one to follow. Between *a*, *b* and *c* it has increased both in size and in brightness; in *d*, *e* and *f* it has increased in size and decreased slightly in brightness; in *g* and *h* the spot has increased still more in size so that it is quite diffuse while the brightness has decreased greatly. The life history of other spots may be similarly traced. As a result of the development of these spots, picture *h* reveals an electron image which is more uniform and more active than that shown in picture *a*.

These spots which initially appeared as pinpoints, are places where thorium is arriving at

[6] See Brüche and Scherzer, *Geometrische Elektronenoptik* (J. Springer, Berlin 1934).
[7] Rose, Phys. Rev. **44**, 585 (1933).
[8] Farnsworth, Phys. Rev. **51**, 378 (1937).
[9] Mendenhall, and DeVoe, Phys. Rev. **51**, 346 (1937).
[10] The electron images vary in width depending on the exact value of the backing plate potential used.
[11] The differences between *b*, *d*, *f* and *h* are due to different degrees of thoriation and will be discussed later.
[12] Clausing, Physica **7**, 193 (1927).

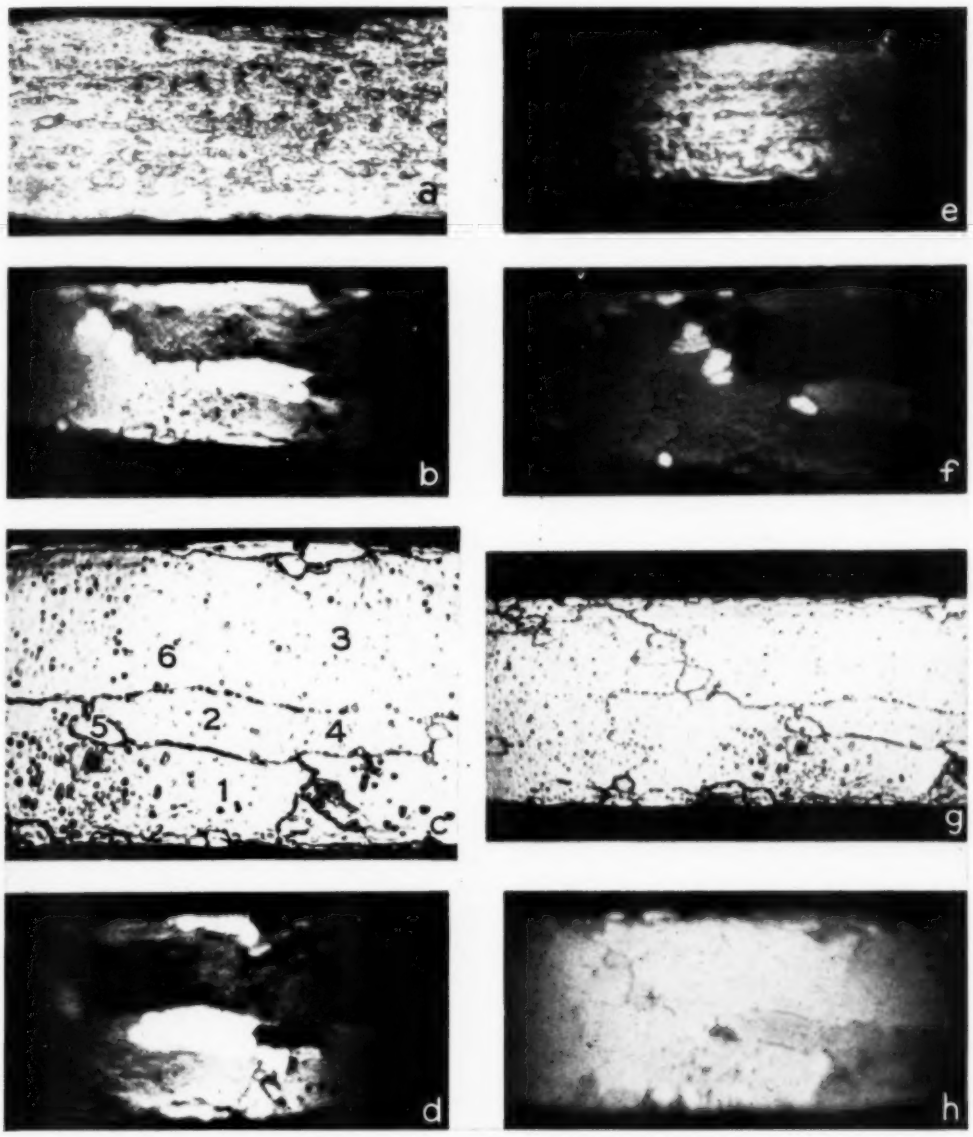

FIG. 3. Comparison of electron images and light images of thoriated tungsten (small grain and large grain ribbons). The average degree of thoriation f and photographing temperature for the electron images are given. *a*, Light (×68); *b*, electron 0.25 1460°K; *c*, light (×100); *d*, electron 0.13 1570°K; *e*, electron 0.80 1250°K; *f*, electron 0.11 1620°K; *g*, light (×71); *h*, electron 0.54 1405°K.

the surface of the filament.[13, 14] Thorium suddenly boils up from the interior at a point on the filament surface. This is followed by the building up of a film of thorium around this point and a migration of thorium over the surface, as revealed by the increase in brightness and size of the spots. After the arrival of thorium at the surface ceases, the surface density of thorium decreases due to the continued migration of thorium over the surface. This is shown by the decrease in brightness of the spot as it increases further in size.

Since this phenomenon of thorium spots resembles volcanic eruptions they are called "thorium eruptions." *Thousands of these eruptions have been observed with several different filaments in wire form as well as in ribbon form.*

[13] Brüche and Mahl, Zeits. f. Tech. Physik, No. 12, p. 623 (1935); No. 8, p. 262 (1936).
[14] Johnson and Shockley, Phys. Rev. **49**, 436 (1936).

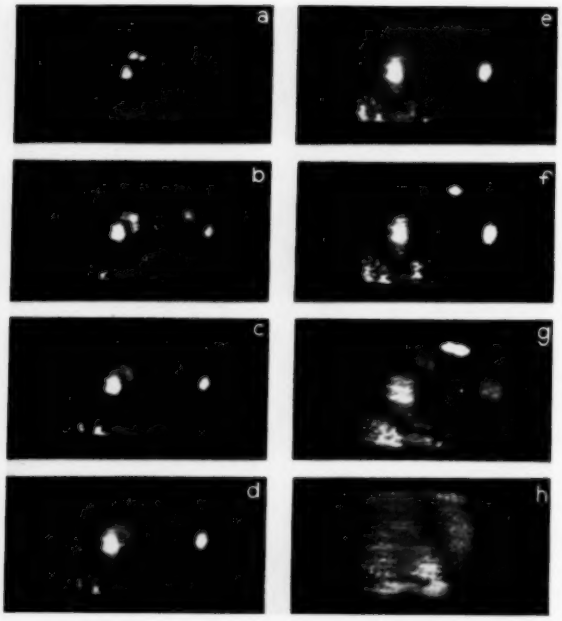

FIG. 4. Thorium eruptions on small grain thoriated tungsten ribbon. Photographing temperature 1490°K. Temperature and time of heat treatment, average degree of thoriation f and exposure time are given in order. *a*, 2550°K, 30 sec. 0.03, 60 sec.; *b*, 1530°K, 1 min. 0.06, 60 sec.; *c*, 1570°K, 1 min. 0.06, 60 sec.; *d*, 1600°K, 1 min. 0.06, 60 sec.; *e*, 1680°K, 1 min. 0.10, 40 sec.; *f*, 1720°K, 1 min. 0.10, 60 sec.; *g*, 1755°K, 1 min. 0.11, 30 sec.; *h*, 1830°K, 2 min. 0.11, 30 sec.

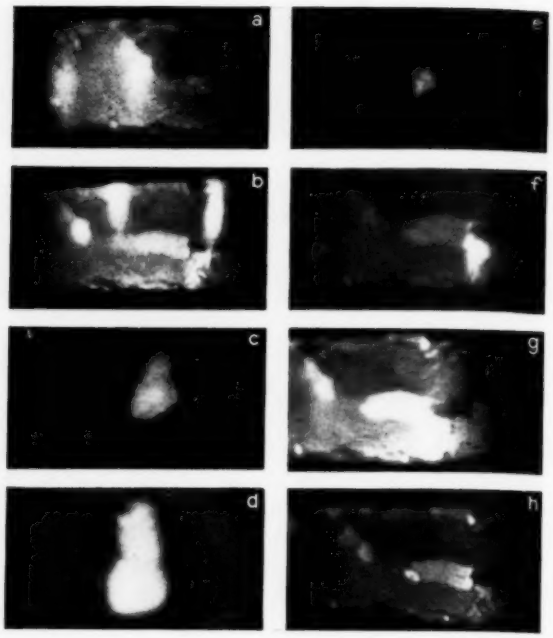

FIG. 5. Thorium eruptions on large grain thoriated tungsten ribbon. Exposure time—*a*, *b*, *c*, *d*, *f*, *g*, *h*, 60 sec., *e*, 120 sec. Temperature and time of heat treatment preceding image, average degree of thoriation f and photographing temperature are given in order. *a*, 2450°K, 7 min. 0.05, 1740°K; *b*, 2520°K, 5 min. 0.05, 1740°K; *c*, (2440°K 9 min., 1930°K 2 sec.) 0.10, 1390°K; *d*, none, 0.20, 1660°K; *e*, 1890°K, 2 sec. 0.05, 1500°K; *f*, none, 0.10, 1605°K; g, none, 0.10, 1710°K; *h*, 1620°K, 1 min. 0.10, 1605°K.

They appear to be the most important if not the only means whereby thorium comes to the surface.

4b. Where do Eruptions Occur?

Figure 5 shows some typical eruptions occurring on grain boundaries of a rather large grain filament. In picture *e* the growth of an eruption was arrested quite early in its life by suddenly cooling the filament. Comparison of the negatives for *e* and *f* (taken after more migration on the filament had occurred) shows very distinctly that the dark irregular lines through the spot in *e* correspond with grain boundaries in *f*. Counts of eruptions occurring on large grain filaments such as shown in Fig. 5 show that about $\frac{1}{3}$ of the eruptions occur on grain boundaries and the remaining $\frac{2}{3}$ definitely occur off grain boundaries. In general, eruptions do not repeatedly occur in the same place. Other studies have shown that eruptions do not occur with the same frequency on all grains. On some grains eruptions were never observed.

The electron emission pattern of a Pintsch single crystal thoriated tungsten filament (in an electron projection tube after the fashion of Johnson and Shockley[14]) consisted of about six active bands parallel to the filament axis alternated with inactive bands. These bands are probably related to the faces of the single crystal filament. Eruptions occurred exclusively on the active bands. This indicates that thorium diffuses in certain directions inside the tungsten crystal much more readily than in other directions.

4c. Factors That Influence the Occurrence of Thorium Eruptions

Eruptions occur at temperatures as low as 1500°K. Fig. 4 shows some that appeared after treatments at slightly higher temperatures. In general, the frequency of eruptions increases with the temperature.

A high temperature flash temporarily increases the frequency of eruptions at a lower tempera-

ture. A wire filament was flashed at about 2900°K for about a minute; then the number of eruptions per minute at 1920°K was counted. The results, plotted in Fig. 6, show that this number decreased rapidly with time soon reaching a constant value of about one-ninth of the initial value. If the filament is then suddenly cooled and reheated, the eruption frequency is temporarily increased.

Eruptions were observed to occur only at values of f below about 0.4. There are reasons for believing that it should be very difficult to observe eruptions at high values of f. The contrast in brightness between the eruption point and its immediate surroundings would be much smaller at high activities. The migration and evaporation of thorium from an eruption point would be faster at high activities. Hence, it would be difficult if not impossible to observe eruptions at high activities.

4d. Comparison of Thorium Eruptions and Thoria Globules

The amount of thorium coming to the filament surface when an eruption occurs was estimated in the following ways. For photographs of electron images like those in Fig. 4 showing the life history of thorium eruptions, the assumption was made that at its maximum brightness the eruption spot was covered with one monatomic layer of thorium. From the magnification, the spot diameter at which this maximum brightness persisted and the number of thorium atoms in a monatomic layer (7.1×10^{14} atoms/cm^2) the number of thorium atoms emitted during an eruption was calculated. These range from 1×10^9 to 52×10^9 atoms per eruption for the fine grained ribbon of Fig. 4 and from 110×10^9 to 540×10^9 atoms per eruption for the large grained ribbon of Fig. 5.

The second method of calculation can be outlined with the aid of Fig. 4. From the measured temperature and emission current density,[15] the average f was found[2] to be 0.11 in picture h. This corresponds to 8×10^{13} atoms per cm^2 and to 1.2×10^{11} atoms in the field of view. In the picture sequence a to h, about 15 eruptions appear. The assumption is made that these eruptions contributed all of the thorium that is on the surface in picture h. The average amount emitted by one eruption is $1.2\times10^{11}/15$ or 8×10^9 atoms of thorium. The two methods give concordant results.

From the known value of N, the number of thorium atoms per eruption, the mass of the corresponding N molecules of thorium oxide was calculated. From this mass and the density of thorium oxide (9.7 g/cm^3) the volume of the thorium oxide was determined. From this the equivalent sphere diameter was calculated. Curve 1 of Fig. 8 gives the distribution curve of such sphere diameters. On the large grain ribbon the necessary data and photographs for these calculations were taken for only a few eruptions. These individual values are indicated by triangles on the diameter axis of Fig. 8. Thus Fig. 8, curve 1, gives the percentage of eruptions, whose equivalent sphere diameters lie in the interval d to $d+10^{-5}$, as a function of their diameter d.

On neither the large nor on the small grain filament did eruptions occur in the same place

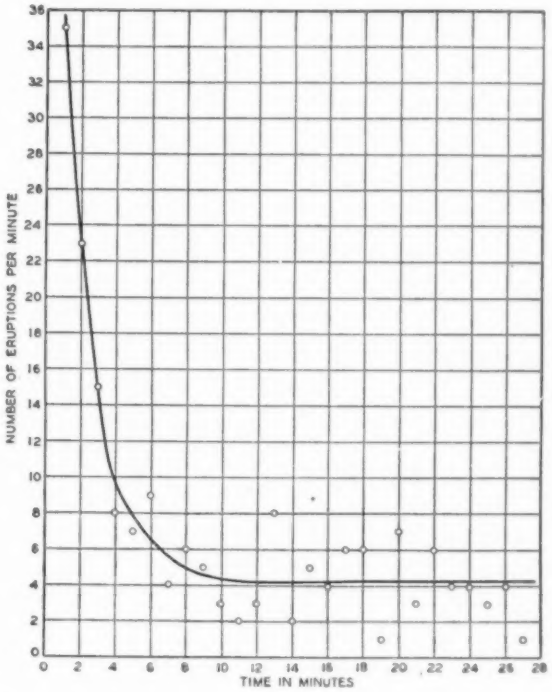

Fig. 6. Variation of eruption frequency with time after flashing thoriated tungsten wire.

[15] For the small grain ribbon, the current density was calculated from the emission and the area of the entire ribbon. For the large grain ribbon, it was calculated from the emission coming from the area of the filament in the field of view.

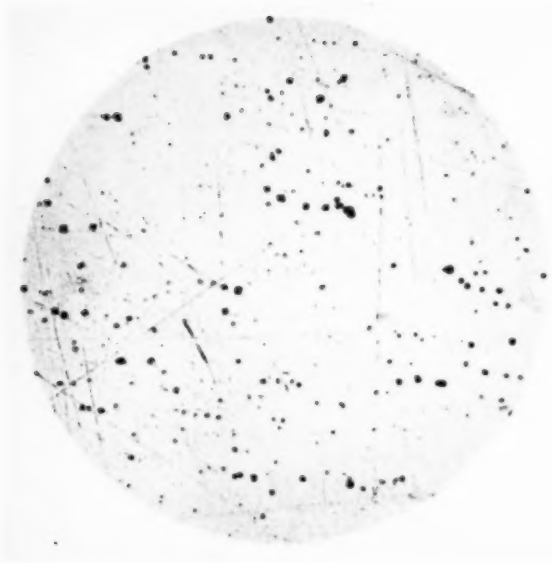

FIG. 7. Photomicrograph of interior section of fine grain thoriated tungsten ribbon (×1000).

repeatedly. Furthermore, the eruptions on the large grain filament were in general much larger than those on the fine grained one. Now it is well known that the globules of thorium oxide increase with the grain size of the tungsten. To explain these facts, the following hypothesis was made; when an eruption occurs, a globule of thorium oxide decomposes and all of the thorium in the globule comes to the surface.

This hypothesis was tested by an independent determination of the size of the thorium oxide globules as follows. The photomicrographs of the ribbons shown in Fig. 3 made after the electron image studies were concluded, reveal a large number of small black spots. The following facts indicated that these spots are related to the thorium oxide in the tungsten.

1. Tests with an optical microscope with different types of illumination show that the spots are depressions or holes whose shapes were roughly parts of spheres. Now in thoriated tungsten which has been heat treated, the thorium oxide is dispersed in little globules.

2. On the large grain filament these spots are larger than on the fine grain one. As stated earlier, the thoria globules increase in size as the grain size of the tungsten increases.

3. More of these spots occur on grain boundaries than within the grains. The thoria globules also occur more frequently on grain boundaries[16] than within the grains.

[16] Jeffries, Proc. Inst. Met. Div. (A.I.M.E.), (1927), p. 395.

These related facts suggest that the spots or holes are former sites of thoria globules at or near the surface and that the size of the globules can be calculated from the size of these holes. The diameters thus calculated were about twice the value deduced from eruption data. Since evaporation of tungsten would tend to enlarge the holes on the surface, it seemed preferable to examine the interior of the ribbon. Therefore, the ribbons were ground down and the new surfaces were polished. Fig. 7 is a photomicrograph of this interior section of the fine grain ribbon at a magnification of 1000. Black spots, i.e., holes again appear. On the large grain ribbon (not shown) they are larger in size and smaller in number than on the fine grain ribbon.

To test further the assumption that the circular spots on these polished surfaces are sections through thorium oxide globules the total volume corresponding to the spots was calculated.[17] This volume ranged from 1 to 3 percent of the tungsten volume for various regions of the ribbon. Chemical analysis of large samples of these ribbons showed that the thorium oxide content was about 2 percent by volume. This confirms the assumption that these spots are sections through thoria globules.

We want to obtain the diameter distribution of the thorium oxide globules that appear in Fig. 7. Unfortunately this photomicrograph does not give a direct measure of these globule diameters. Due to the grinding and polishing of the ribbon the resulting sections of globules of a given diameter d appear as spots whose diameters range from zero to d. Curve 3 of Fig. 8 which is for the region shown in Fig. 7 gives the distribution of the section diameters of the globules.

Suppose we now calculate the distribution of sections to be expected if the true globule diameters are given by curve 1, Fig. 8. Consider a sphere cut by a large number of parallel equally spaced planes. The resulting section diameters will increase rapidly from zero as the intersecting planes go from the pole to the equator. Thus it is evident that a plane, cut through a volume containing a number of spheres

[17] In making this calculation section diameters were converted to true sphere diameters as explained in subsequent paragraphs.

of equal diameter d, will reveal many sections whose diameters are nearly equal to d and relatively few that are nearly zero. The distribution function for the section diameters is

$$f(x) = x/(d^2 - x^2)^{\frac{1}{2}}, \qquad (1)$$

where the section diameter x ranges in value from zero to the sphere diameter d.

By means of Eq. (1) it is possible to derive the distribution of section diameters that would be expected from the distribution of globule diameters given by curve 1 of Fig. 8. Curve 2 gives this section distribution derived from eruption data. Curve 3 gives the section distribution observed in an optical microscope. The agreement between curves 2 and 3 is probably better than would be expected. These curves are for the fine grain ribbon.

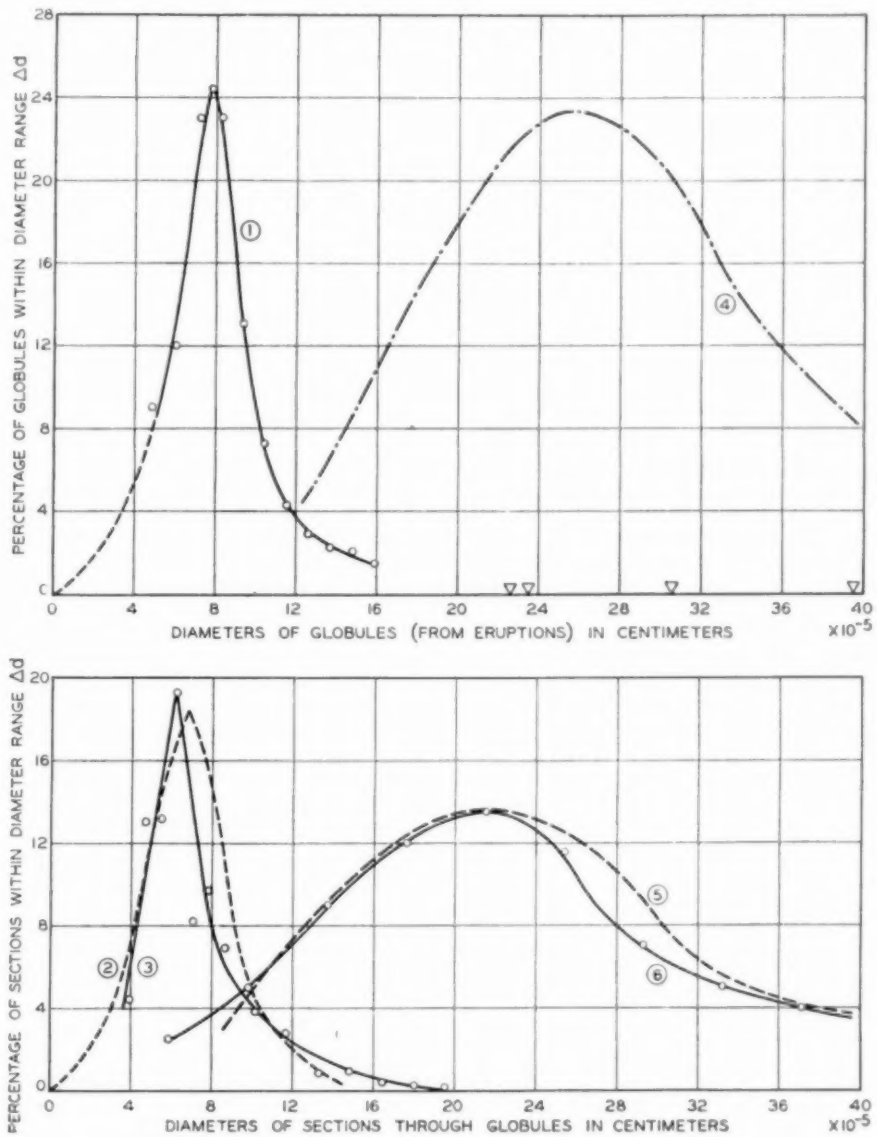

FIG. 8. Distribution of thorium oxide globule diameters. Fine grain ribbon ($\Delta d = 1 \times 10^{-5}$ cm). Curve 1, calculated from electron images of thorium eruptions. Curve 2, distribution on a section expected from curve 1. Curve 3, distribution observed on photomicrograph of section. Large grain ribbon ($\Delta d = 5 \times 10^{-5}$ cm). ▽ calculated from electron images of thorium eruptions. Curve 4, assumed distribution. Curve 5, distribution on a section expected from curve 4. Curve 6, distribution observed on photomicrograph of section.

On photomicrographs of the coarse grain filament, the distribution of section diameters given by curve 6, Fig. 8, was observed. By trial and error, curve 4 for sphere diameters was found which gave a section diameter distribution (curve 5) that is in good agreement with the observed curve 6. As previously stated, only four values of globule diameters were obtained from eruption data. They are shown by the triangles along the diameter axis in Fig. 8. These four measured values fall within the expected range given by curve 4.

The data of Fig. 8 particularly curves 1, 2 and 3 indicate very strongly that the distribution curve obtained from the eruption data gives the actual distribution of thorium oxide globules. Now in the eruptions, the phenomenon is one in which thorium has come to the surface. This confirms the hypothesis proposed at the beginning of this section; *when an eruption occurs approximately all of the thorium in a globule of thorium oxide comes to the surface.*

On the basis of these observations and deductions, we believe that a thorium eruption occurs when a vent is opened between a thorium oxide globule and the surface of a filament. When this happens, all of the thorium oxide is reduced and the thorium diffuses to the surface, where it migrates or evaporates. This suggestion is supported by the evidence of Wartenburg and Moehl[18] that tungsten reduces thorium oxide. A thorium oxide globule embedded in a mass of tungsten represents a closed system in which the following reaction would be in equilibrium

$$\mathrm{Th\,O_2 + W \leftrightarrows WO_2 + Th.}$$

Of the four constituents, the tungsten oxide and the thorium have the higher vapor pressures. When a vent between the cavity and the tungsten surface is opened they escape more rapidly than the thorium oxide and tungsten. Thus the equilibrium is upset and the reaction proceeds from left to right until the thorium oxide is completely reduced.

The particular part played by the tungsten oxide in this process is not yet clear. It may evaporate much more readily than thorium; or tungsten oxide on tungsten may not greatly alter the emission properties of thorium on tungsten. There is some evidence that a thoriated filament gives off oxygen,[19, 20] or an oxide, which deactivates another tungsten filament in the same tube.

5. Migration of Thorium on Tungsten

Migration of thorium occurs at the lowest temperature at which eruptions occur, i.e., about 1500°K. Fig. 4 shows this migration from the eruption centers over the surface of the tungsten. During their growth the spots remain approximately circular in shape. This shows that on the fine grained filament, the thorium migrates with equal ease in all directions.

In contrast to this isotropic migration of thorium on the polycrystalline ribbon, Fig. 9 shows the migration phenomenon after an initially small grained filament had been grown into a single crystal.[21] Here the thorium migrates in a preferred direction over the surface of the tungsten crystal. This preferred direction of migration makes an angle of from zero to 12° with the cross direction of the ribbon, the most probable angle being about 7°.

After the microscope was dismantled, this filament was examined by x-rays.[22] An 11 mm section of the filament containing the field of view consists of one single crystal with the exception of some small crystals on the two edges. The orientation of this (body-centered cubic) single crystal is as follows. The surface of the ribbon is a (211) plane with a (110) normal at an angle of 8° with the rolling direction (the length of the ribbon) and a (111) normal making an angle of 8° with the cross direction. The direction of most probable migration (about 7°) is in excellent agreement with this (111) direction. These two facts show that *on the (211) plane of a tungsten crystal, thorium prefers to migrate in the (111) direction.* In this plane, this is the direction in which the separation between rows of atoms is greatest. This probably means that in this direction the migrating atom encounters the lowest potential hills.

[18] Wartenburg and Moehl, Zeits. f. physik. Chemie **128**, 439 (1927).

[19] Nottingham, Phys. Rev. **49**, 78 (1936).

[20] Coomes, Phys. Rev. **53**, 936 (1938).

[21] The circular spot near the center is due to light from the filament.

[22] We are grateful to Mr. F. E. Haworth of these laboratories for this analysis.

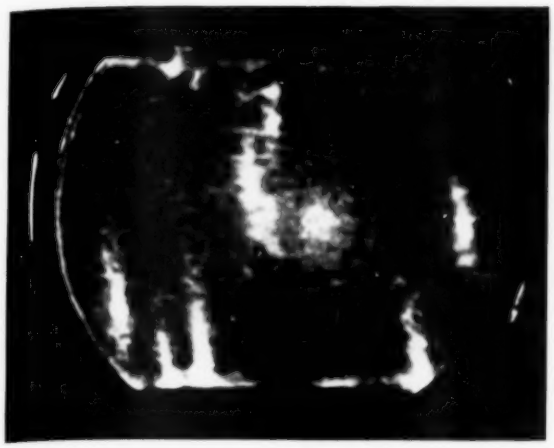

FIG. 9. Thorium eruptions and the migration of thorium in a preferred direction over the surface of a single crystal of thoriated tungsten.

At one stage in the growth of this single crystal, the field of view as shown diagrammatically in Fig. 10 consisted of an island of polycrystalline tungsten surrounded by the single crystal. When an eruption occurred in position 1, the thorium migrated in the preferred direction shown by the arrows, corresponding to the preferred direction of Fig. 9. When one occurred in position 2, the thorium migrated equally in all directions until it reached the edge of the polycrystalline island. Then the thorium migrated in the preferred direction over the single crystal. Conversely when an eruption occurred in position 3, the migration took place in the preferred direction until the thorium reached the polycrystalline island; then it migrated fanwise over this island.

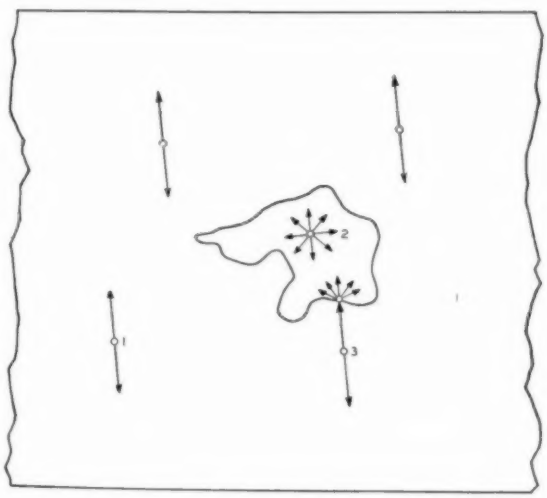

FIG. 10. Directional migration of thorium. Polycrystalline surface *vs.* single crystal surface thoriated tungsten ribbon.

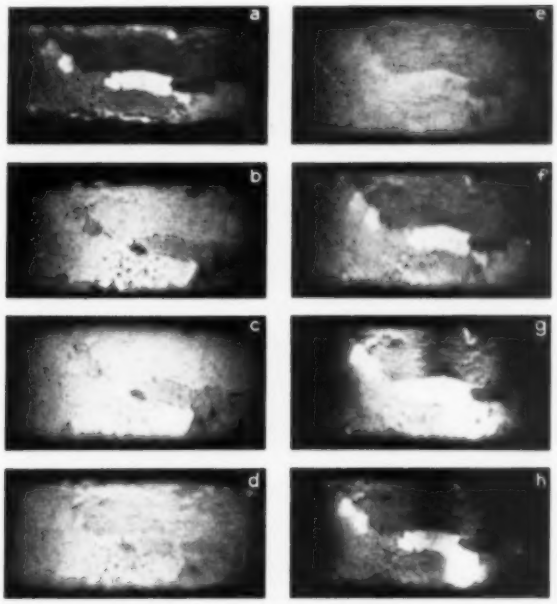

FIG. 11. Reversal of electron image pattern with change in degree of thoriation. Exposure time—*b*, *c*, *d*, *e*, *f*, *g*, *h*, 5 sec., *a*, 60 sec. Temperature and time of heat treatment preceding image, average degree of thoriation *f* and photographing temperature are given in order. *a*, 0.11, 1620°K; *b*, 0.54, 1405°K. Further activation treatments raised *f* to 0.70. *c*, 1970°K, 10 min. 0.56, 1440°K; *d*, 2100°K, 1 min. 0.42, 1515°K; *e*, 2140°K, 1 min. 0.32, 1580°K; *f*, 2180°K, 5 min. 0.22, 1675°K; *g*, 2220°K, 6 min. 0.13, 1755°K; *h*, 2340°K, 5 min. 0.07, 1840°K.

Some of the photographs in Fig. 5 also show a preferred direction of migration. The direction of migration on one ribbon which contained only 3 or 4 large grains varied as much as 90° for different grains.

6. Reversal of Pattern with Degree of Thoriation

How do the relative electron emissivities of different crystal grains vary as the average amount of thorium on the filament surface is varied? The series of photographs in Fig. 11 shows the changes in the electron image as the degree of thoriation was varied from about 0.11 to about 0.70 and then down again to about 0.07. A comparison of pictures *a* and *b* shows that the relative emissivity of nearly every grain with respect to its neighbors is markedly

changed. Moreover, in most of these cases, this change is so great that the relative emissivities are reversed. The degree of this reversal, however, varies considerably from grain to grain.

During the dethoriation process, as shown by the picture sequence c to h, the image reverses back to the original pattern shown in a. At $f=0.4$ approximately, the electron image is quite uniform and lacking in contrast.

One factor which probably contributes to the reversal is the different rates of accumulation of thorium on different grains. The rate of accumulation on any one grain is probably determined by the surface forces associated with the particular exposed face of the grain or single crystal. It is probably conditioned also by the abundance of thorium oxide globules within the grain or in its neighborhood. Furthermore, the phenomenon of migration in a particular direction characteristic of the face of the grain may be a factor influencing the rate of accumulation.

Another factor which contributes to the reversal phenomenon is suggested by the probable fact that of two surfaces the one having the higher work function when clean will have the lower work function when covered with the optimum amount of adsorbed electropositive material. If this is true, the emission from two grains of tungsten having different work functions would vary as shown schematically in Fig. 12 as thorium is deposited thereon. The electron images of grains A and B of Fig. 12 would become "reversed" beyond $f=0.3$.

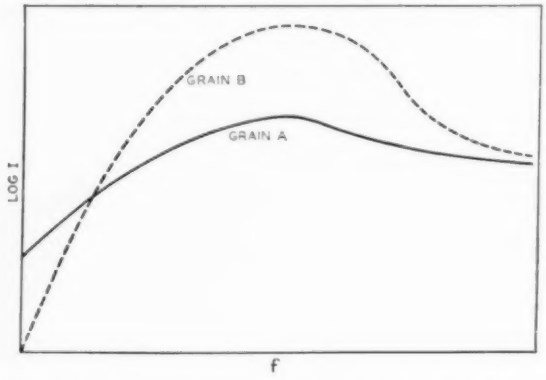

FIG. 12. Activation curves for different grains of thoriated tungsten suggested by reversal of pattern of electron image.

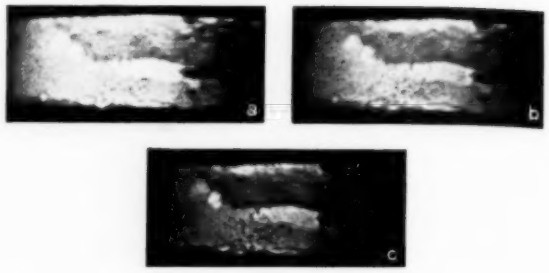

FIG. 13. Work function differences between grains of thoriated tungsten. Filament temperature 1460°K. Degree of thoriation f 0.25. Exposure times, a, 120 sec.; b, 60 sec.; c, 30 sec.

7. Work Function Differences

The electron microscope is readily adapted to a quantitative measure of work function differences between grains of filaments. The method consists in taking photographs of the electron image, keeping all conditions such as temperature, applied voltages, etc., constant but varying the time of exposure. To determine work function differences between a pair of grains from such a series of photographs one selects the shortest time exposure of the more active grain and determines the exposure on which another grain shows the same degree of blackening. To a first approximation one may then conclude that the inverse ratio of the two exposure times gives the ratio of their electron emissivities and from this ratio, by means of the equation

$$i=120T^2\epsilon^{-\phi e/kT} \qquad (2)$$

one can calculate the difference in work function for pairs of grains.

Figure 13 contains 3 photographs in which only the exposure time is varied. These show the grains numbered in Fig. 3. Matching densities of grains 2 and 1, 1 and 6, 6 and 3, 3 and 4 showed that the electron emissivity of grain No. 2 is about one hundred twenty-eight times as great as that of No. 4. Eq. (2) then gives a work function difference between grain No. 4 and 2 of about 0.6 of a volt. The electron images of Fig. 13 where $f=0.25$ reveal work function differences between grains ranging from 0 to 0.6 volts. The electron images of Fig. 11 show that this work function range depends upon f.

Construction of Filament Surfaces*

R. P. JOHNSON
Research Laboratory, General Electric Co., Schenectady, N. Y.

(Received May 12, 1938)

An incandescent tungsten filament gradually loses its die marks and comes to display a surface whose structure depends on whether the lamp was evacuated or gas-filled, and on whether it was run on a.c. or on d.c. Filaments heated in vacuum with a.c. remain smooth and nearly round. In neutral gas, with a.c., the filament tends to expose smooth concave (100) faces. The d.c. vacuum structure is steplike, is polarized with respect to the current, and seems to be due to a drift of W ions in the field along the filament. Surface migration of Th adsorbed on W, during d.c. heating, has been demonstrated in a simple electron-optical tube. Structure identical in form with the d.c. structure appears on a.c. filaments where a temperature gradient exists, and is attributable directly to surface diffusion in the temperature gradient. On d.c. gas filaments the d.c. structure and the gas structure are concurrent. No small-scale structure is found microscopically; probably the only substructure is atomic in scale. Preliminary study of Ta, Mo, Pt, Fe and Ni filaments in vacuum indicates that these metals also develop a roughened surface on d.c. heating, but remain smooth on a.c.

INTRODUCTION

THIS study was undertaken in the hope of finding answers to two questions. Imagine some simple solid, such as a sphere, cut out of a single crystal of metal at 0°K, with its surface as nearly smooth as the atomic nature of the lattice will allow. If this sample is heated so that atoms evaporate from it irreversibly, how will its shape change, and what sort of structure will the surface, originally smooth, come to display? If the sample is held in equilibrium with the vapor for a long time, what shape and what surface structure will result?

These questions, aside from their intrinsic interest, are of importance in the study of thermionic emission, adsorption and surface reactions, pyrometry, and lighting. A cylindrical filament of tungsten, heated by electric current, is, for well-known reasons, the metal sample most commonly used in experiments in all these fields. The tungsten filament is also a most convenient test object for studying the surface effects of drastic heating. Burned-out incandescent lamps afford a plentiful supply of specimens which have been held at high temperatures for about 1000 hours. Much of this investigation, then, has been a microscopic study of filaments from several hundred burned-out incandescent lamps, of various sizes and from various manufacturers.

* This investigation began at the Massachusetts Institute of Technology in 1936. The results were reported in part at the Washington Meeting of the American Physical Society in April, 1938.

RECRYSTALLIZATION OF TUNGSTEN WIRE; GAS IN LAMPS

The fibrous crystals in raw drawn tungsten wire have a [110] axis preferentially along the wire direction,[1] with this preference more marked near the axis.[2] When a straight wire recrystallizes on heating, the resulting equiaxed crystals have the same degree of alignment locally as the original fiber structure if they are so small that a cross section of the wire comprises many of them. If the final crystals are so large that they extend through the wire, they have the same degree of alignment as the original fibers near the outside. Apparently the large crystals grow from nuclei near the surface; this view is consistent with the idea that the material near the surface is most highly strained in the process of drawing.

The size of the final crystals depends chiefly on the impurity content. Wires containing 1 to 2 percent of thoria usually grow only small crystals; the "218" wire generally used in lamps is so doped that it grows overlapping crystals many wire diameters long; very pure tungsten, like other pure metals, grows crystals one or two wire diameters long, with boundaries nearly transverse to the wire. Helical lamp filaments of 218 wire often contain crystals 20 to 30 turns long; the helix is as if it were hewn from a single-crystal block.

[1] M. Ettisch, M. Polanyi and K. Weissenberg, Zeits. f. physik. Chemie **99**, 332 (1921).

[2] This, and succeeding statements in this paragraph, are based on unpublished x-ray studies by Mr. R. B. Nelson and the writer.

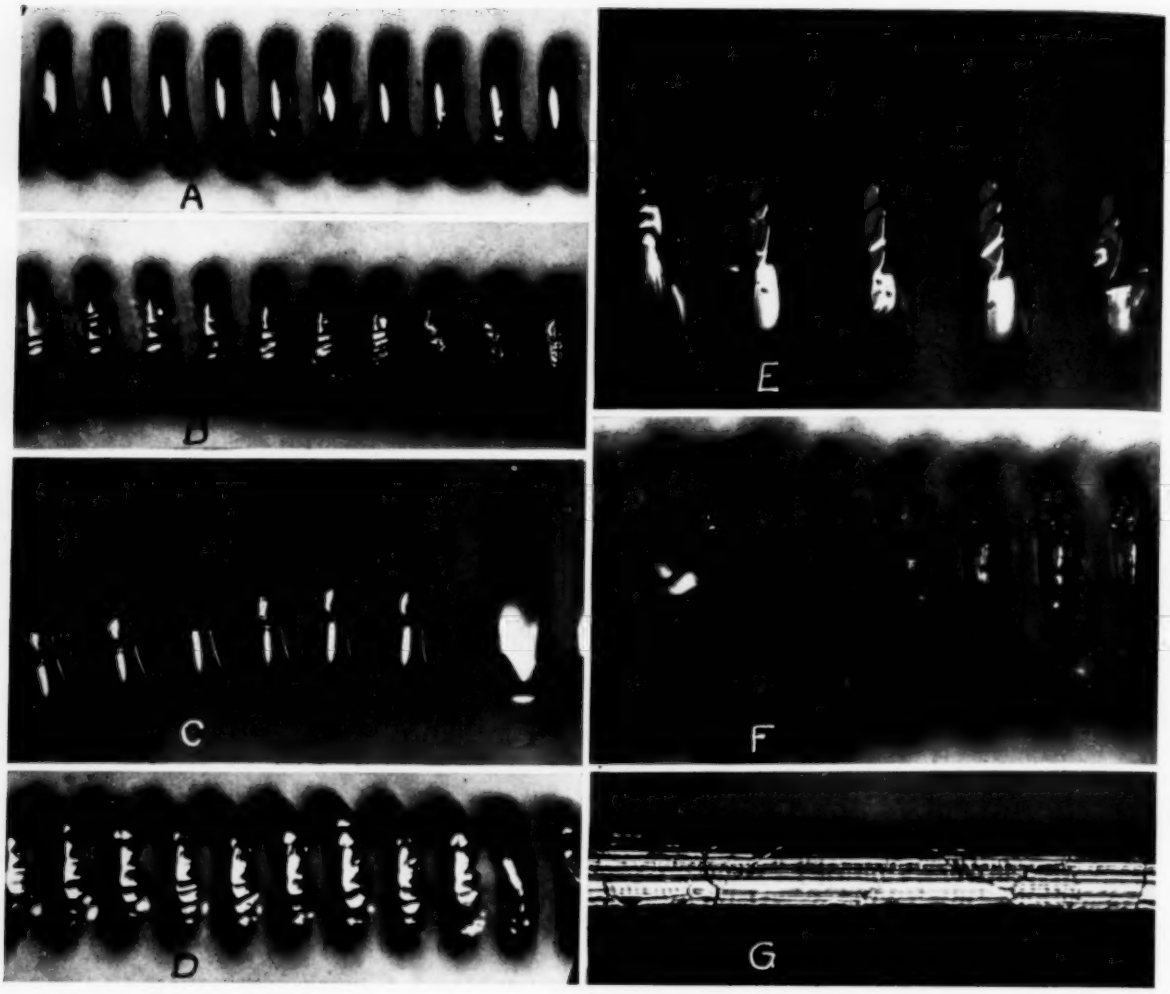

FIG. 1. *A*, Typical a.c. vacuum helix, with wire round and smooth except for grain boundaries. *B*, Hook-region structure on an a.c. vacuum helix. *C*, Structure on a small (50 w) helix heated with a.c. in lamp gas. *D*, Helix heated in vacuum with d.c., top of turns negative. *E*, Stile structure on a helix heated with a.c. in pure argon. *F*, Spine growth near a burnout in lamp gas. *G*, Residual die marks on pure tungsten heated with a.c. in vacuum.

Mazda lamps of 40 watt size and larger are currently filled with 86 percent A+14 percent N_2 ("lamp gas") at 60 cm cold pressure. Lamps of smaller size are evacuated.

THE FOUR TYPES OF SURFACE STRUCTURE

Judged solely by surface appearance, helical filaments from used incandescent lamps fall unambiguously into four classes. Surface structure is correlated with voltage supply and gas filling as follows:

(1) Alternating current in vacuum

To the naked eye, these filaments over most of their length look uniformly gray. Microscopically they are smooth and round, showing no irregularities except occasional grain boundaries with rounded edges (Fig. 1(*A*)). However, at the ends of the wire and at each support hook, for about 8 turns there is a characteristic step-like structure (Fig. 1(*B*)). This structure is repetitive, except for prominence, on all the turns in a single crystal, and hence is related to the lattice arrangement.

(2) Alternating current in gas

The glint of these filaments under a light indicates reflecting surfaces unrelated to the original cylinder surface. Under the microscope there appears a regular structure of smoothed

curved faces with linear dimensions of the order of magnitude of the wire diameter (Fig. 1(*C*)). The structure is repetitive on all turns of a single crystal and therefore is oriented with respect to the lattice. The structure increases in complexity with increasing wire size. It is quite unlike the step surface on a.c. vacuum wires at hooks and ends. At hooks and ends of a.c. gas wires the characteristic step structure appears, seemingly superposed on the typical a.c. gas structure.

(3) Direct current in vacuum

To the naked eye, the filaments look like the a.c. gas filaments. Microscopically, the structures are entirely different. The d.c. vacuum structure is apparently identical with the hook-region etching on a.c. wires. The original surface is approximated by a series of steps, smooth and nearly plane, somewhat smaller in scale than the wire diameter, and alike for all the turns in a single crystal (Fig. 1(*D*)).

(4) Direct current in gas

On these wires, the gas structure found on a.c. filaments and the d.c. structure found on vacuum filaments are apparently concurrent.

Straight filaments and coiled-coils also fit uniformly into these four groupings.

On samples of all these various surface types, etching on a smaller scale has been sought with a Leitz Ultropak illuminator and magnification up to 2500. No trace of regular structure appears. If substructure exists, its linear dimensions cannot exceed a few thousand atom diameters.

Mechanism and Detail of the Gas Etching

Since the gas structure and the d.c. structure are superposable, they can be attributed to independent mechanisms. We consider first the difference between the smooth a.c. vacuum wires and the strikingly "etched" a.c. gas wires, and overlook for the moment the hook-region structure which is common to both.

The wires in gas have not suffered more net evaporation: weighing of several thousand counted turns showed that the wires burned out in vacuum had lost about 17 percent of their weight, while the wires burned out in gas had lost only about 5 percent.[3] Etching in $HF+HNO_3$ showed that the crystals in both groups have the same average size. The deep gas structure obviously could not be formed by gouging tungsten from a new wire, without losing at least 20 percent of the material. Clearly, tungsten must have been transported from one part of the wire to another. The stationary gas jacket, through which evaporated tungsten atoms diffuse, with high probability of returning to the wire and recondensing,[4] obviously provides a mechanism for moving tungsten from surfaces with high evaporation rate to surfaces with low evaporation rate. The observation that the gas structure is less prominently developed on the inside of helices and coiled-coils, where the wire surface is slightly hotter and the gas is more tenuous, is consistent with this view.

The gas structure, then, seems to merit attention as an intermediate stage between the original helical filament and the form that would develop if the wire attained equilibrium with the vapor. Helical single crystals, exposing every possible crystallographic surface twice in each turn, are particularly apt for study. The 40-watt filaments have the gas structure in its simplest form. The feature most readily identified is a small projecting face, about $\frac{1}{5}$ the wire diameter in size, approximately plane, generally rhombic, and quite often hollowed out in the center with an elliptical dimple. From each corner of the rhombus a ridge runs away, and from each edge a long concave smooth surface extends to an edge of the next such dimpled flat. The complicated structure on larger wires is actually of the same sort: The single dimples are replaced by groups of dimples, 10 or 12 in a group on 200-watt wires. The ridges running from corners, and the long concave smooth surfaces, occur on the larger wires as on the smaller. Goniometric study of 50 long crystals in wires of different sizes, checked by Laue pictures, has led to the following crystallographic assignment: the dimpled flat faces and the ridges are both approximately normal to the dodecahedral [110] axes, and the large concave smooth surfaces are approximately normal to [100] axes.

[3] See G. R. Fonda, G. E. Rev. **32**, 206 (1929) for similar results on weight loss from straight wires.
[4] I. Langmuir, A.I.E.E. **32**, 1913 (1913).

Interpretation of the Gas Etching

Several considerations might deter us from taking the cube, which these helical crystals are apparently approaching, as the approximate form of a tungsten single crystal in equilibrium with the vapor. First, there is the possibility, since a.c. and d.c. produce widely different surfaces, that the electric current itself influences the surface form, and that heating in lamp gas without current would give yet another surface. That this caution is probably extreme appears when the frequency of the heating current is varied. Filaments of various sizes, straight, helical, and coiled-coil, in vacuum and in gas, were run on 60-cycle a.c., 25-cycle a.c., 500-cycle a.c., 25-megacycle a.c., and square-wave a.c. with a period of two minutes. No dependence on frequency was found. It can be concluded with fair reason that heating with a.c. is equivalent to heating without passage of current.

Second, there is the effect studied by Langmuir,[5] that a tungsten atom evaporating into an atmosphere containing N_2 readily (probability near unity for a single gas-kinetic collision) combines with a nitrogen molecule to form the nitride WN_2. This molecule, if it reaches the bulb wall, contributes to a brown deposit. Since the lamp gas contains N_2, heating in lamp gas is not, at first glance, even approximately equivalent to heating in a Hohlraum; in the lamp gas, many tungsten atoms that return toward the surface bring with them two nitrogen atoms. It seems unlikely, however, that this difference will have any effect on the developing surface structure. It could be effective only if the WN_2 molecules reached the filament without dissociating, and if the condensation coefficient for these were a different vector function from that for W atoms. The experimental fact that the gas jacket does greatly retard net evaporation indicates that the condensation coefficient must be near unity for all the surface—such small local differences as may exist are not probably decisive for the structure.

Third, there is a possibility that N_2 may be attacking the wire slightly, at a rate which varies markedly with lattice direction. Fonda[3] has noted that lamp filaments suffer a greater average loss of weight in pure A than in lamp gas, and a greater loss in lamp gas than in pure N_2. If there is a slight direct attack by some mechanism involving N_2, at a rate which increases with temperature more rapidly than does the evaporation rate of W, the disastrous effect of thin spots in the wire will be accelerated in the presence of N_2, and the observed order of weight-loss at burnout is to be expected.

To check these last two possibilities, several lamps were exhausted and refilled, some with pure A and some with pure N_2. On 60-cycle a.c., the filaments in N_2 developed the same structure as appears in lamp gas. The structure in A was different in one major particular; the small (110) faces, instead of being dimpled, were built up in a symmetrical stile-like arrangement of flat steps and short risers; the larger wires had more steps in each stile (Fig. 1(*E*)).

It can be concluded tentatively that the dimpling of the residual (110) faces in gas containing N_2 is due to an attack on the metal, the reaction rate of which is a vector function. Conversely, the structure developed in pure A by a.c. heating can be taken as an approximation to the equilibrium structure. Recalling that the sample is not growing slowly from a nucleus, but is slowly modifying an imposed form, we may plausibly assume that if equilibrium were attained the (110) faces would have disappeared, and only the (100) surfaces would remain exposed. The (100) surfaces are concave, probably because they have a temperature gradient from the center outward—the Joule heating is more widely dispersed near a projecting edge, and the wire is not in an isothermal enclosure. Material will obviously be transported down such a temperature gradient, whether the mechanism be one of evaporation-condensation or one of surface diffusion. Concavity of true equilibrium faces need not be expected. It is to be noted that the cubic (100) surfaces, which are apparently increasing their exposure in this simple evaporation-condensation process, are not so densely populated as the dodecahedral (110) surfaces, which an elementary theory would regard as the most stable bounding planes for a body-centered cubic lattice.

[5] I. Langmuir, J. Am. Chem. Soc. **35**, 931 (1913); Zeits. f. anorg. allgem. Chemie **85**, 261 (1914).

The projecting spines, sometimes found on several helix turns at each side of a burnout in gas, are other evidence for anisotropy of crystal growth. These spines spring almost without exception from the raised edges of the original structure (Fig. 1(*F*)). The concave (100) faces remain smooth; the dimple in each (110) face remains depressed and is surrounded by a rosette of spines grown out from the neighboring flat region. The ends of spines are often flat, or pyramidal with flat faces. Occasionally the "spines" are clusters of quasi-perfect crystals. It seems necessary that atoms, after diffusing from the vapor and striking the spines, migrate on the surface to favorable permanent locations. Spine structure occurs only in gas, and is comparatively rare. More often the end at a burnout is a polished sphere which, etching shows, comprises 3 or 4 crystals.

Mechanism of the d.c. Etching

We next inquire why d.c. heating in vacuum produces a step-like structure, in contrast to the smooth surface developed on a.c. Alternating current at any frequency greater than about 1 cycle/min. produces the typical smooth a.c. surface. Half-wave 60-cycle rectified current produces the typical rough d.c. surface. Intermittent heating with an on-off period of about 1 sec., on either d.c. or 60-cycle a.c. produces the same sort of surface as continuous heating from the same sort of voltage supply. From this evidence it is clear that the frequency, form, and amplitude of the temperature oscillations are not concerned. Whether the a.c. or the d.c. structure develops depends only on whether the current is unidirectional or alternates in direction. The d.c. structure occurs with equal average prominence on all sides of a helical wire, inside as well as outside. This observation rules out any significant action of the magnetic field or of the electric field on evaporating ions or atoms. Any mechanism primarily involving tungsten ions in the vapor is ruled out by the rarity of ion evaporation: a rough estimate gives 10^{-7} as the probability that a tungsten atom in evaporating shall leave a valence electron with the metal.

The d.c. structure is apparently due to a migration, over the surface, of positive tungsten atom-cores, driven by the longitudinal electric field. If we assume that the rate of drift depends on the type of underlying surface, and is different for different directions on a surface of given type, obviously the development of steps on a surface which is continually changing in character in the direction of the field (a helix, for example) can be qualitatively explained. This assumption is inherently reasonable, and is supported by two pieces of evidence on the analogous process of diffusion. One of these is the spine growth mentioned above; the other is the observation, by electron-optical methods, that activating material diffusing from a source spot out over a heated single-crystal surface of metal, spreads symmetrically but not circularly, with the contours of equal concentration oriented with respect to the lattice.[6] Once steps have started, cooling from the edges and dispersion of the Joule heating will both act to accelerate their growth.

Detail and Polarization of the d.c. Structure

Study of a large number of d.c. helical crystals (chiefly from small size gas-filled lamps, with the simpler gas structure as an orienting background) has shown that the flat steps are approximately (100) planes. The d.c. structure on helices has a definite polarization, easily recognizable. In silhouette, the etching shows sawteeth of greater or less pitch, which point always toward the negative end of the wire.

On straight wires, the d.c. structure consists of steps which run diagonally across the wire, giving a herringbone effect. These herringbone stripes first begin to come out on sides of the single-crystal cylinder where (110) planes are most nearly coincident with the surface, while other sides of the wire are still smooth. Where the etch on straight wires is well developed, it is polarized with the sawteeth pointing toward the negative end. It will be noted that the hypothesis advanced above for the d.c. structure will not account for steps running diagonally across a straight cylindrical crystal. No fully satisfactory way of avoiding the symmetry con-

[6] A. J. Ahearn and J. A. Becker, Phys. Rev. **54**, 448 (1938). I am indebted to Dr. Ahearn for a discussion of this point.

sideration, that all points on an element of a single-crystal cylinder are equivalent, has yet appeared. Some phenomenon of "rhythmic precipitation" is seemingly involved. Only a few straight large-crystal wires have thus far been studied.

It has been remarked that current reversal once a minute results in the typical smooth a.c. surface. When the current is reversed every 24 hours, the d.c. steps develop noticeably. Some lamps were run for 100 hours on d.c., then for an additional 415 hours with reversed polarity. The d.c. structure appeared with full prominence, and the polarization appropriate to the original polarity of current was preserved. In these tests, involving some 40 lamps, no marked difference was found among filaments of different sizes and therefore of different operating temperatures, nor among helices, straight wires, and coiled-coils, nor between gas-filled and evacuated lamps. It appears that a lamp filament in a few minutes of d.c. heating at normal temperature can develop enough structure to be barely "remembered" during a like interval of heating with reversed current.

Surface Drift of Th on W[7]

It seemed worth determining whether Th atoms adsorbed on a W filament migrate toward the negative terminal. A simple electron-optical tube was used for the test. A loop of 1-mil thoriated wire 6 mm long was mounted on 30 mil leads at the center of a spherical bulb 3 inches in diameter coated inside with willemite. The final anode, a wire ring near the neck of the bulb, was made a few thousand volts positive to the filament, and the emitted electrons formed on the screen a magnified orthogonal image of the loop. A 10-mil Ni wire, welded to one filament lead and projecting between the ends of the loop, cast an electrical shadow on the pattern which permitted distinguishing the emission from the two ends, and also prevented evaporation of Th from one end across to the other.

With no voltage on the anode the filament was first flashed and then was heated, from a 2 v supply, for 20 or 30 minutes at a low activating temperature. The electron image, observed briefly at a low temperature where the Th is immobile, was then brightest opposite the negative end of the loop, with a sharp cut-off toward the lead and a gradual decrease toward the center. The positive side of the screen was dark. With 60-cycle a.c. heating the activation was always symmetrical about the center of the wire. The processes involved in activation of a short filament are obviously complicated, but the net result, that Th accumulates preferentially at the negative end, strongly suggests a drift of ions in the electric field. Ionization in the space is ruled out by the low voltage of the heating supply, the shadow-caster stops evaporation from one end to the other, and thermionic emission from one end to the other is at the worst limited by space charge to a value too low to give appreciable cooling.

Etching at Hooks and Ends

The step-like etching at hooks and ends of a.c. wires, in vacuum and in gas, might be due to a rectifying effect of the temperature gradient on the drift in the electric field, or it might arise directly from diffusion in the temperature gradient. On wires heated with 25 megacycle current (reversal every 2×10^{-8} sec.) the hook region etch is identical in prominence with that on 60-cycle wires. Ten lengths of 1-mil wire about 1 mm long, between heavy leads, were heated on d.c. in vacuum for several hours to burnout. The etch structure was polarized with sawteeth pointing toward the cool ends of the wire, in the direction of the conventional current on one-half of the wire, but against it on the other. The conclusion from these two observations is that the structure developed in a temperature gradient is due primarily to diffusion of atoms toward cooler regions. That it is identical in form with the d.c. structure means that the surfaces and directions which are favorable for drift in an electric field are also favorable for migration down a temperature gradient—a plausible analog to the well-known universal relation between mobility and diffusion coefficient for ions in gases.

[7] This experiment has been reported: Phys. Rev. **53**, 766L (1938).

Die Marks

Grooves left by the diamond die are plainly visible on raw tungsten wire under a microscope; these grooves are not entirely removed from lamp filaments until after about 50 hours at normal temperature; except in a.c. vacuum lamps, they are followed immediately by the d.c. or gas structure. The treatment recommended for producing a "well-aged" tungsten filament,[8] which involves heating 10 minutes at 2900°K, does not remove the die marks.[9] Wire used in recent studies of thermionic emission[10] and of the properties of tungsten as functions of temperature[11] still show, after removal from the tubes, surfaces deeply grooved. From the fact that a brief heating which does not remove the die marks does make the surface properties constant during the course of experiments, the inference is that the die marks, long before they suffer any large-scale changes, adjust themselves to some standard condition. Probably a rearrangement, by surface migration and by differential evaporation between the sides of grooves, rapidly replaces the hodge-podge surface of the raw wire with a surface exposing only low index planes. As this adjustment proceeds simultaneously with evaporation, the die mark should move into the wire, should become smoother and less prominent, and should shift parallel to itself and change the tilt of its sides to conform with the lattice orientation. Such sidewise displacement and change in character of the residual die marks as they cross crystal boundaries can readily be observed on straight large-crystal wires that have been evaporated to an intermediate degree (Fig. 1(*G*)).

Effect of Normal Electric Field[12]

Open-wound helical filaments in two commercial rectifier tubes were burned out slowly, one filament on d.c., the other on 60-cycle a.c., with the anodes kept at $-10{,}000$ v during life ($\sim 10^5$ v/cm at the wire surface). As controls, filaments in two similar tubes were burned out, with the anodes floating. The two a.c. filaments were alike, smooth, while both d.c. filaments showed the typical rough structure. No effect of the field on either type of surface could be found. A straight 5-mil filament in an experimental tube was run on d.c. for 350 hours with a constant average field of $\sim 10^6$ v/cm at the surface. The filament was etched in the usual d.c. fashion, and was indistinguishable from filaments heated with d.c. in plain glass envelopes. Filaments from 100,000 v Kenotrons after 2000 hours at normal temperature on a.c. show the usual smooth surface, with the usual etching toward the cool terminals. It appears that a strong normal field has little effect on the character of the surface developing in vacuum. No large effect is to be expected, if the suggested mechanisms are correct.

Small-Grain Filaments

Some 30 or 40 thoriated filaments, in which the equiaxed crystals remain much smaller than the wire diameter, have been examined after long heating in vacuum. The a.c. crystals are smooth, and are markedly convex, because of the rounding-off of the exposed grain edges. The d.c. crystals are also smooth, but are tilted at various angles up to $\sim 45°$ away from the mean surface. Regular step-like d.c. structure rarely appears on one crystal—presumably one would-be step reaches clear across each tiny grain. Polarization of the d.c. structure appears as a preferential tilting of the exposed crystallite surfaces; in silhouette, the wire looks to be budding toward the negative terminal.

Etching by Water Vapor

When water vapor is present in a lamp, the wire surface tends to develop a characteristic rough structure on a smaller scale than the crystal size, which exposes flat faces with sharp edges—a surface quite similar to that brought out in an acid etch bath. The character of this structure is independent of the gas filling and the type of voltage supply. Its prominence depends on the quantity of H_2O present; it may

[8] H. A. Jones and I. Langmuir, G. E. Rev. **30**, 310 (1927).
[9] Z. Jeffries, Trans. Am. M. and M. Eng. **60**, 588 (1919); see photomicrographs on p. 641.
[10] W. B. Nottingham, Phys. Rev. **49**, 78 (1936).
[11] W. E. Forsythe and E. M. Watson, J. O. S. A. **24**, 114 (1934).
[12] Changes in the rate of evaporation from W and Mo wires when a strong field is applied have been reported: A. G. Worthing, Phys. Rev. **17**, 418 (1921); G. B. Estabrook, Univ. Pittsburgh Bull. **29**, No. 3 (Jan. 1933).

completely obscure the typical d.c. or gas structure which would appear in a bulb thoroughly dried. The well-known water cycle,[13] a mechanism which transports tungsten from the hot wire to cooler surfaces in the neighborhood, is presumably responsible for this etching. The structure has not been systematically studied. Most of the observations have been on small-grain filaments in bulbs which by accident contained some H_2O.

Metals Other than Tungsten

Some rather sketchy experiments with hairpins of Ta, Mo, Pt, Fe and Ni in vacuum have shown that these metals, like tungsten, become and remain smooth with 60-cycle a.c. heating, but develop a rough surface on d.c. On none of these metals is the d.c. structure brought to prominence with so little evaporation as on W. The character of the structure seems to differ markedly among these different metals.

Evaporated Surfaces and Equilibrium Surfaces

The first of the two questions posed in the introduction appears to be answered by the observations, if the one assumption is allowed, that heating with a.c. is equivalent to heating without passage of current. A single-crystal tungsten sample evaporating in vacuum first loses such projections as die marks, and thereafter presents a smooth convex surface, with no regular structure larger than a few thousand atom diameters. On a multicrystal sample, the edges of the grains round themselves off so that finally each crystallite is smoothly convex outward. Since the evaporation rate is a vectorial function, a single crystal originally in a simple, perfect geometrical form (a cylinder, for example) should, as evaporation proceeds, gradually become idiomorphic. Helical tungsten filaments in vacuum, however, lose up to 17 percent of their weight before this tendency toward distortion becomes noticeable under the microscope.

These are the observations. The assigned upper bound of a few thousand atom diameters for regular substructure is set by the magnification used. There is no evidence that regular structure on a smaller scale actually exists. It seems probable that the sample after long evaporation has no surface structure larger than a few atoms in scale. If one draws a plane square array of atoms bounded on one side by a jagged line in which the steps and risers are many atoms broad, one finds, on considering energy bonds between nearest and next-nearest neighbors, that energy can be continually derived from the system by shifting atoms from corner positions into re-entrant angles, until the mean direction of the surface is approximated as closely as the atomic nature of the lattice will allow—until no step and adjacent riser are both more than one atom broad. Obviously, similar analysis applied to the three-dimensional body-centered lattice of tungsten is not likely to lead to a result precisely opposite, that a surface originally smooth can increase its stability by digging out grooves and pits in itself. Curvature of the smooth surface is not incompatible with minimum energy, since the specific surface energy is a continuous function of surface orientation.[14]

The second question, what surface will be displayed in equilibrium with the vapor, is not so definitely answered by the observations. If the structure developed by long heating with a.c. in argon is taken as an intermediate stage between the original helix and the equilibrium form, then in equilibrium the (100) surface will certainly predominate. It is not certain whether it will appear exclusively, or whether other faces, such as the more dense (110), will also be present; it is also uncertain whether the equilibrium faces will be flat or curved. In equilibrium, atoms from the vapor are striking the surface at random places; by the principle of statistical balance, atoms must also be leaving the surface from random places. Hence, at first glance, either the surface atoms must be in such disorder that the surface is effectively an isotropic liquid, or else all parts of the surface must be alike—the sample must expose only one kind of crystallographic plane. The former hypothesis is clearly untenable at low temperatures. The latter hypothesis cannot be readily accepted, since the edges and corners of faces

[13] C. J. Smithells, *Tungsten* (D. Van Nostrand, New York, 1927), p. 62.

[14] P. Ehrenfest, Ann. d. Physik **48**, 360 (1915).

patently need special consideration. For practical purposes, it is sufficient to conclude that trend of a tungsten filament toward equilibrium increases the exposure of cube-face type (100) surface. The considerations mentioned in the preceding paragraph obviously also apply to the case where some or all of the evaporated atoms are returned to the filament surface; tungsten filaments heated in an atmosphere of neutral gas, or in an isothermal enclosure with tungsten walls, presumably have no regular surface substructure larger in scale than a very few atom diameters.

Previous Observations on Tungsten Filament Surfaces

Langmuir's conclusion[15] which has been generally used in the interpretation of thermionic and adsorption data, that a tungsten sample heated in vacuum rapidly develops a faceted surface and exposes only (110) planes, is not supported by the results of the present study. The samples studied by Langmuir had been heated in wet H_2, and the water cycle is presumably responsible for the sharp etching he observed. Bien,[16] studying the optical reflections from filaments briefly heat treated, concluded that the surface is grooved longitudinally, and that the groove sides are predominantly (110) and (211) planes. There is good reason to believe that this grooved structure consisted of residual die marks, and was not a result primarily of the evaporation. Seemann[17] shows photomicrographs of a straight filament burned out in an amplifier tube after 800 hours life, which has prominent typical d.c. herringbone structure. It is unlikely that the new wire Seemann used in his experiments, after a few minutes of heating, had any surface resemblance to this veteran. Simon[18] shows a longitudinal section of a single-crystal Pintsch filament after 8000 hours life, which has a pronounced sawtooth edge. This structure he attributes to a vectorial evaporation rate; presumably it is actually the result of heating with d.c. Lieb[19] shows pictures of helical and straight filaments, run on a.c. and on d.c., in gas and in vacuum, which agree perfectly with the present observations. Lieb erroneously supposed that in the d.c. wires, since the surface is rougher, the crystals are correspondingly smaller.

It may be mentioned incidentally that Lieb's study showed a slightly more rapid decline in luminous efficiency of lamps on d.c. than on a.c., and that a similar difference in rate of change of chromaticity has been tentatively noted by Judd.[20] Differences of this sort are to be expected, since the developing d.c. roughness gives the filament some black-body character and acts to nullify the favorable selective emissivity of smooth tungsten.

I am particularly indebted to Dr. M. Pirani, Dr. Wm. Shockley, Dr. F. Seitz, Dr. I. Langmuir, Dr. H. M. Day, Mr. L. L. Wyman, and Mr. W. J. Gorman, Jr., for assistance and for helpful discussions.

[15] I. Langmuir, Phys. Rev. **22**, 374 (1923).
[16] R. P. Bien, Phys. Rev. **47**, 806A (1935).
[17] H. Seemann, Zeits. f. Physik **92**, 253 (1934).
[18] H. Simon, *Handbuch der Experimental Physik*, Vol. 13 (Leipzig 1928), p. 292.
[19] J. W. Lieb, Trans. Ill. Eng. Soc. **18**, 5 (1923).
[20] D. B. Judd, Nat. Bur. Stand. J. Research **17**, 679 (1936).

Polymorphic Transitions in Metallic Halides

ROBERT B. JACOBS
Physics Laboratory, Harvard University, Cambridge, Massachusetts
(Received May 13, 1938)

An x-ray powder analysis of RbI made at 4500 kg/cm² pressure and room temperature shows the crystal form of RbI to be body-centered cubic under these conditions. The lattice constant is 4.33$_8$A. The volume change from the face-centered lattice which is stable below 4000 atmospheres is 0.037 cm³ per gram. This is about 0.009 cm³ per gram greater than Bridgman's piston displacement value and the difference may be significant.

With the exception of the fluorides, all of the rubidium and potassium halides undergo polymorphic transformations under pressure, which in the light of the present knowledge of RbI are assumed to be of the face-centered to body-centered type. The method of Born and Mayer is used to calculate the lattice constants for both face- and body-centered types of each halide at the experimentally known temperature and pressure of equilibrium. From these the volume changes of the transformation are computed. They are found to agree quantitatively with the experimental values. Theoretical values for the transition pressure are also given. These are confirmed by experiment only in a qualitative manner, but the method may be used to explain, for instance, the nonoccurrence of transitions in the sodium halides up to 50,000 atmospheres. Similar calculations are made for AgI, the crystal form of which has been previously shown by the author to be face-centered cubic at pressures beyond 3000 kg/cm².

INTRODUCTION

THE alkali halides are known experimentally to exist in two cubic crystal forms (NaCl and CsCl types). The rubidium and the potassium halides (with the exception of the fluorine salts) have been found by Slater[1] and Bridgman[2,3] to exhibit crystal polymorphism under pressure. These salts are of the NaCl type under atmospheric conditions. Intuitively, it is to be expected that the high pressure forms are of the CsCl type, and a supposition to that effect has generally been made. The present work includes an x-ray analysis of one of these halides (RbI) at a pressure considerably beyond the equilibrium pressure. The x-ray diffraction lines thus obtained show definitely that RbI at 4500 kg/cm² pressure is body-centered cubic (CsCl type). This would indicate a high probability that the other transitions are of the same type, i.e., face-centered to body-centered cubic.

The equilibrium lattice constants for the alkali halides may be determined theoretically by the method due to Born and Mayer.[4] With the various parameters empirically adjusted at one atmosphere the agreement between theoretical and experimental lattice values is excellent.[5] The parameters thus determined (on the basis of the known interatomic distances in the crystal forms, stable under atmospheric conditions) are used in the present case to determine the lattice distances for both crystal forms of each alkali halide, under conditions of temperature and pressure at which the two forms are known to be in equilibrium. This calculation involves an extension of the usual procedure to include the effect of pressure. The necessary additions to the theory will be described in a later part of this paper. From the lattice constants so determined one can readily deduce the change in volume which occurs when a given salt is transformed from the one crystal form to the other. These values may be compared with the experimentally determined values. For the rubidium halides the agreement is excellent. For the potassium salts the agreement is not so good, but is, nevertheless, quite satisfactory. Bridgman has failed to find transitions in the sodium halides up to pressures of 50,000 kg/cm². The present calculations show (in the case of NaI) that at 49,000 kg/cm² the volume change which would take place if a transition were to occur is already too small for a certain and accurate detection. If

[1] J. C. Slater, Phys. Rev. **23**, 488 (1924).
[2] P. W. Bridgman, Zeits. f. Krist. **67**, 363 (1928).
[3] P. W. Bridgman, Phys. Rev. **48**, 893 (1935).
[4] M. Born and J. E. Mayer, Zeits. f. Physik **75**, 1 (1932).
[5] M. L. Huggins and J. E. Mayer, J. Chem. Phys. **1**, 643 (1933).

the transition were to take place at a slightly higher pressure, there would be no volume change at all. At still higher pressures the volume change is in such a direction as to favor the stability of the face-centered type of lattice. Since considerations of the energy involved in this transition indicate that the transition would not take place at a pressure lower than this (50,000 kg/cm²), it may be logically predicted that the transition under hydrostatic pressure will not be found.

For the transformations which do occur, it should be possible to predict theoretically the equilibrium pressures. However, it is actually found that the uncertainties in the energy terms are usually too large to allow an accurate determination of these pressures. This is to be expected since the calculation of the pressure involves the difference in two energy terms, each of which is about a hundred times as large as the difference term. Nevertheless, the agreement with the experimental pressures is in all cases qualitatively satisfactory insofar as the pressure sequence for the six transitions involved is in perfect agreement with experiment. Numerically, the calculated pressures are found to be from $2\frac{1}{2}$ to 7 times greater than the experimental.

AgI has been previously shown by the author to exist under pressure in the face-centered cubic form.[6] AgCl and AgBr are known to be stable at atmospheric pressure in this crystal form, but have been found by Bridgman[7] to transform to another crystal form under pressure (presumably body-centered cubic). A similar transition from the face-centered form of AgI might reasonably be expected. Yet, efforts to detect the same have been unsuccessful up to pressures of 50,000 atmospheres. One may calculate the various factors involved in such a transition by using the same method as for the alkalis. The parameters computed by Mayer[8] are employed for this purpose. These calculations indicate that the transition will probably take place at a pressure beyond 50,000 atmospheres. The volume change to be expected is small, but increases with increasing pressure (in contrast to NaI). This excludes the chance of its changing sign, thus making the occurrence of the transition an impossibility.

The Transformation: RbI(I) into RbI(II)

The transition pressure for RbI(I) and RbI(II) is given by Bridgman[2] as 3,900 kg/cm² at 25°C. There is a certain region of "indifference" (region of possible metastable equilibrium) which amounts to something like 200 kg/cm² on either side of the equilibrium curve. By use of the pressure camera described by the author in a previous publication,[6] an attempt was made first to obtain a diffraction pattern from RbI(II) at 4700 kg/cm², which is 800 kg/cm² beyond the equilibrium pressure, and 600 kg/cm² beyond the region of indifference as found by Bridgman. The diffraction lines so obtained indicated that the salt remained completely in the form of RbI(I). Several attempts were then made on pretreated specimens (specimens previously subjected to high pressures) since it is sometimes found that the transitions take place more readily for these. The results of these experiments were likewise negative, as were attempts to transform the salt through heating by mounting it on a resistance wire in the camera and passing a current through the same after the application of pressure. The material used in these experiments was Eimer and Amend's C.P. (presumably of about the same purity as the stock used by Bridgman). Through the generosity of Professor Archibald of the University of British Columbia, the author obtained some rubidium salt of "atomic weight" purity. Professor Baxter of Harvard University kindly converted the same into RbI, by utilizing "atomic weight" iodine for this purpose. Several runs were made with this salt, and it was found to transform readily at pressures as low as 4000 kg/cm².

A certain significance is attached to these experiments. In the x-ray pressure camera used in the present case, the *pressure is perfectly hydrostatic*, since the individual crystal grains are acted upon only by helium gas. In the case of Bridgman's experiments the pressure is only approximately hydrostatic, since he employed a free-piston type of piezometer. The salt was placed under kerosene in an accurately machined

[6] R. B. Jacobs, Phys. Rev. **54**, 325 (1938).
[7] P. W. Bridgman, Proc. Am. Acad. **72**, 63 (1937).
[8] J. E. Mayer, J. Chem. Phys. **1**, 327 (1933).

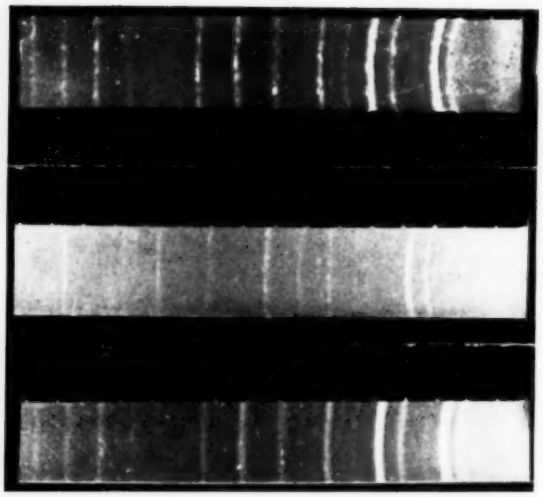

FIG. 1. Above: RbI(I) before transformation. Center: RbI(II) at 4500 atmospheres. Below: RbI(I) after transformation.

cylinder and was separated from the external hydrostatic compressive medium by means of an accurately fitted, freely-moving piston. In this case the pressure was partially transmitted from grain to grain as a mechanical force, which certainly cannot be regarded as hydrostatic as far as single grains are concerned. Shearing forces are unquestionably present. The effect of large shearing forces on polymorphic transitions has been demonstrated by Bridgman,[9] but the role played by small accidental shearing forces in the usual "hydrostatic" pressure experiment has not been previously recognized. In the present case the lack of these in the pressure camera undoubtedly is a large factor in accounting for the inability to transform the commercially obtainable C.P. salt.

The actual mechanism of a polymorphic crystal transformation has not been well explained. The role of an impurity is not known. The large effect produced by the impurities present in the "C.P." RbI in the present investigation is not a common experience. In the first place a foreign atom is generally regarded as a favorable site for the nucleus of a new crystal, and hence as a catalyst rather than as an inhibitor of a transition. The instantaneous crystallization of an undercooled liquid upon the introduction of foreign particles is a familiar example of this action. The role of the impurities in the RbI appears to be of a different nature. It is possible that they are segregated to a certain extent and localized on the intercrystalline boundaries of the mosaic crystals. Here it is possible that their action might be such as to prevent cooperative action from one mosaic to the next. It would not be difficult to explain the action of shearing forces in overcoming the effect of such impurities.

The question also arises as to the role of the individual crystal grain in a polymorphic transition, i.e., does it transform as a unit, or does it break up into smaller parts? In the case of transitions induced by temperature, the grain size is generally reduced materially. Here thermal agitation may be an important factor in breaking up the crystal grains. This is a factor which is eliminated in a pressure transition, and hence it becomes of interest to study the grain size with the pressure camera. In the case of $CsClO_4$, it has already been observed[6] where two crystal forms were simultaneously present, that the new phase was composed of the larger crystal grains, and showed in this case that a transformation is more likely to occur in a large grain than in a small one. Fig. 1 shows the effect of a transformation on the grain size of RbI. The three diffraction diagrams represent the condition of the same sample before, during, and after the application of pressure. The upper diagram is "splotchy" and indicates a large grain size. The lower diagram is uniform and the lines broadened which indicates a considerable "breaking up" of individual grains. The x-ray evidence would then unmistakably show first, that the larger crystals are the more likely to transform,

TABLE I. *Diffraction data for* RbI(II). *Temp.* 25°C. *Pressure* 4500 *kg/cm²*.

Bragg Angle (×2) 2θ (degrees)	Miller Indices h, k, l	Interplanar Distance $d_{h,k,l}$ (A)	Lattice Constant d (A)
28.88	110	3.08_6	4.36_3
41.46	100(2)	2.17_4	4.34_8
51.43	121	1.77_5	4.34_8
60.15	110(2)	1.53_7	4.34_7
68.16	130	1.37_2	4.33_9
82.94	123	1.15_9	4.33_6
97.97	101(3)	1.02_1	4.33_0
105.13	120(2)	0.968_1	4.33_0
129.60	431	0.850_2	4.33_6
		Lattice constant = 4.33_5A	

[9] P. W. Bridgman, Proc. Am. Acad. **71**, 387 (1937).

and second, that there is an appreciable subdivision of grains in a pressure transition.

The data for the crystal structure of RbI(II) are given in Table I, in which the measured values from the more intense lines of the diffraction pattern are used.

From the lattice constant thus found one may compute the volume change from RbI(I) to RbI(II). This gives a value of 0.037 cm³/gram at 4500 kg/cm² which is about 0.009 cm³/g greater than Bridgman's piston displacement value. The scattering of Bridgman's experimental points would indicate a maximum allowable error of 0.005 cm³/gram in his measurements. The uncertainties in the lattice constants should not introduce more than 0.003 cm³/g error. In the most unfavorable case, the difference between the piston-displacement and the x-ray values could then possibly be attributed to experimental uncertainties. In the case of AgI the author found a similar situation, which could not be attributed reasonably to experimental error. In that case it was pointed out that an incomplete transition will result in too low a measured volume change for the piston-displacement method. Definite evidence was also given for the existence of a partial transition. It is possible that the present investigation affords another example of this phenomenon.*

Calculations

It is desirable to calculate the lattice constants of the various halides at the pressures at which the two crystal forms are known to exist in equilibrium. Since it is the usual procedure to make such calculations at zero pressure, some small alterations in the method are necessary. We use the thermodynamic potential Φ, defined as follows:

$$\Phi = U - TS + PV. \tag{1}$$

For equilibrium of a single phase,

$$(\partial\Phi/\partial V)_{T,\,P} = 0 = \partial U/\partial V - T(\partial S/\partial V) + P,$$

or

$$\partial U/\partial V = T(\partial S/\partial V) - P. \tag{2}$$

The "temperature term," $T(\partial S/\partial V)$, may be further reduced, since

$$(\partial S/\partial V)_T = (\partial P/\partial T)_V = -(\partial V/\partial T)_P/(\partial V/\partial P)_T = \alpha_T/\beta. \tag{3}$$

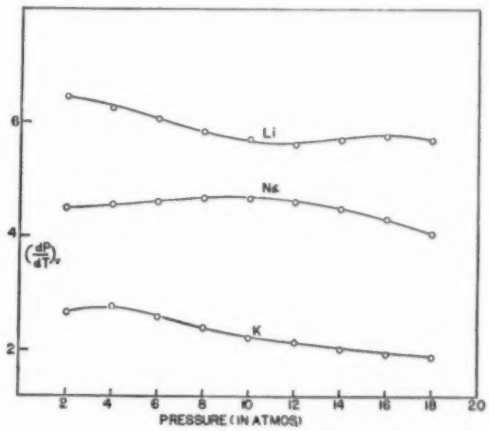

FIG. 2. $(\partial P/\partial T)V$ as a function of pressure for the alkali metals. (Data from Bridgman.)

At atmospheric pressure the values of α_T and β (thermal expansion and compressibility, respectively) are known and may be used to compute $(\partial P/\partial T)_V$. On the other hand, at high pressures the values for α_T are not known in the case of the alkali halides, and one cannot compute $(\partial P/\partial T)_V$ directly at any optional pressure. However, it seems reasonable that the quantity is invariant with pressure. In the case of the alkali metals Bridgman[10] has given sufficient data for the evaluation of $(\partial P/\partial T)_V$ over a considerable range of pressures. The values thus obtained are shown plotted in Fig. 2. Here no significant variation of the quantity with the pressure is in evidence. In the following calculations on the metallic halides, the assumption is made that $(\partial P/\partial T)_V$ is constant with respect to pressure. This assumption is not too hazardous, since even a considerable variation in the value of this quantity would affect the lattice constants only slightly. Physically, this

* Professor Bridgman has informed the author that he has recently repeated his experiments on AgI, using a somewhat modified procedure. He now subjects the salt to a pressure far in excess of the equilibrium pressure. The volume change is then measured as the pressure is reduced below its equilibrium value, and again when the pressure is raised a second time. He now obtains a volume change of about 0.0280 cc/g which is in agreement with the x-ray values. Apparently the treatment at very high pressures overcomes the inability of the salt to completely transform near equilibrium pressure.

[10] P. W. Bridgman, Proc. Am. Acad. **70**, 93 (1935).

TABLE II. *Calculations for transitions in rubidium halides.*

PRESSURE USED IN CALCULATIONS (kg/cm²)		RbCl f.c. 5,500	RbCl b.c. 5,500	RbBr f.c. 5,000	RbBr b.c. 5,000	RbI f.c. 4,500	RbI b.c. 4,500
r (obs.)	$\times 10^8$ cm	3.23$_5$		3.38		3.61$_5$	3.75
r (cal.)	"	3.24	3.39	3.38	3.54	3.61	3.78
C	$\times 10^{60}$ erg-cm^6	691	1,023	898	1,348	1,330	2,039
D	$\times 10^{78}$ erg-cm^8	96	147	134	209	224	367
$C/r^6+D/r^8$	$\times 10^{12}$ ergs	0.68	0.76	0.68	0.77	0.68	0.79
$\alpha e^2/r$	"	12.27	11.83	11.76	11.33	11.02	10.61
$(3T/NB)(dV/dT)$*	"	0.90	0.79	0.91	0.81	1.06	0.94
$(3V/N)P$	"	1.10	0.98	1.14	1.01	1.24	1.10
$B(r)$	"	1.72	1.67	1.65	1.56	1.45	1.39
E	"	11.23	10.92	10.80	10.54	10.25	10.41
Vol. (cal.)	$\times 10^{24}$ cm^3	68.$_0$	60.$_0$	77.$_2$	68.$_3$	94.$_1$	83.$_2$
ΔV (cal.)	"		8.$_0$		8.$_9$		10.$_9$
ΔV (obs.)	"		9.$_7$		8.$_7$		(9.$_5$, 12.$_9$)†
P (cal.)	kg/cm²		39,000		30,000		22,000
P (obs.)	"		5,500		5,000		4,000

TABLE III. *Calculations for transitions in potassium halides.*

PRESSURE USED IN CALCULATIONS (kg/cm²)		KCl f.c. 19,000	KCl b.c. 19,000	KBr f.c. 17,000	KBr b.c. 17,000	KI f.c. 17,000	KI b.c. 17,000
r (obs.)	$\times 10^8$ cm	3.05		3.19$_5$		3.40$_5$	
r (cal.)	"	3.04	3.21	3.19	3.37	3.40	3.60
C	$\times 10^{60}$ erg-cm^6	452	682	605	930	924	1,472
D	$\times 10^{78}$ erg-cm^8	560	893	800	1,343	1,420	2,521
$C/r^6+D/r^8$	$\times 10^{12}$ ergs	0.65	0.70	0.65	0.72	0.68	0.77
$\alpha e^2/r$	"	13.08	12.49	12.47	11.90	11.70	11.14
$(3T/NB)(dV/dT)$	"	0.91	0.82	0.95	0.87	1.02	0.94
$(3V/N)P$	"	3.14	2.85	3.35	3.04	3.92	3.60
$B(r)$	"	2.12	1.96	1.98	1.82	1.86	1.72
E	"	11.61	11.24	11.14	10.80	10.51	10.19
Vol. (cal.)	$\times 10^{24}$ cm^3	56.$_2$	51.$_0$	64.$_9$	59.$_0$	78.$_6$	71.$_8$
ΔV (cal.)	"		5.$_2$		5.$_9$		6.$_7$
ΔV (obs.)	"		6.$_7$		6.$_4$		7.$_5$
P (cal.)	kg/cm²		74,000		59,000		49,000
P (obs.)	"		20,000		19,000		18,000

* α/B—taken as same for both body-centered and face-centered types.
† —piston displacement and x-ray values, respectively.
NOTE.—For a summary of values used for compressions, thermal expansions, etc., see reference 5.

quantity gives the difference between the lattice constants at absolute zero and at the temperature at which the calculation is made.

The internal crystal energy may be subdivided, i.e.

$$U = U(T) + E(r) + h\nu_0/2. \tag{4}$$

$U(T)$ represents the thermal energy and $E(r)$ the lattice energy proper. The latter quantity is given by the expression:

$$E(r) = -\alpha e^2/r - C/r^6 - D/r^8 + B(r). \tag{5}$$

These terms represent the electrostatic, the dipole-dipole, the dipole-quadrupole, and the repulsion energies, respectively. Eq. (5) substituted into Eq. (2) gives the equation:

$$3TV\alpha_T/N\beta + 3PV/N = \alpha e^2/r + 6C/r^6 + 8D/r^8 + \partial B(r)/\partial r. \tag{6}$$

This expression may be solved for r, the distance between nearest neighbors in the crystal. The values for the van der Waals coefficients C and D, and for the repulsion coefficients in $B(r)$ are taken from papers by Huggins and Mayer[5] and by Mayer.[11]

Equation (5) serves for the evaluations of $E(r)$ after the values for (r) are obtained. Equilibrium between the two phases of the crystals (b.c. and f.c.) requires that their thermodynamic potentials be equal, or that:

$$\Phi_1 = \Phi_2,$$

or
$$U_1 - TS_1 + PV_1 = U_2 - TS_2 + PV_2. \tag{7}$$

[11] J. E. Mayer, J. Chem. Phys. **1**, 270 (1933).

For the alkali halides it is known from experiment that the equilibrium curves in the $P-T$ plane run almost parallel to the temperature axis. This indicates that the temperature terms are very nearly the same for each phase, and hence they can be neglected in comparison with the pressure terms. With this simplification, Eq. (7) becomes

$$E_1(r) + PV_1 \leq E_2(r) + PV_2$$

or
$$P \leq \frac{E_2(r) - E_1(r)}{V_1 - V_2} \tag{8}$$

from which one may solve for P, the equilibrium pressure. Not much accuracy can be expected here because P will be a small difference between two large terms.

In the calculations given below, the interatomic radii are solved for at the experimental equilibrium pressures and at room temperature. These radii are substituted into Eq. (8) for the solution for P. This is a first approximation for P. More accurately, one would take this value of P, and again solve for the equilibrium radii, and use these in turn for a better approximation of P. Actually, this is not done, since the very approximate nature of the P's obtained does not warrant the effort involved in carrying out the second approximation.

The results of these calculations for the rubidium and potassium halides are given in Tables II and III. Sodium iodide is given in Table IV.

DISCUSSION OF RESULTS

A comparison of the calculated and experimental interatomic distances for the face-

TABLE IV. *Calculations for transitions in* NaI.

PRESSURE USED IN CALCULATIONS (kg cm²)		f.c. 0	b.c. 0	f.c. 49,000	b.c. 49,000
r (obs.)	$\times 10^8$ cm	3.23		3.03$_5$	
r (cal.)	"	3.23	3.50	3.04	3.31
C	$\times 10^{60}$ erg-cm^6	482	864	482	864
D	$\times 10^{76}$ erg-cm^8	630	1,436	630	1,436
$C/r^6+D/r^8$	$\times 10^{12}$ ergs	0.48	0.53	0.70	0.76
$\alpha k^2/r$	"	12.31	11.46	13.08	12.12
$(3T/NB)(dV/dT)$	"	1.16	1.13	0.97	0.96
$(3V/N)P$	"	0	0	8.10	8.05
$B(r)$	"	1.40	1.28	2.54	2.30
E	"	11.39	10.72	11.24	10.57
Vol. (cal.)	$\times 10^{24}$ cm^3	67.$_4$	66.$_1$	56.$_2$	55.$_9$
ΔV (cal.)	"		1.$_3$		0.$_3$
ΔV (obs.)	"		—		—
P (cal.)	kg/cm²				No trans.
P (obs.)	"	—	None to 50,000		—

centered lattices shows good agreement in all cases over a wide pressure range. This is particularly significant in the case of sodium iodide in which the over-all volume change is almost 20 percent in 50,000 atmospheres and where the final compressibility is roughly one-fourth the original.[12] This agreement would indicate that the van der Waals coefficients were of about the correct magnitude, and that the exponential form of the repulsion coefficient gives a fairly good representation of experimental fact. Rubidium iodide furnishes the only experimental observation of a body-centered halide in this group. The agreement here is not quite as good as for the face-centered types.

The volume changes provide the most interesting part of the calculations. They, of course, involve the lattice constants of both the face-centered and the body-centered structures (assumed, except RbI). It will be observed that in every case the experimental and theoretical volume changes check within the limits of accuracy to be expected. The method can therefore be regarded as entirely satisfactory for such calculations.

Enough has been said about pressure calculations to indicate that no especial agreement can be expected here. However, it may be pointed out that for the six salts which are known to have high pressure modifications, the pressure sequence as given by the theory is confirmed by experiment.

It has been suggested in the literature[13] that better energy relations may be obtained in the case of NH_4Cl and CsCl by multiplying the van der Waals coefficients by some arbitrary factor, which, in turn, involves a recalculation of the repulsion coefficients. Since the energy difference between a body-centered and a face-centered lattice is not very sensitive to variations in the van der Waals forces, an appreciable energy change can result only from a large variation in the forces. This, of course, results in a new calculated compressibility. In view of the apparent validity of the present theoretical compressibilities, one could not justify a serious alteration of the van der Waals constants as used. It is possible that the energy discrepancies may be traced to some nonionic force. It is pointed out, however, that the pressure calculations can be expected to be more accurate for very high pressure transitions, since the energy deviations are approximately constant for any halide series. Thus if the values 19, 20, and 26×10^{-14} erg/molecule are subtracted from the calculated energy differences of the iodides, the bromides, and the chlorides, respectively, the calculated pressures will in all cases agree with the experimental to better than 1000 kg/cm². Hence, if the sodium halides were to exhibit polymorphism under pressure, one would expect the calculated pressures to approximate more closely the experimental values than they did in the case of rubidium or potassium.

No pressure transformations have been observed in the sodium halides up to 50,000 kg/cm². By analogy we would expect NaI to transform first in the sodium series. It is worth while to consider the theoretical predictions for this salt. The calculations (Table IV) are made for atmospheric and for 49,000 kg/cm² pressure. For the latter pressure the calculated volume change is very small (of the order of magnitude of a probable deviation of an experimental point). At still higher pressures the volume change will reverse its algebraic sign. The energy difference between the two crystal phases at 49,000 kg/cm² and below is sufficiently large to indicate with some certainty that the face-centered lattice is always stable in this region. Above 49,000 kg/cm², the reversal of sign in the volume term will preclude the possibility of building a sufficiently high external work term ($p\Delta v$) to equal the internal energy difference. In view of these

[12] P. W. Bridgman, not yet published.
[13] A. May, Phys. Rev. **52**, 339 (1937).

considerations, it is fairly safe to predict that NaI will not experience a face-centered to body-centered transformation under hydrostatic pressure alone.

Silver Iodide

Mayer[8] has evaluated the van der Waals and the repulsion coefficients for AgI, and has pointed out that a NaCl type of lattice is theoretically more stable than the ZnS type *unless* homopolar energy is associated with the latter type of lattice. The experimental values for the lattice constant which he derived for the ZnS type of lattice were too large. This was likewise explained by the presence of homopolar binding. At the present time it is possible through the knowledge of the existence of AgI in the NaCl type lattice at high pressures to test further the validity of Mayer's assumptions. The calculations for AgI are summarized in Table V. The agreement between theory and experiment for the lattice constant of the face-centered lattice at 3750 kg/cm² is here regarded as a check on the correctness of the van der Waals and repulsion terms used. This would remove doubt as to a possible explanation of Mayer's results through his use of incorrect values in these quantities rather than in the existence of the homopolar energy assumed. The calculated energy difference between the face-centered lattice and the ZnS type amounts to 55×10^{-14} erg per molecule at 3,750 kg/cm², where the two forms are now known to exist simultaneously. The external work and temperature terms can account only for a few percent of this energy. The conclusion that the ZnS lattice is not purely ionic, appears inescapable at this point.

AgBr and AgCl at atmospheric pressure crystallize into the face-centered cubic form. Bridgman[7] has found each of these to have polymorphic transitions at pressures around 13,000 kg/cm² (presumably from f.c. to b.c.). It appeared probable that AgI could be further transformed; i.e., from its high pressure face-centered lattice to a body-centered crystal. Professor Bridgman[14] tried the experiment up to 50,000 atmospheres without success. It is possible that the transition will take place at a higher pressure. Two approximations are shown in Table V for the theoretical pressures. Because of the small volume change to be expected the uncertainties in pressures are large. They do, however, agree with the experiment insofar as no face-centered to body-centered transition is predicted below 50,000 atmospheres. It is pointed out that here the face-centered lattice is the least compressible. The calculated volume change *increases* with pressure, and makes the eventual occurrence of the transition highly probable.

In conclusion the author wishes to express his gratitude to Professor Bridgman for many discussions on this subject and for the extensive use of his experimental material.

Table V. *Calculations for transitions in* AgI.

Pressure Used in Calculations (kg/cm²)		(ZnS) 3,750	f.c. 3,750	b.c. 3,750	f.c. 145,000	b.c. 145,000
r (obs.)	$\times10^{8}$ cm	2.80	3.03_5		—	
r (cal.)	"	(~2.95)	3.05	3.30	2.85	3.07
C	$\times10^{60}$ erg-cm^6	850	1,450	2,209	1,450	2,209
D	$\times10^{78}$ erg-cm^8	1,467	2,460	4,000	2,460	4,000
$C/r^6+D/r^8$	$\times10^{12}$ ergs	2.15	2.14	2.00	3.27	3.14
$\alpha l^2/r$	"	13.34	13.04	12.15	13.95	13.06
$(3T/NB)(dV/dT)$	"	1.47	.62	.61	.51	.49
$(3V/N)P$	"	.74	.63	.61	19.72	19.00
$B(r)$	"	3.05	2.19	2.10	4.79	4.74
E	"	12.43	12.98	12.05	12.43	11.47
Vol. (cal.)	$\times10^{24}$ cm^3	—	56.7	55.5	46.3	44.4
ΔV (cal.)	"		10.7	1.2		1.7
ΔV (obs.)	"		*(9_2), (11_2)	—		—
P (cal.)	kg/cm²			~8×10^5		~6×10^5
P (obs.)	"			None to 5×10^4		None to 5×10^4

* Piston displacement and x-ray values, respectively.

[14] Not yet published.

Unusual Range of Radio Signals

J. A. Pierce and H. R. Mimno
Cruft Laboratory, Harvard University, Cambridge, Massachusetts

ON June 5, 1938, unusual long distance transmission of signals in the 56–60 megacycle band was observed by radio amateurs in the United States. Many of them have reported the contacts made and stations heard by them to the American Radio Relay League. Mr. Hull and Mr. Battey of that organization have been kind enough to permit us to study the data which have been submitted.

These reports cover some seven hundred contacts between amateur stations in nearly thirty states, primarily in the eastern part of this country. We have analyzed these data and have put them into the form exhibited in Fig. 1. The circles indicate the distribution of contacts made (or stations heard) over various distances, expressed as the number in each fifty-mile zone. We are dealing here with reflections from an ionized region in which the ionic density is so limited that a skip distance exists. One would, therefore, expect that such a distribution curve would be simple, rising from zero to a single maximum, and might possibly be similar to the normal curve of errors. The smoothed curve shown by the heavy line of Fig. 1 differs from such a curve in two respects. There is a minimum at 250 miles with indications of a sharp rise at smaller distances. Ground wave transmission over distances of two hundred miles is not possible at these frequencies, so that it seems reasonable to conclude that refraction was especially marked and was responsible for transmission up to 300 miles or so. It undoubtedly also facilitated the other contacts made on this day, rays from the ionosphere being curved toward the earth so that they reached locations which would otherwise have been behind obstacles.

In Fig. 1 a small second maximum will be noted at a little more than 1100 miles. This maximum is due to reports of stations located to the west of the Mississippi River. The ninety contacts reported by them have been plotted separately to give the smoothed curve B of Fig. 1, which has the expected type of distribution. Since there was no dearth of reporting stations at shorter distances, the displacement of the maximum of curve B from that of curve A

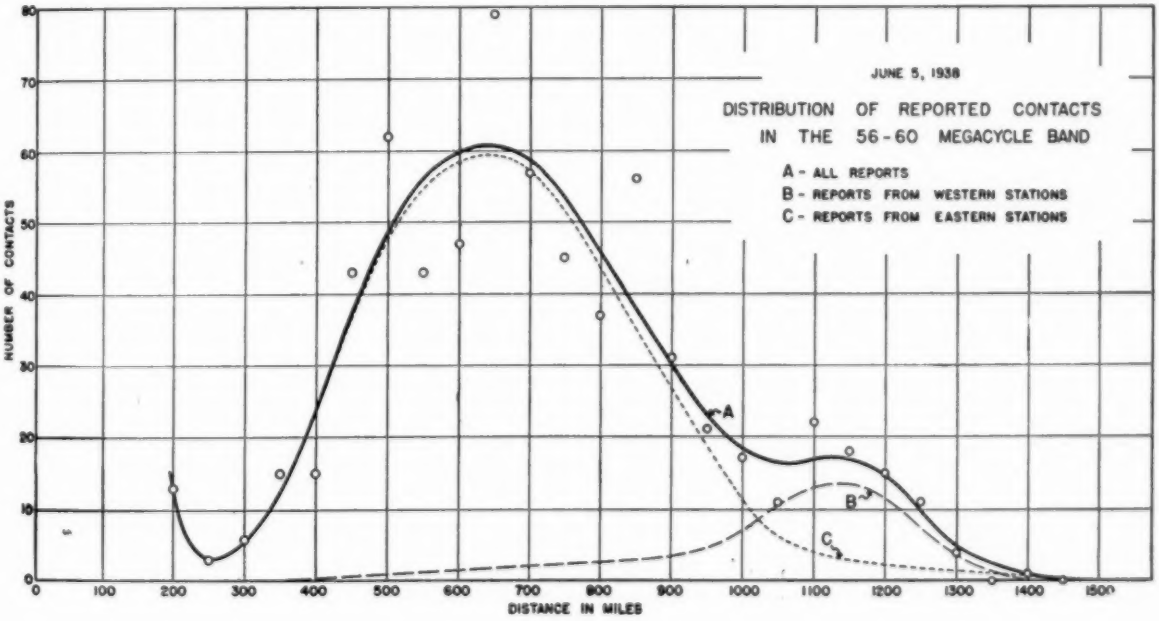

FIG. 1.

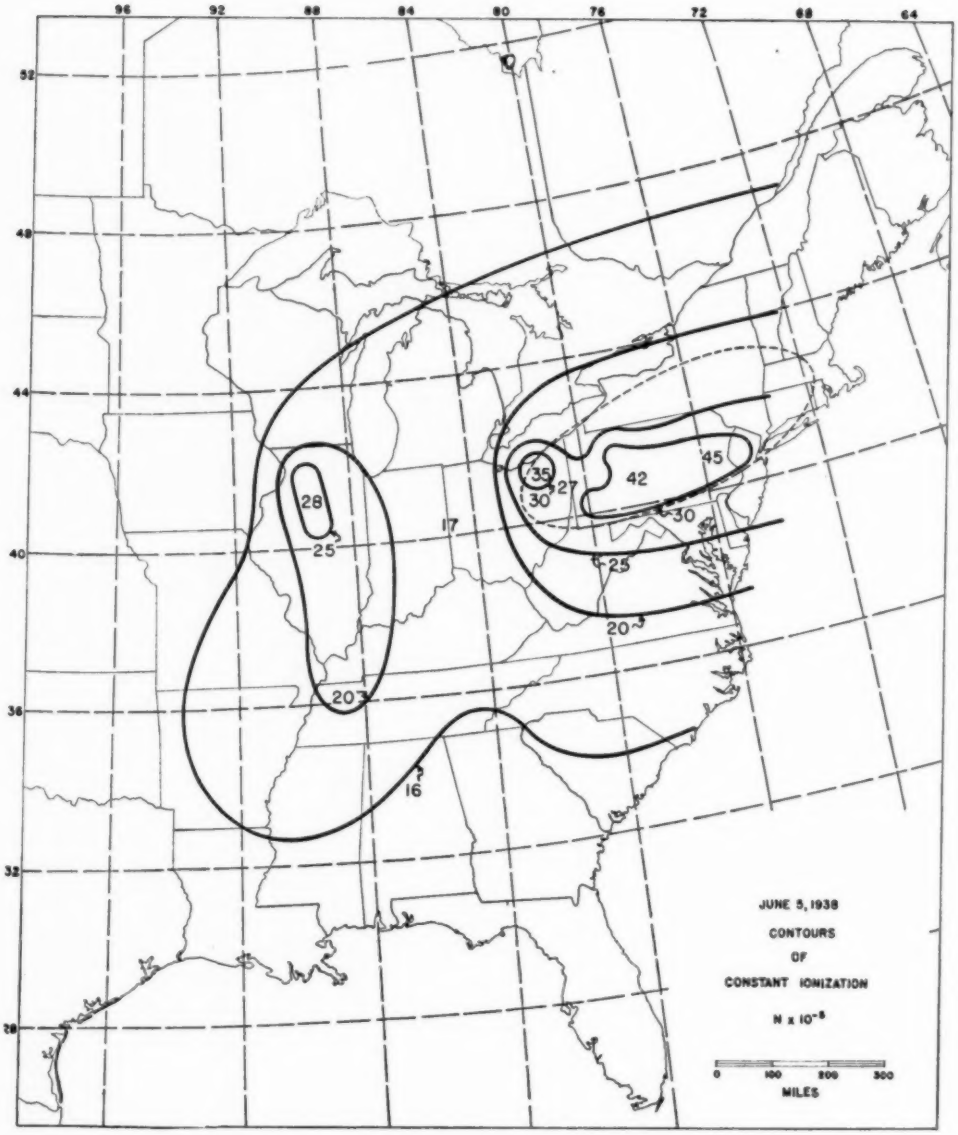

FIG. 2.

seems a valid indication of a smaller degree of ionization at the points where reflection took place. Curve C of Fig. 1 is curve A minus curve B, and represents, therefore, the distribution found from all reports from east of the Mississippi River.

On this date very strong abnormal *E* layer ionization was observed above Cambridge, Massachusetts, using another technique, and has been reported elsewhere.[1] This enables us to assume that the height of reflection was about 120 kilometers. It should be noted that the greatest distance shown in Fig. 1 (1400 miles) is the maximum to be expected from a single reflection at such a height. This confirms the assumption that reflection from the *E* region is the mechanism causing this type of transmission.

By noting on a map the locations of stations heard in a fairly small area, the skip distance can be estimated and the location of the point of reflection marked. From this skip distance and the assumed height of reflection we can calculate the ionization density necessary to reflect a

[1] Nature **142**, 163 (1938).

58-megacycle signal over that path. We have computed many such values, noted them on the map at each of the midpoints, and drawn the contours of constant ionization shown in Fig. 2. It must be understood that these contours are rough and serve only to show the limits throughout which a high level of ionization existed, and the locations of regions of maximum ionization. The highest value observed was nearly 5×10^6 electrons/cm^3, while a value of about 1.6×10^6 was the smallest which could be determined by this method of observation. Unfortunately, little is known about the times of day when these various contacts took place. In general a period of maximum activity occurred during the latter part of the morning and another, perhaps more pronounced one, in the early hours of the evening, but the band was "open" for nearly the whole day.

After deducing that the short distance transmissions (i.e., less than 300 miles) could be attributed to atmospheric refraction, these cases were re-examined. It was found that they all occurred within a rather small region near the Atlantic coast between North latitudes of 40 and 43. This region has been outlined by the light dotted line of Fig. 2. It should be of interest in this connection to study the tropospheric weather, especially the temperature and humidity distributions, over this and surrounding areas.

On this occasion the *E* region ionization reached a level which is rare even at a time of maximum solar activity, and at the same time a temperature inversion, or similar phenomenon, produced remarkable atmospheric refraction. Such a coincidence is probably rare, so that it is unlikely that the number of contacts enjoyed on this occasion will soon be exceeded. It seems wise, therefore, to read into the literature such data as we have so that they may be available for reference and study when our knowledge of these phenomena shall have increased.

LETTERS TO THE EDITOR

Prompt publication of brief reports of important discoveries in physics may be secured by addressing them to this department. Closing dates for this department are, for the first issue of the month, the eighteenth of the preceding month, for the second issue, the third of the month. Because of the late closing dates for the section no proof can be shown to authors. The Board of Editors does not hold itself responsible for the opinions expressed by the correspondents.

Communications should not in general exceed 600 words in length.

Sidereal Daily Variation of Barometric Pressure

Barometric pressure, plotted against sidereal time for sixty-two stations ranging from 80° N to 55° S latitude and including 28 American, 9 Russian, 8 English, 4 Japanese, and 3 South African stations, a total of 308 station-years of records, shows the sidereal daily variations of Fig. 1. The pressure in millimeters of mercury, plotted against the sidereal hour angle as abscissa, shows a maximum sidereal daily variation of 0.167 mm at 60° Nl atitude. The greatest pressure is reached at sidereal hour angle 11 which is approximately the position of the pointer stars of the Great Dipper.

The position of the crest and trough of the pressure wave, as viewed from a fixed star, shows a drift to the east with change in latitude toward the south. This effective time lag suggests that the driving force is applied in the northern hemisphere. The amplitude of the wave south of the equator is nearly as large as in the northern hemisphere. This suggests a high degree of resonance in the effect.

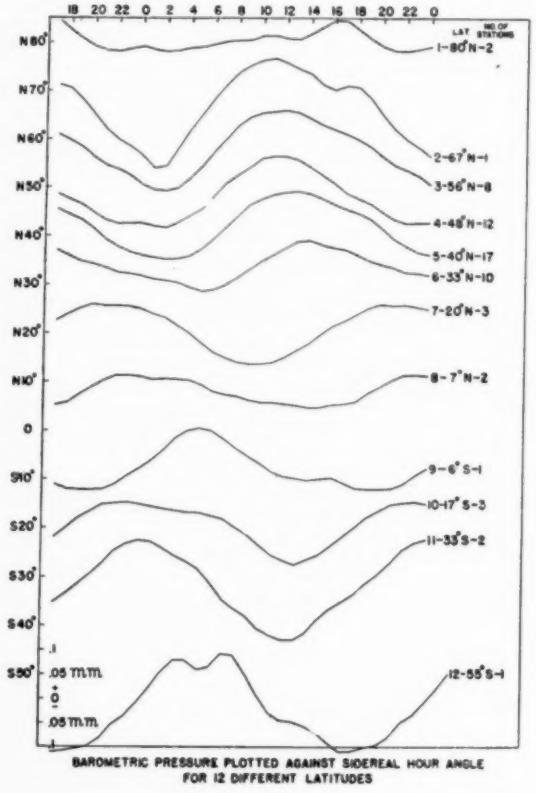

BAROMETRIC PRESSURE PLOTTED AGAINST SIDEREAL HOUR ANGLE FOR 12 DIFFERENT LATITUDES

FIG. 1.

The average daily sidereal pressure variation for 37 stations between 39° and 60° N latitude and including 160 years of station records is given quite accurately in millimeters of mercury by the equation:

$$P=0.072\cdot\sin t-0.0076\cdot\sin 2t+0.0024\cdot\sin 3t,$$

where t is the sidereal hour angle. When the coefficients of this equation are compared with those given by Chree[1] for the average diurnal variation for seven English stations, we find that for the 24-hour cycle the sidereal component is 5.5 times the solar component, but for the 12-hour cycle the sidereal component is only 1/28 of the solar component. It is also interesting to note that the sidereal wave decreases to a minimum at the equator where the solar diurnal wave is a maximum.

The sidereal pressure tide accounts for much of the observed seasonal change in the solar diurnal tide.

H. B. MARIS

Naval Research Laboratory,
Washington, D. C.,
August 10, 1938.

[1] Chree, J. Roy. Meteorolog. Soc. **50**, 247 (1924).

Crystal Fields in Rare Earth Ethylsulphates

The recent appearance of Ketelaar's[1] approximate structure determination of the series of rare earth crystals $Me(C_2H_5SO_4)_3\cdot 9H_2O$ has brought hope of determining a crystalline potential which will explain the absorption spectra and magnetic properties of these salts. The rare earth ion is surrounded by a group of three equilateral triangles of water molecules which has the symmetry C_{3h}. If one places a charge Q at each of the nine H_2O positions, the first two terms of the potential which contribute to the energy are:

$$V=A_2[x^2+y^2-2z^2]+A_4[(x^2+y^2)^2+\tfrac{4}{3}z^4-\tfrac{4}{5}r^4],$$

where $A_2>A_4$. Because of its axial symmetry this potential will split each free-ion level into $J+1$ or $J+\frac{1}{2}$ components. Each component will have an integral or half-integral M value and all except $M=0$ will be doubly degenerate. Such a picture, dominated by the second-degree axial term, is in definite disagreement with the published experimental data on spectra and magnetic properties of the ethylsulphates.

Other possibilities present themselves, however. There is another triangle of oxygen atoms coming from the three ethylsulphate radicals which lies almost as close to the rare earth ion as do the water molecules. If, following previous suggestions for sulphate crystals, one assumes a charge on the ethylsulphate oxygens, the symmetry and the algebraic expressions in the potential are unchanged but great variations in the relative magnitudes of A_2 and A_4 may be caused. For a charge of about $\frac{1}{2}Q$, A_2 vanishes. It is also true, on the other hand, that A_2 can be made to vanish for zero charge on the ethylsulphate oxygens, if one shifts the water molecules from Ketelaar's positions by only 3 or 4 degrees (maintaining the same symmetry). Because of this high sensitivity of the coefficients it is impossible to be sure of a definite potential from the x-ray data alone.

If A_2 is made very small in one of these ways, the resulting picture seems to give much better agreement with the experimental data. The patterns are determined principally by the fourth-degree term (they are often quite similar to those arising from a cubic potential), and the sixth-degree term becomes noticeable. The latter contains an expression which in polar coordinates is $\cos 6\phi$ and which causes a slight doubling of those components whose M values are multiples of 3 and departures from integral or half-integral M values in many other components.

The applicability of such a predominantly fourth-degree axial field *consistent* with the x-ray structure, even if not demanded by it, will be reported upon shortly.

CECIL B. ELLIS
HARVEY HALL

College of the City of New York,
New York, New York,
August 22, 1938.

[1] Ketelaar, Physica **4**, 619 (1937).

Viscosity of Helium

Recent experiments of Itterbeek and Keesom[1] on the viscosity of helium from room temperatures to about two degrees Kelvin have served to emphasize the inadequacy of the elastic sphere model for the atoms of an inert gas. Results of calculations by one of the authors,[2] based on this model, are shown to be in serious disagreement at both high and low temperatures. In view of the adequacy of experimental data and the limitations of the elastic sphere model as revealed by a comparison of these data with the theory, it is of some importance to obtain the consequences of the latter when an appropriate van der Waals interaction is assumed. This question has been considered already by Massey and Mohr[3] in the temperature region above 15°K by assuming a Slater field to describe the interaction of helium molecules. Their results likewise reveal serious discrepancies in the low and the high temperature regions, which are of the order of twenty percent at 15°K and seven percent at room temperature. The question of density dependence in an intermediate range of densities conforming to the validity of existing theories is not considered by these authors. In view of the experiments of Itterbeek and Keesom in the temperature region below 15°K where the quantum density dependence may be expected to be appreciable, this question is still of an academic nature, but is being considered by the present authors together with a choice of interaction potential giving an improved temperature dependence.

To choose correctly the best form of van der Waals field involves considerable difficulty. First, an exact quantum mechanical calculation of the field reveals a rather complicated form not suited to computation. Even this expression may be questioned on the basis of the correctness of the perturbation theory when the overlap and the attractive terms are comparable. To represent this field then, two terms, one a repulsive and the other an attractive, requires that we give up any attempt to fix the constants entirely by theory. In addition it must be pointed out that the kinetic theory of viscosity developed, takes into account no inclusion of ternary and higher order collision processes. The appropriate van der Waals field should be based on a binary collision theory of a gas and experiment should serve to determine adjustable constants.

Following the preceding arguments, we have been led to select the expression for the helium interatomic field as given recently by Lennard-Jones.[4] Calculations with this field revealed that the transport cross section is reduced in the high and low velocity ranges giving rise to the proper corrections for the two extremes of temperature considered by Itterbeek and Keesom. In the intermediate velocity range a slight increase in cross section was obtained, such that for intermediate temperatures the overlap from all three regions maintained elastic sphere values of the viscosity. It is just in this intermediate region that the elastic sphere model gives correct values for the coefficient.

As an indication of the fit at low and high temperatures, we list the values found in our preliminary calculations for the van der Waals field along with the experimental data from the tables of Itterbeek and Keesom and corresponding values from the quantum mechanical calculations of the elastic sphere model. (The coefficient η is given in micropoises.)

T(°K)	η(exp.)	η(v. d. W.)	η(elastic sphere)
273	187.0	182.	173.
4.23	12.67	12.6	10.8

With regard to the density correction arising from the quantum-statistical modification in the Stoss-zahlansatz, preliminary calculations show that with a Lennard-Jones potential, this correction, as for the elastic sphere model, can at most amount to only a few percent in the range of variation in density to which the theory can be legitimately applied. In this range of density variation and at all temperatures the experiments are inconclusive with regard to any density dependence of the viscosity coefficient.

E. A. UEHLING
E. J. HELLUND

University of Washington,
Seattle, Washington,
August 25, 1938

[1] Itterbeek and Keesom, Physica **5**, 257 (1938).
[2] E. A. Uehling, Phys. Rev. **46**, 917 (1934).
[3] Massey and Mohr, Proc. Roy. Soc. **A144**, 188 (1934).
[4] Lennard-Jones, Physica **4**, 941 (1937).

Tentative Theory of Novae

As has been indicated by the author,[1] a star model having an ordinary thermonuclear source of energy must show a steady increase with time in luminosity and effective temperature, moving slowly upward along the main sequence of the Hertzsprung-Russell diagram. At the point of maximum luminosity all hydrogen will be finally used up and the star will be suddenly deprived of any source of nuclear energy. At the succeeding stages of its evolution we should expect a progressive contraction, the radiation being supplied by utilizing gravitational energy only. However at this turning point of evolution a redistribution of mass in the stellar interior must take place (from "point source" to "contractive" distribution). The gravitational energy liberated in such a redistribution is likely to cause a sudden short increase of luminosity and it is possible that such phenomena may account for the explosions of stars known as novae. From this point of view the observed pre-nova stage of the star should correspond to a vanishing hydrogen-content and should correspondingly possess a luminosity about a hundred times larger than that of a normal star of the same mass. The history of the star after the contraction has started will depend essentially on its mass. For masses smaller than the critical mass of Chandrasekhar-Landau (about 3.2 sun masses) the contraction will lead through all stages of hot and dense stars to the well-known type of white dwarfs, having a degenerated electron gas inside and very small energy production. For larger masses the formation and growth of a neutron core, representing a practically unlimited source of energy, should be expected. The growth of such a core, accompanied by increasing energy liberation (and probably expansion of the atmosphere), may bring the star into the Giant branch of the H-R diagram. The explosion of massive stars thus will lead to extremely bright novae and might be identified with the so-called super-novae of Baade and Zwicky.[2]

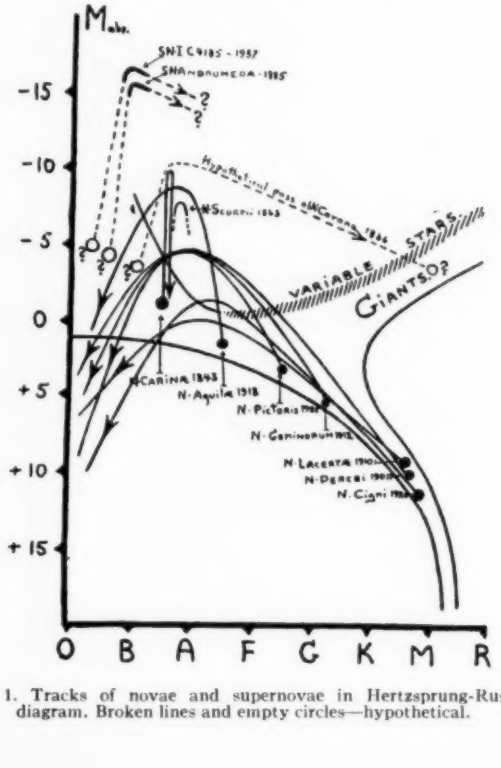

FIG. 1. Tracks of novae and supernovae in Hertzsprung-Russel-diagram. Broken lines and empty circles—hypothetical.

We see from Fig. 1, where the tracks of the explosions of various novae with known absolute magnitudes[3] are schematically shown in the frame of the H-R diagram, that there is no marked gap in intensity between ordinary novae and the so-called super-novae. The hypothetical pre-nova stages of super-novae (indicated by empty circles) are visually too faint ($m_{vis}=18.5$ and 19.5) to be observed against the background of an extra-galactic nebula. We see that stars of small initial luminosity, after passing through the maximum (average increase 11 magnitudes) come finally to the region of higher effective temperatures (i.e., smaller radii) in agreement with the above theoretical considerations. However the "anomalous" Nova Carinae (1843) which, judging from its initial luminosity, possesses the largest mass of all observed novae, behaves in a rather different way, returning to its initial spectral class and radius. Still more interesting is the "anomalous" Nova Corona (1866) which shows at present the spectrum of class *M*. Such behavior should be expected on the basis of the above considerations for stars of rather large masses. Unfortunately the parallax of this nova is not measured and hence we do not know its absolute magnitude. Since the star is visually very faint, one should predict a very small (probably unmeasurable) parallax. Another way to check the above thermonuclear considerations regarding stellar energy and evolutionary behavior would be to prove that the present spectrum of *N*-Corona belongs to the M_{giant} class; no work in this direction, however, is known to the author. A more detailed knowledge of the location of novae of large masses in the H-R diagram is necessary for the further check of this proposed point of view.

G. GAMOW

George Washington University,
Washington, D. C.,
August 20, 1938.

[1] G. Gamow, Phys. Rev. **53**, 595–604, 907–908 (1938); Zeits f. Astrophys. **16**, 113–160 (1938).
[2] F. Zwicky, Phys. Rev. **53**, 1019–1020 (1938).
[3] F. J. M. Stratton, *Handbuch für Astrophys.* Vol. VI$_2$ (1928), p. 251.

Gamma-Rays from Li+H[1]

Indications of a gamma-ray resonance from Li+H[1] at about 200 Kev were obtained by Bothe and Gentner.[1] Using isotope targets, Roberts and Heydenburg[2] found that the gamma-rays emitted in this voltage region are due to Li^7, while Gentner,[3] in a later paper, observed a smooth rise in the thick target yield, following a curve similar to that of the well-known alpha-particle yield. We have repeated the experiment both by counting gamma-rays alone and by counting alpha-particles and gamma-rays simultaneously. In both cases we observed the smooth rise indicating the absence of a resonance. Fig. 1 shows the results of the latter experiment, giving the proportionality of the alpha- and gamma-yield, along with the data published by Gentner.

For this work we have used the transformer-rectifier

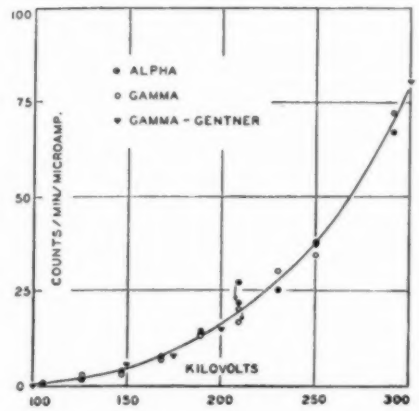

FIG. 1. Gamma-ray and alpha-particle excitation curves of Li+H[1]. At 210 kv two points are given for both alpha-particles and gamma-rays. The high point in both cases includes data taken while the lithium film was fresh, while the lower points include only data taken after the film had reached an "equilibrium."

equipment described by Haworth, King, Zahn, and Heydenburg.[4] The gamma-rays were detected by a Geiger-Mueller counter filled with a mixture of air and alcohol,[5] and shielded from x-radiation produced by the apparatus itself by $\frac{3}{4}$ in. lead. The radiation entering the window of this shield was filtered by $\frac{1}{16}$ in. brass, $\frac{1}{16}$ in. lead, and $\frac{3}{8}$ in. aluminum. Despite this shielding, the background count with the proton beam coming down the tube was above the cosmic-ray background. This additional background was probably caused by x-rays produced by secondary electrons striking the high voltage end of the tube. Corrections were made, for the greater part, on the basis of background runs made immediately after corresponding gamma-ray runs, even though the corrections were a fairly regular function of voltage and proton current. The alpha-particles were counted by an ionization chamber and a Dunning-type linear amplifier. The target assembly has been described by Haworth and King.[6]

The data presented in Fig. 1 were obtained from a single lithium film, the yield from which decreased very rapidly for a time, but later gave reproducible results. At 210 kv two points are given for both alpha-particles and gamma-rays. The high point in both cases includes data taken while the film was fresh, while the lower points include only data taken after the film had reached an "equilibrium." We found no radiation in this voltage region from a target of pure carbon, so the inevitable carbon deposit cannot make the proportionality of the two yields fortuitous.

The authors wish to express their gratitude to Professor Breit for many helpful discussions and to the Wisconsin Alumni Research Foundation for financial support.

W. R. KANNE
G. L. RAGAN

University of Wisconsin,
Madison, Wisconsin,
August 19, 1938.

[1] Bothe and Gentner, Zeits. f. Physik **104**, 685 (1937).
[2] Roberts and Heydenburg, Phys. Rev. **53**, 929 (1938).
[3] Gentner, Zeits. f. Physik **107**, 354 (1937).
[4] Haworth, King, Zahn, and Heydenburg, Rev. Sci. Inst. **8**, 486 (1937).
[5] Trost, Zeits. f. Physik **105**, 399 (1937).
[6] Haworth and King, Phys. Rev. **54**, 38 (1938).

The Variation with Heat Treatment of the Cold Resistance of Nickel

In order to obtain a clean, stable nickel wire for the study of surface energy losses, the wire was subjected to prolonged heat treatment and its cold resistance (resistance at 0°C) measured at various stages. The initial bakeout at 450°C caused a 13.3 percent decrease in resistance, and subsequent flash annealing at gradually increasing temperatures up to about 900°C caused a gradual decrease in cold resistance to a value 16.8 percent less than the original. Upon increasing the annealing temperature to about 950°C, instead of a continued decrease, an increase of 0.8 percent over the lowest resistance was found. (This difference was well over the experimental error.) In this connection it may be noted that Bittel,[1] investigating the influence of heat treatment on the cold resistance of much purer nickel, reports a gradual decrease in resistance for annealing temperatures up to about 600°C, followed by a sharp increase. Measurements previously made by Tammann[2] and Credner[3] (maximum temperature reached: 800°C and 750°C, respectively) show no rise in cold resistance. This difference Bittel attributes to the greater impurities present in the specimens used in the earlier work, which would cause recrystallization to begin at a higher temperature. This view is confirmed by the present work, for the nickel used approximates Credner's in purity, and the first increase in resistance was found for an annealing temperature higher than any used by Credner.

The above aging process was repeated approximately (except for much shorter annealing times), with quite different results: upon heating for one hour at each of several temperatures from about 400°C to about 950°C the resistance consistently increased, the final resistance being 8.5 percent higher than that previously observed after flashing for 23 hours at the same temperature.

These results suggest that the wide variation in the electrical and thermal properties of nickel as reported in the literature are due in part to the lack of a standardized aging procedure. Different investigations of the temperature variation of the thermal conductivity of nickel, for example, have not even agreed on whether the thermal conductivity increases or decreases as the temperature is raised above room temperature. Sager,[4] who measured the thermal conductivity first with increasing temperature and then with decreasing temperature, found about a 14 percent increase in the value at 54°C, yet in some other reports on the thermal conductivity of nickel, no comparable check on the stability of the specimen seems to have been made.

From work done on the aging of other metals, notably that of Langmuir and Taylor[5] on tungsten, it was expected that an annealing temperature could be found such that after sufficient heat treatment at that temperature, treatment at lower temperatures would produce no change in cold resistance. This was not found to be the case with nickel, at least for annealing temperatures up to about 950°C. For, although after many hours of heating at 950°C, further heating at that temperature did not change the

cold resistance, several hours of heating at about 700°C caused a decrease of 4.0 percent in the cold resistance. Further heating at 950°C brought the cold resistance back to the value formerly characteristic of annealing at that temperature: part of the change in cold resistance with heat treatment appeared reversible.

Further work on the aging of "A" nickel and of 99.9 percent pure nickel is contemplated.

I wish to express my thanks to Dr. Walter C. Michels for his guidance in this work.

BARBARA RAINES

Bryn Mawr College,
Bryn Mawr, Pennsylvania,
August 30, 1938.

[1] Bittel, Ann. d. Physik **31**, 219 (1938).
[2] Tammann, Ann. d. Physik **16**, 667 (1933).
[3] Credner, Zeits. f. physik. Chemie **82**, 457 (1913).
[4] Sager, Renss. Poly. Inst. Publ. 27, (1935).
[5] Langmuir and Taylor, J.O.S.A. **25**, 321 (1935).